DESIGN AND MECHANICAL BEHAVIOUR OF BRAZED PLATE HEAT EXCHANGERS

A Thesis Submitted to
the Graduate School of Engineering and Sciences of
İzmir Institute of Technology
in Partial Fulfillment of the Requirements for the Degree of

MASTER OF SCIENCE

in Mechanical Engineering

by
Yiğit GÜRLER

July 2018
İZMİR

We approve the thesis of **Yiğit GÜRLER**

Examining Committee Members:

_____

Assoc. Prof. Dr. H. Seçil ARTEM
Department of Mechanical Engineering, İzmir Institute of Technology

_____

Prof. Dr. M. Evren TOYGAR
Department of Mechanical Engineering, Dokuz Eylul University

_____

Assist. Prof. Dr. Sinan KANDEMİR
Department of Mechanical Engineering, İzmir Institute of Technology

9 July 2018

_____

Assoc. Prof. Dr. H. Seçil ARTEM
Supervisor, Department of Mechanical Engineering, İzmir Institute of Technology

_____

Prof. Dr. Metin TANOĞLU
Head of the Department of Mechanical Engineering

_____

Prof. Dr. Aysun SOFUOĞLU
Dean of the Graduate School of Engineering and Sciences

ACKNOWLEDGMENTS

I would like to express my deeply and sincerely thanks to the precious scientist and my advisor Assoc. Prof. Dr. H. Seçil ARTEM. I could not imagine to finish this study without her help and continuous support.

I would like to thank Mr. Saim Kırgız, BOSCH Thermotechnology Manisa Research and Development Center Director and Mr. Erden Akdarı, Research and Development Center Design Section Manager for giving me chance to proceed this study. I am grateful to my workmates Zafer Turhan, Dr. Caner Şenkal, Ozan Mert Balcı and Simge Yalçın for their endless support during the working and writing period of my thesis.

I would like to thank Prof. Dr. Metin Tanoğlu and M. Deniz Güneş for their helping and valuable comments during experimental study of this thesis.

Finally, I would like also thank to my parents and express my gratitude to my mother, father and grandmother for their endless support, motivation and understanding at every stage of my life.

ABSTRACT

DESIGN AND MECHANICAL BEHAVIOUR OF BRAZED PLATE HEAT EXCHANGERS

In recent years, the developments in clean, renewable and efficient energy policies have been enabled to design new and innovative heat exchangers. The plate heat exchangers have crucial importance among these innovative products due to compact size and thermally efficient behaviour. There are many studies dealing with the thermo-fluidic behaviour of brazed plate heat exchangers. However, since the usage of these products often includes relatively high pressure and toxic fluids, the examination of structural stability of these products is cruical from the point of scientific perspective view. There are very few studies of plate heat exchangers regarding to mechanical aspects. Accordingly, in this thesis it is intended to investigate structural behaviour of brazed plate heat exchangers by numerical methods. For this purpose, the material properties of brazing interface of plate heat exchangers have been determined by experimental methods. The tensile and stress based fatigue experiments are carried out and the material models have been obtained. The validation of material model which is used in numerical analysis has been carried out by explicit method using maximum displacement as a boundary condition. The mechanical behaviour of chevron type brazed plate heat exchangers has been investigated by considering effect of chevron angle under different pressure conditions. The results have been obtained numerically in two stages; static structural analysis results and fatigue analysis. The numerical results show that the chevron angle has a significant effect on the formation of brazing points of plate heat exchangers. The dimensions of brazing points directly affects the overall structural behaviour of plate heat exchanger. It is observed that the single brazing point surface area and homogeneous distribution of brazing points on the plates are more critical than the total surface area. Finally, it is thought that the developed numerical methodology will lead to the structural design of brazed plate heat exchangers before the production of protoype molding and experimental testing. Eventually, it will be advantageous in terms of mold costs and time spent for experimental testing.

ÖZET

SERT LEHİMLİ PLAKALI ISI DEĞİŞTİRGEÇLERİNİN TASARIMI VE MEKANİK DAVRANIŞI

Son yıllarda, temiz, yenilenebilir ve verimli enerji politikalarındaki gelişmeler yeni ve inovatif ısı değiştirgeci tasarımlarına olanak sağlamaktadır. Plakalı ısı değiştirgeçleri kompakt boyut ve ısıl verimlerindeki potansiyelleri açısından bu inovatif ürünler arasında önemli bir yere sahiptir. Sert lehimli plakalı ısı değiştirgeçleri ile ilgili ısıl ve akışkan davranışını inceleyen birçok bilimsel çalışma olmasına rağmen bu ürünlerin kullanımı çoğunlukla yüksek basınç altında çalıştığından ve toksik akışkanlar ile etkileşimde olduğundan yapısal karalılık konusununda bilimsel açıdan irdelenmesi önem kazanmaktadır. Literatürde, plakalı ısı değiştirgecin yapısal davranışını inceleyen bilimsel çalışma sayısı oldukça azdır. Bu bağlamda, tez kapsamında plakalı ısı değiştirgecinin yapısal davranışının nümerik methodlar yardımıyla incelenmesi hedeflenmektedir. Bu amaca yönelik olarak plakalı eşanjörlerdeki sert lehim noktalarının malzeme özellikleri deneysel olarak elde edilmiştir. Çekme testi ve gerilme genliğini esas alan yorulma testleri yapılmış olup elde edilen veriler ile malzeme modelleri kurulmuştur. Nümerik analizlerde kullanılan malzeme modelinin validasyonu maksimum yer değiştirme sınır şartını kullanarak eksplisit yöntem ile doğrulanmıştır. Plakalı ısı değiştirgeçlerinin mekanik tasarımı çavuş açısı esas alınarak yapılmış ve yapısal davranışı farklı basınç değerleri altında incelenmiştir. Nümerik analizlerde çavuş açısının sert lehim noktalarının oluşumu üzerinde oldukça etkili olduğu gözlemlenmiştir. Mekanik dayanım açısından tek bir sert lehim noktası yüzey alanı değerinin ve sert lehim noktalarının homojen dağılımının etkisinin toplam yüzey alanı değerinden daha kritik olduğu görülmüştür. Sonuç olarak, tez kapsamında geliştirilen methodoloji ile prototip kalıp üretimi ve deneysel testler öncesinde sert lehimli plakalı ısı değiştirgeçlerinin tasarımına yön verileceği düşünülmektedir. Bu sayede kalıp maliyetleri ve testlere harcanan zaman açısından avantaj sağlanmış olacaktır.

TABLE OF CONTENTS

LIST OF FIGURES

LIST OF TABLES

CHAPTER 1

INTRODUCTION

Over the last decades, the increasing demand on efficient and clean energy management has brought about the development of numerous innovative heat exchanger designs. The plate heat exchangers have crucial importance among these innovative products due to their compact size and thermally efficient behaviour. There are many studies in the literature considering the investigation of thermo-fluidic behaviour of heat exchangers in terms of design aspects. However, the requirements on these equipments often include a fully sealed construction and a high structural stability for the use in applications with high pressures and toxic fluids. There are very few studies of plate heat exchangers regarding to mechanical aspects.

Structural stability of plate heat exchangers were directly caused sealing problem between central heating water and domestic hot water. Hence any structural failure will be caused heavy metal and burnt waste contamination problem into domestic hot water circuit. Besides that issues structural failure was brought along some thermo-fluidic problems wihich were caused to decrease thermal effectiveness of system. Another issue of about heat exchangers is cyclic high pressure thermo-mechanical loading. The mechanical stability of heat exchangers during life time is strongly depends on fatigue response of desired system.

A plate heat exchanger is mechanical device that is used for the thermal energy conversion between two or more fluids by using corrugated plates. As a common rule, the corrugation of plates is necessary for the increasing of heat transfer surface area. Although, there is a various type of corrugation geometry, the chevron type plate configurations is commonly used shown in Fig. 1.1. Plate heat exchangers (PHEs) can be produced in several methods, but mostly exhibit certain common characteristics. The PHEs are usually have a compact size and they are lighter and cheaper than the tubular type of heat exchangers. However, PHEs have some limitations on application side because they can not tolerate as relatively high temperatures and pressures.

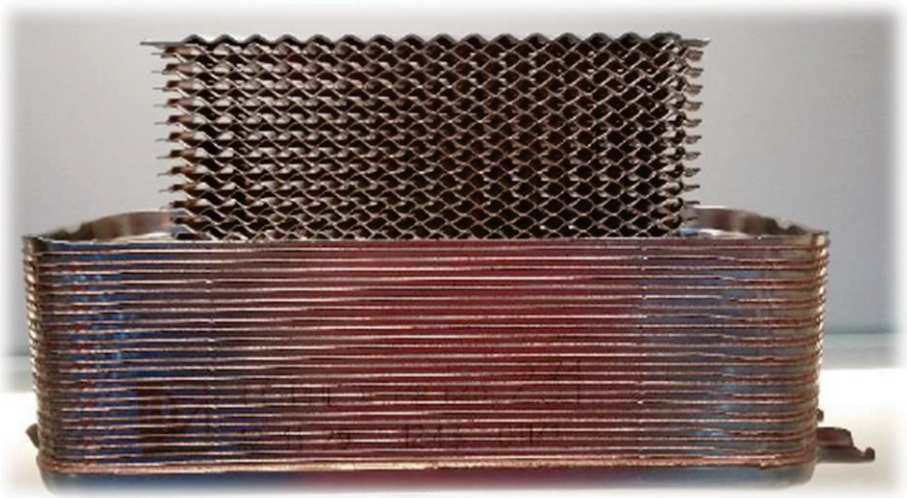

Figure 1.1. Chevron type asymmetric Brazed Plate Heat Exchanger (BPHE)
(Source: Bosch TT, 2015)

The production cycle of PHEs can be listed as below in case of vacuum environment and using copper filler,

- ✓ Stainless steel sheet and copper foil are stamped in knuckle joint press
- ✓ Stamped plates are stacked onto each other and introduced to vacuum brazing furnace

Finally, the two fluid mediums are not mixed into each other thanks to copper brazed sealed surfaces. The PHEs works according to principle of cross-flow of cold and hot waters. This cross-flow principle is achieved by arranging the chevron directions in the opposite way as can be seen in Fig.1.2.

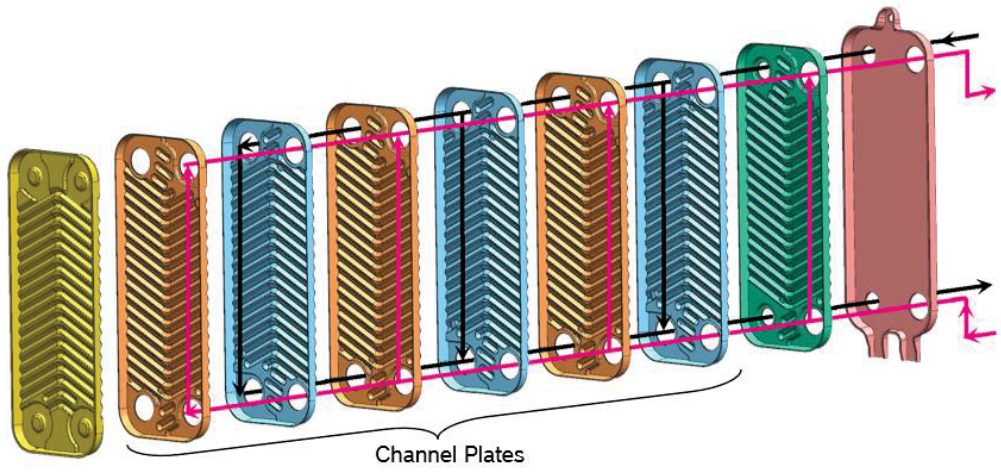

Figure 1.2. Stacking sequences of plates in opposite chevron directions
(Source: Bosch TT, 2015)

1.1. Literature Review

The recent research studied and developments on the mechanical stability and fatigue life behaviour of brazed plate-plate or plate-fin heat exchangers have been summarized in this section.

The effect of filler metal thickness on the tensile strength behaviour of plate-fin structures made of 304 type stainless steel have been studied both numerically and experimentally. The experimental results showed that the filler thickness has a great importance on the tensile strength of plate-fin stucture. Finally, the experimental and numerical studies have been condensed on the prediction of optimum filler thickness for the best tensile strength performance (Jiang, et al. 2009).

The fatigue properties of austenitic type 316L stainless steels have been investiagted at constant amplitude cyclic loading. The cyclic experiments have been run at R = 0,1 stress ratio. At the end of experimental studies fracture surfaces were scanned by electron microscopy to understand crack initiation and propagation ways (K.A.Mohammad, et al. 2011).

The mechanical reliability characterization of low carbon stainless steel brazed joints by copper filler materials have been studied by Morvarid, et al. It has been observed that the Power Law mixed mode failure theory which is based on single mode tensile and shear tests well predicts the biaxial failure of brazed joints.

The fatigue life time prediction of plate-fin type heat exchangers made of 304 stainless steel has been studied numerically by using equivalent homogeneous solid method. The finite element analysis interface has been developed to predict fatigue aspects and numerical results have been validated experimentally. The proposed methods gives a posssibility to predict stress concentrations around brazed joint and fatigue life of plate-fin structure. The crack nucleation locations and propagation way has been discussed for the further improvements (W.Jiang, et al. 2011).

The high temperature structural design procedure and methods for plate-fin heat exchangers were investigated by both experimental and numerical techniques. The allowable stress limits have been given for brazed joints as a result of experiments. The procedure of design and used finite element analysis techniques were validated by partial model tests. In order to understand decreasing of material strength by thermal aging and helium gas environment, several experiments have been carried out. The failure mode

and failure limits were given. Pressure burst test and thermal fatigue behaviours have been investigated by validated numerical approach with partial model (Mizokami, et al. 2012).

The mechanical integrity of tube type heat exchangers have been investigated by taking into account local and global material properties. The prediction of boundary conditions properly for local stress analysis of heat exchanger, the global fluid-structure interaction analysis have been run accordingly. The local mechanical properties of brazing joints have been introduced by using nano-identation tests and used as input for finite element analysis. Stress concentration and fatigue limit of U-type tube heat exchanger have been determined by changing fillet radius of brazed joint (S.H. Kang, et al. 2012).

The fatigue failure can be occured by elastic or elasto-plastic strain accumulation on the material. The structural response of investigated part is drastically changing according to accumulation is whether elastic or not. Hence, the fatigue method which will be used in simulations should be selected thanks to structural response of investigated part. It is strongly recommended that, if the desired system has a plastic strain after first step of loading, the strain life based fatigue methodlogy must be used and experiments had to be done accordingly. But some research studies reveal that a small amount of plastic strain after first cycle of loading may be acceptable for the usage of stress life based fatigue methodology.

The experimental test to characterize the cyclic plastic behaviour of austenitic type 316 L stainless steel has been investigated by J.Shit, et al. (J.Shit, et al. 2013). The strain controlled symmetric low cycle fatige experiments has been carried out and the cyclic hardening character was revealed.

The prediction of fatigue life of austenitic type 316 L stainless steels under cyclic loading conditions has been studied at constant load amplitude and 5 Hz loading frequency. The fatigue test specimens have been prepared according to ASTM E466-96 standarts. The endurance fatigue limit of material has been determined (Khairul A.Mohammad, et al. 2013).

The plate heat exchanger is composed of channels which are stacked up onto each other to direct the cold and hot waters with opposite directions from inlet to oulet ports. Plate heat exchangers are classified according to connection type; sealed type and brazed type. The mostly current applications require to use brazing technique for the

connection of plate channels. Hence, the endurance of brazed joints is gaining importance in both static and cyclic loading conditions.

The fatigue and cyclic deformation behaviour of brazed steel joints has been investigated experimentally. Stress controlled fatigue test of 4313 stainless steel with its brazed joints has been carried out to capture failure modes during repitative mechanical loading. The production conditions of brazing is crucially important for mechanical behaviour of final part. The brazing process has been realized in the shielding gas furnace under H_2 atmosphere by using Au 18 wt % Ni filler material. The cyclic experiments have been run at constant stress ratio (M.Koster, et al. 2013).

The low cycle fatigue life prediction of stainless steel have been investigated by using plain speciments in both experimentally and numerically. The effect of temperature and notch have been added into content of study (R.Agrawal, et al. 2014).

The influence of elasto-plastic base material properties of on the fatigue life and cyclic deformation behaviour of brazed steel joints have been discussed. The 316 C-NM type stainless steel has been used as a base material and AuNi18 has been selected as a filler metal. To understand effect of heat treatment on the cyclic deformation behaviour of inspected material, the series of heat treatments were planned. Hence, the artificial defects has been removed. The study reveals that significant effect of heat treatment on the fatigue life (M.Koster, et al. 2015).

The production method of plate heat exchangers directly effects the geometrical dimensions and mechanical properties. The investigation of stamping process effect on the thichkness reduction behaviour of brazed plate heat exchangers has been discussed via both experimental and numerical techniques. The orientation of grains and crystall plasticity effects are successfully implemented on finite element analysis. The thickness reduction map of plates were given comparatively (D.Canadinc, et al. 2015).

The low cycle and thermo-mechanical fatigue behaviour of 316 FR type stainless steel material has been investigated via experimental methods for fully reversed loading conditions. Strain controlled isothermal tests have been perforated at 650 °C temperature conditions for the different strain ranges such as ; $\Delta\varepsilon$ = + / - 0.4, 0.8, 1.0, 1.2 %. The thermo-mechanical cyclic tests have been run for the 500 – 650 °C conditions. The final results has been discussed by doing scanning electron microscopy analysis for the fractured sample surfaces (R.Hormozi, et al. 2015).

The mechanical properties of austenic type X6CrNiTi18 – 10 stainless steel have been investigated for the short time creep and fatigue life. Tensile and cyclic fatigue tests have been performed at constant stress ratio. The stress limit of fatigue life have been obtained (Brnic, et al. 2016).

The low cycle fatigue behaviour of compact heat exchanger made of 316 L stainless steel has been studied numerically with proper material models which are obtained from mechanical characterization tests. According to this manner, the finite element analysis method has been developed which confirms experimental study. The bending tests have been done for the usability of multilinear kinematic hardening model in numerical analysis. The new methodlogy gives a possibility to predict life time of heat exchangers based on Coffin-Manson law (M.Laurent & R.Estevez, et al. 2016).

Most of the studies in literature have been focused on obtaining of mechanical properties of materials. Meanwhile, the fatigue behaviour of the brazed joints is generally studied for fully reversed loading type. There are almost no studies that include stress based fatigue tests in which the stress ratio was taken close to 0. Another factor in literature studies is that the frequency of the applied load is much higher than our application in this thesis. The increment of frequency makes the fatigue behaviour dependent on the strain rate. Thus, since the strain rate is not desired to have an effect on fatigue behaviour of plate heat exchangers in our application, the experimental fatigue tests have been carried out suitable for the operating and test conditions of plate heat exchanger. After that, for the prediction of overall structural behaviour and mechanical integrity of heat exchangers, the numerical approach suitable for application and operating conditions of plate heat exchangers have been developed in this thesis. The findings about the material properties of brazed joint which are obtained from experimental works have been used as an input data in numerical models.

Finally, it is thought that this thesis fills the gap in the literature on point of examination of the fatigue behaviour of brazed compact plate heat exchangers, under specific load conditions such as zero based loading and relatively low frequency.

CHAPTER 2

THEORETICAL BACKGROUND

In this chapter, it is intended to give basic informations about the theories used in this study experimental and numerical parts. This chapter gives fundamentals of tensile testing, stress-strain relations, plastic deformation of metal alloys, hardening law of metallic materials, brief description about vacuum furnace brazing process and fundamentals of fatigue theory. The last part of this chapter will give a some fundamental and basic informations about the finite element analysis techniques.

2.1. Tensile Testing

The tensile testing is commonly used experimental method to obtain fundamental design informations of engineering applications. The test can be used as an acceptance criteria to specify engineering materials which are using in component design. The test specimen is subjected to a continously increased uniaxial force up to break of tested sample and the load – displacement curve is automatically saved by data acquisition system. The extensometer can be used as a data collection insturement to derive load – displacement curve (George E.Dieter, 1988).

2.1.1. Testing Machines

The tensile testing machines can be electromechanical or hydraulics. The main difference between them is the application of load on the specimen. Electromechanical tensile machnies are applying load based on a variable-speed electric motor while hydraulic testing machines are based on whether a single or dual acting piston that moves cross-head up or down. The typical hydraulic tensile testing machine shown in Figure 2.2.

The tensile testing machines can be used for several material testing applications such as, tension test, compression test, three or four point bending tests and some fatigue applications. The electromechanical testing machines are able to do tests for wide range speeds and they have longer cross-head displacements. However, the hydraulics testing machines are cost effective for applications at higher forces. In Figure 2.1, the elements of hydraulic tensile testing machine are shown (ASM, 2014).

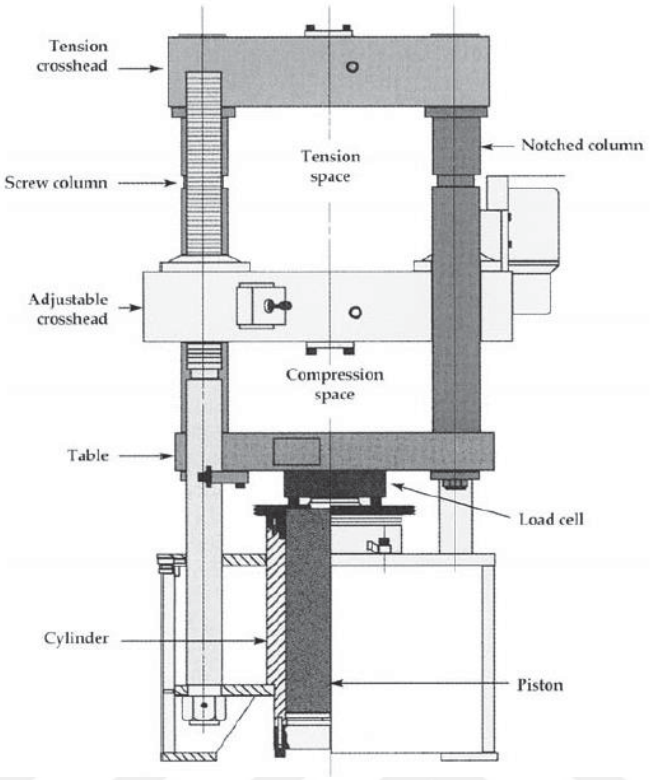

Figure 2.1. Components of a hydraulic universal testing machine (Source: ASM, 2014)

Figure 2.2. Tension test equipment (hydraulic tensile testing machine) (Source: NDE Research center)

2.1.2. Tensile Specimens

The main two types of tensile specimen can be classified according to its cross-section as, dog-bone or circular type. The selection of a type of tensile specimen is changing application by application. The important dimensions of specimen are gage length and gage diameter. The cross-sectional area of gage section is decreased to have stress intensity on that region. So, the fracture and failure of material will be from this reduced region because of the locally accumulated stresses. The gage length is region which the deformation measurements are made to calculate elongation at yield or break. The typical dog-bone and circular type tensile specimens are shown in Figure 2.3 and 2.4 respectively (ASM, 2014).

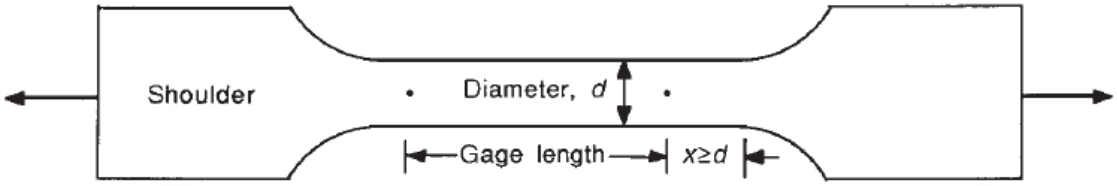

Figure 2.3. The typical dog-bone shaped tensile specimen
(Source: ASM, 2014)

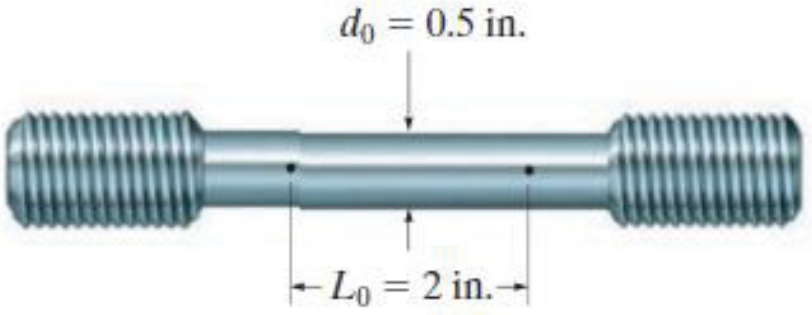

Figure 2.4. The typical circular shaped tensile specimen
(Source: Hibbeler, 2014)

There are several methods of gripping the specimen to avoid from bending effect during the tests. The most important concern in the selection of gripping method is to be ensured that the specimen can be withstand by maximum applied tensile load without ant slippage.

(ASM, 2014)

2.2. Stress – Strain Relations

In this section of chapter, it is intended to give some fundamental informations about the engineering and true stress- strain curves, differences between them and Hooke's Law under the part of stress-strain relations with subheadings respectively.

2.2.1. Stress – Strain Curve

The stress-strain curve can be obtained after uniaxial tensile testing and the deformation mechanisms of tested material can be investigated by looking up test results. The several engineering design inputs are coming from this test by gaining engineering curve such as, modulus of elasticity (Young's modulus), yield strength and ultimate tensile strength etc. The engineering stress – strain curve is obtained from the load – displacement curve by using cross-sectional area and elongation metrics of tested specimen. The most important point of engineering stress – strain curve is that the obtained stress is the 'average longitudinal stress (ALS)' of tensile specimen. The ALS value can be calculated by dividing the tensile load by the corss-sectional area of the specimen (George E.Dieter, 1988).

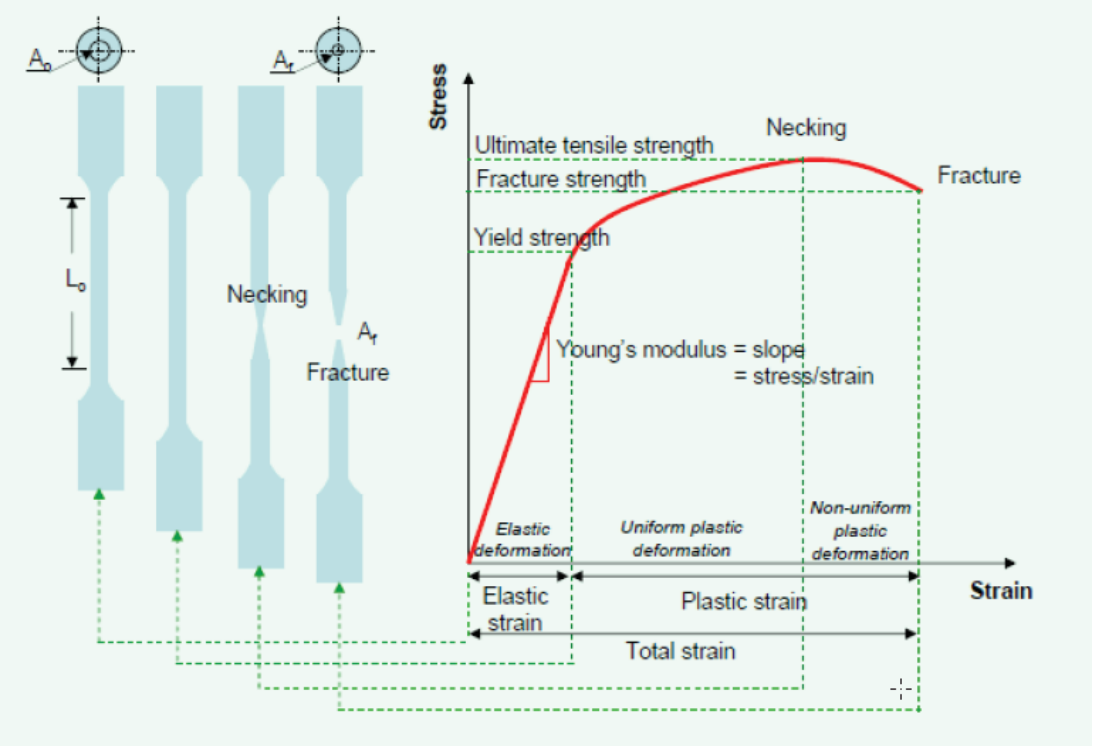

Figure 2.5. Classical stress-strain curve of engineering material (metal alloys) (Source: ASM International, Tensile testing, 2nd edition)

In Figure 2.3, the typical engineering stress-strain curve of metal alloys is given with the important points and regions. The left side of figure represents the deformation shapes of dog-bone based tensile specimen. It is important that to understand physical meanings of each region of that curve. Firstly, the elastic region of curve and Hooke's Law will be discussed in order to understand elastic deformation of materials.

2.2.2. Elastic Deformation and Hooke's Law

There is a linear relation between stress and strain in elastic region which means if the applied load is removed, the material will turn back its original position. In other sense, there will be no damage on the material. This rule has been explained as Hooke's Law. It's mathematical expression can be given as in Eq. (2.1).

$$\sigma = E.\varepsilon \tag{2.1}$$

In this equation the E represents the slope of straight curve and it is called as '*Modulus of Elasticity* or '*Young's Modulus*'. Because of the strain is dimensionless, the unit of elastic modulus will be same as with stress such as Pa, ksi, psi etc.

2.2.3. Engineering and True Stress-Strain

To understand yielding, strain hardening and other deformation mechanisms better, it is required to investigate differences between engineering and true stress-strain curves. The main difference between them is coming from the assumption on the change of cross-sectional area of tensile specimen during material testing. (İrizalp, 2015)

- *Engineering values*: If it is assumed that to apply uniaxial tensile force on a sample, the engineering stress can be calculated by dividing the applied force by the initial cross-sectional area of a testing sample. The term of initial cross-sectional area is the value which has been taken from undeformed shape of a sample.
- *True values*: If the narrowing (necking) in the cross-sectional area will be considered in stress and strain calculations, then, the calculated stress value can be called as 'true stress' . Because, although the tensile force has been applied along the uniaxially, the cross-section of the specimen will be constricted along the other axes.

The transformations between engineering and true values for stress and strain can be made by using constant volume assumption during the deformation of material. The equations (2.2), (2.3), (2.4) and (2.5) represents the formulas for engineering and true stress-strain definitions respectively.

$$S = \frac{P}{A_o} \tag{2.2}$$

$$e = \frac{\Delta l}{l_0} \tag{2.3}$$

$$\sigma = S.(1+e) \tag{2.4}$$

$$\varepsilon = \ln(1+e) \tag{2.5}$$

The Figure 2.6 represents the engineering and true stress-strain curves together to see difference clearly. The main difference between them is starting after yielding or post yielding and finalized with the fracture of material. The divergance of two curves are increasing especially after necking of specimen. It should not be forgotten that even the cross-sectional area of sample staying same up to necking point, there will be a diffrence in ultimate tensile strength and tensile strain values.

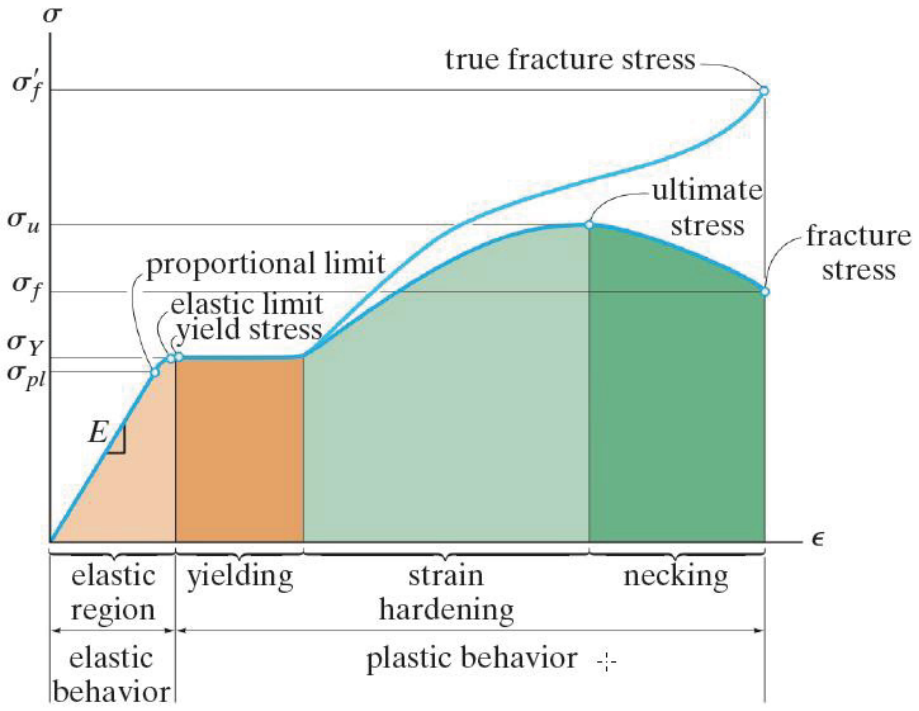

Figure 2.6. Engineering and true stress-strain diagram for ductile materials (steel) (Source: Hibbeler, 2016)

2.2.4. Yielding

The applied force on material is increased to elongate a specimen. After the stress amount reaches a critical value, the elastic deformation will be finalized and te permanen deformation is starting. This point or small region can be called as yield point or yield strength of material σ_y. The stress and strain at that value are defined as yield stress and strain to yield, respectively. The yield point may be apparent for some type of engineering materials such as steels with low carbon contamination, however, it may be inapparent for other type of egineering material such as some steels and polymer based materials etc.

2.2.5. Necking

The deformation of a tensile specimen is being uniformly up to apllied force reaches a critical. After the applying a load which will cause the ultimate tensile stress on the material, the cross-sectional area of sample will begin to decrease in localized region of a specimen shown as in Fig. 2.7. So, this region of a curve is called as necking.

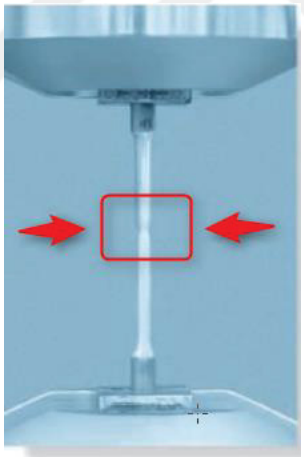

Figure 2.7. Typical necking pattern on the specimen just before fracture

2.3. Stress-Strain Relations in Plastic Deformation

The plastic deformation with several types and mathematical expressions in theory of plasticity is more complex than theory of elasticity. The elastic deformation of material depends on the initial and final cases of stress and strain while the plastic deformation is changing by tracked loading way on the material. There is also no linear relationship

between stress and strain in plastic deformation. The theory of plasticity must be taken as a reference to better understand the mechanism of plastic deformation. The attentions in this area are focused on the imperfection of crystalline structures. The most important subjects of effects on plastic deformation are metallurgical variables and imperfections on a crystallines structures.(İrizalp, 2015)

2.3.1. The Mathematical Description of Plastic Flow

The elastic deformation had been explained with Hooke's law. It is required to define similar relation for the region of plastic deformation. However, the defined relation or expression will be valid only up to necking point. Because, after the necking is occured, the plastic instabillity of material is starting. So that, the region between yielding and necking points is called as homogeneous plastic deformation are and its represented by asimptotic curve shown as in Fig. 2.8.

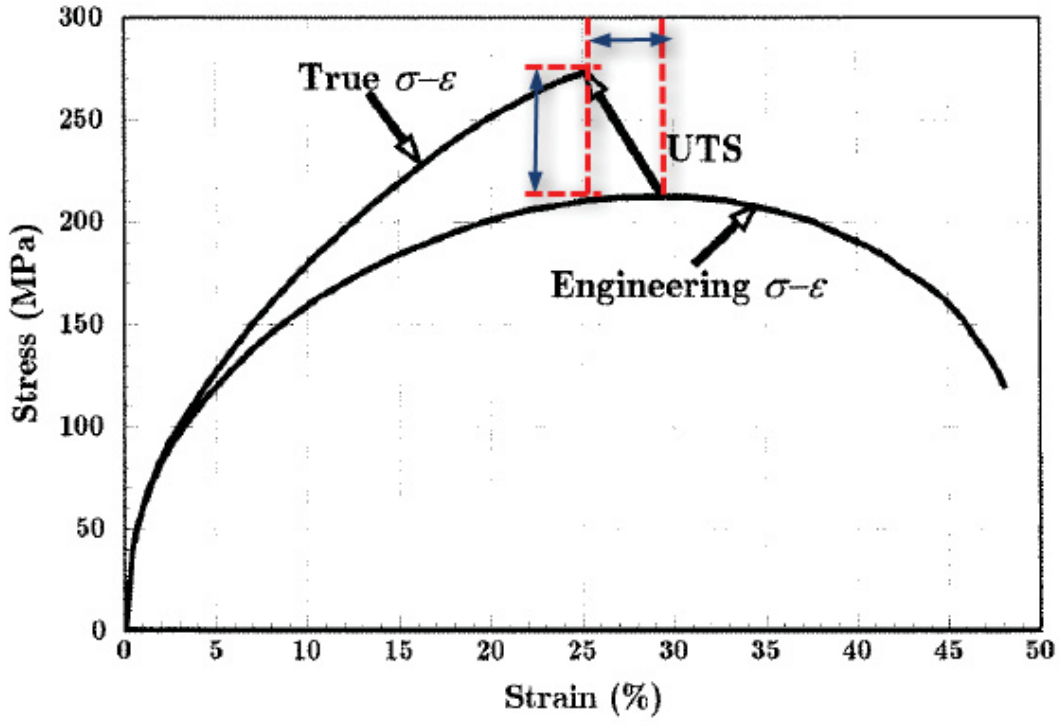

Figure 2.8. The conventional asimptotic plastic flow curve
(Source: Roylance, 2001)

2.3.2. Strain Hardening

When the applied stress exceeds the yield strength of material, the stress on a specimen must be increased for further elongation (strain formation) on the material. The amount of work required for the continuation of the plastic deformation increases as the material elongates. It means that the material is strengthened as the strain increases. This is called as ‘ *strain hardening* ’ which is observed only during plastic deformation. If summarized the definition, *strain hardening* or *work hardening* describes the increase of stress necessary to continue deformation at any stage of *plastic* strain. There are various type of true stress-strain curves describing the work hardening is shown as in Figure 2.9 (W.F.Hosford, 2010).

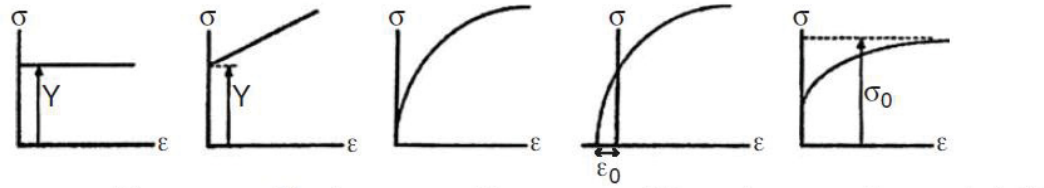

Figure 2.9. Mathematical approximations of the true stress-strain curve
(Source: W.F.Hosford, 2010)

The phsyical meanings of true stress-strain curves are described as;

a. The simplest model of true stress-strain curve with no wprk hardening, the plastic or flow stress is independent from strain, it is so called as *elastic-perfectly plastic* behaviour.
b. The widely used linear approximation for the modelling of plastic flow curve, , it is so called as *linear work hardening* behaviour.
c. It is more common model that used for work hardened metals, The hardening rate of material is decreases as strain increases, it is so called as *Power-law work hardening* behaviour.
d. The model is based on power-law work hardening which modified for the better fit plastic flow curve, it is so called as *modified power-law* relationship.
e. Another model is saturation model offered by Voce, which is more applicable for aluminum alloys.

2.3.3. Power – Law Approximation (Holloman's Equation)

There are various type of approximations which describes the plastic flow curve shown as in Fig 2.9. The widely used expression is the simple power law equation of it given as in Eq. (2.6). The power law model is called as ' *Hollomon's law or equation* ' due to the model is found by John Herbert Hollomon.

$$\sigma = K.\varepsilon^{n} \tag{2.6}$$

The equation parameters K and n can be defined as,

K: Strength coefficient (MPa)

n: Strain hardening exponent

The typical values of K and n for different types are listed of material shown in Table 2.1.

Table 2.1. Typical values of n and K
(Source: Hosford, 2010)

Material	**Strength coefficient, K (MPa)**	**Strain hardening Exponent, n**
Low – carbon steels	525-575	0.20-0.23
HSLA steels	650-900	0.15-0.18
Austenitic steels	400-500	0.40-0.55
Copper	420-480	0.35-0.50
70/30 brass	525-750	0.45-0.60
Aluminum alloys	400-550	0.20-0.30

Then, the shape of a plastic flow curve is described by the parameters of Hollomon's equation. The height of curve is determined by a strength coefficient of K and the length of curve is determined by a strain hardening exponent n. Also, the strain hardening exponent of n gives an idea about the toughness of a material. If n is relatively small the material will exhibit a brittle behaviour otherwise as the value of n increases the ductility of material will increase. The Hollomon's parameters can be obtained by emprical methods such as tensile testing, however, the linearization of a mathematical expression is a must for the determination of n and K. As a conventional rule, high strength materials

have lower strain hardening exponent (n) values than low-strength materials. The durability of hardening is described by change of the shape of true stress-strain curve for different n values shown in Figure 2.10 (Irizalp, 2015).

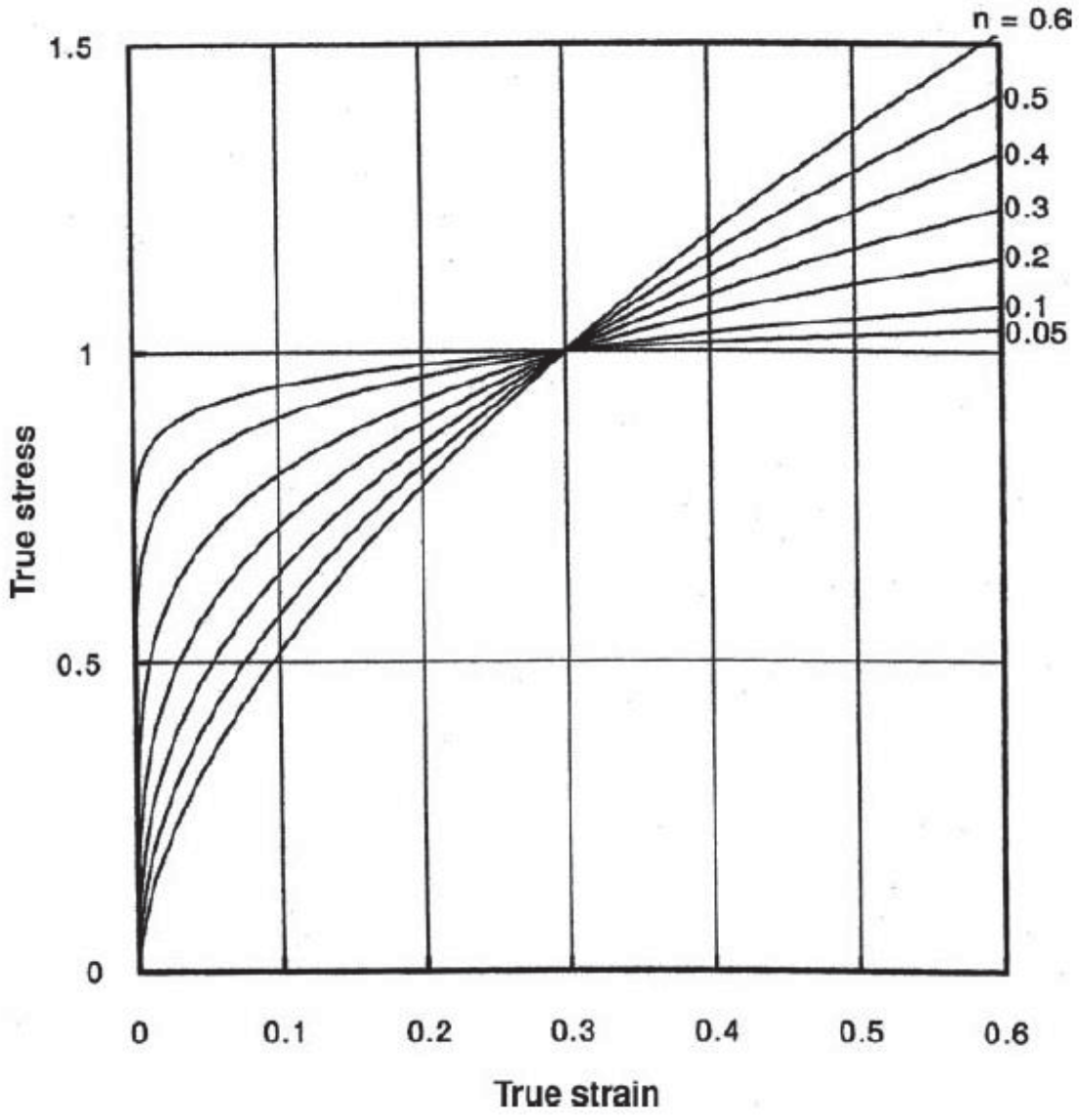

Figure 2.10. True stress-strain curves for Power-law with various values of n (Source: Hosford, 2010)

To make the effect on strain hardening exponent (n) on the shape of the plastic flow curves transperent, the value of strength coefficient (K) has been fixed for each curve so that it passes through $\sigma = 1$ at $\varepsilon = 0.3$. If n is low, the work hardening rate is high in beginning, but the rate decreases rapidly with strain. On the other hand, with a high values of n, the initial work hardening is less rapid but continous to high strain. (Hosford, 2010)

To find out power-law parameters n and K, the linearization process is a must and should be performed as described in equations 2.7 and 2.8.

The logarithm of both side of Hollomon's equation (2.6) should be taken to have linear equation,

$$\ln(\sigma) = \ln(K.\varepsilon^n) \tag{2.7}$$

$$\ln(\sigma) = \ln(K) + n.\ln(\varepsilon) \tag{2.8}$$

$$y = ax + b \tag{2.9}$$

The components of linearized equation (2.8) will be a counterpart of a equation (2.9), so the each elements of equation has been explained as below,

$$\ln(\sigma) = y$$

$$\ln(K) = b$$

$$n = x$$

$$\ln(\varepsilon) = a$$

However, the log-log plot of the true stress-strain curve often deviates from linearity at low or high strains. For many cases, it is convenient yet to use equation (2.6) over the strain range of concern. The slope of a linear portion of the curve will be given as strain hardening exponent (n) shown in eq. (2.10)

$$n = d(\ln\sigma) / d(\ln\varepsilon) = (\varepsilon/\sigma).(d\sigma/d\varepsilon) \tag{2.10}$$

Finally, the representation of true stress-strain curve on logarithmic scale is given in Fig. 2.11.

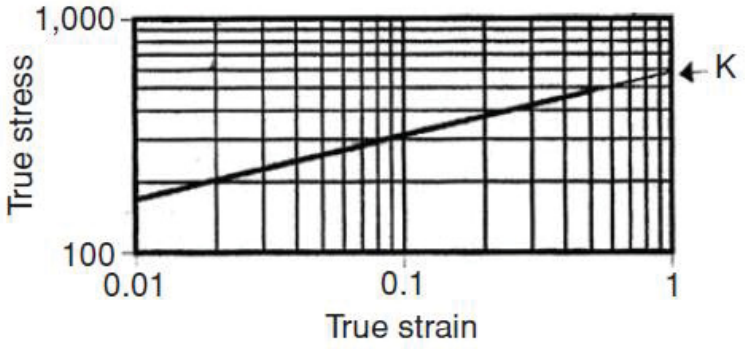

Figure 2.11. A plot of the true stress-strain curve on logarithmic scales
(Source: Hosford, 2010)

2.4. Fatigue

In strength of materials, the formation of stress on a material is affected by shape of the applied load. So that, the selection of dimensioning concept and safety coefficients are gaining importance. Fatigue is a process in which damage accumulation because of the cyclical applied loads that may be well below the yield point. The fatigue is dangerous due to a single application of the load would not produce any catastrophic effects, and classical stress analysis could lead to a assumption of safety that does not exist. The mechanical parts can be work under severel types of loading such as, constant loading, fully reversed loading, vibration induced loading, zero based loading etc. It is important that the stresses on a component consists thanks to applied loading type. The fatigue failure can be defined as the breakage of a material under the generally variable dynamic loading. The most of fatigue failures occur under the yielding strength of material except special cases. The fatigue is generally can be investigated by dividing into two categories as, high cycle and low cycle fatigue (Kaymaz, 2015, D.Roylance, 2001).

The fatigue failure is generally occurs in the following order,

- ✓ The micro crack formation in the material
- ✓ Elasto-plastic stress accumulation on the crack tip
- ✓ The propagation of crack at macro scale under elastic stresses.
- ✓ Fatigue fracture

2.4.1. Stress Cycles

There are three basic factors necessary to cause fatigue: a maximum tensile stress of sufficiently high value, enough fluctuation in applied stress and a sufficiently large number of cycles of the applied stress. With various type of fluctuating stresses, the most common types are shown in Figure 2.12, 2.13 and 2.14 respectively.

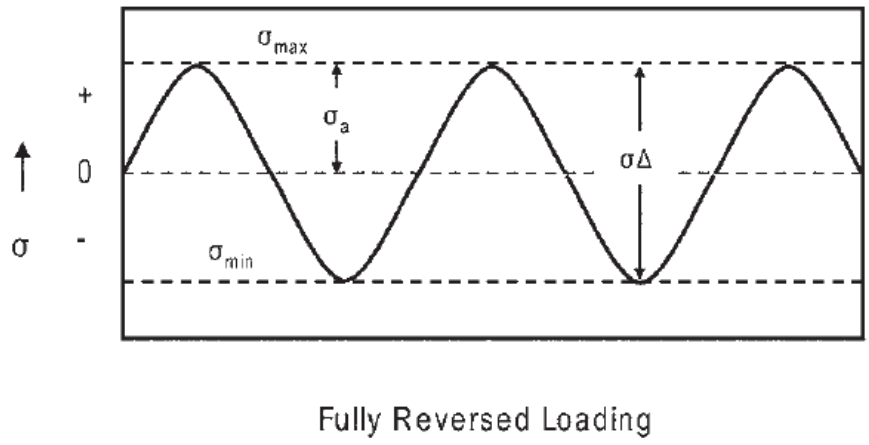

Figure 2.12. Fully reversed loading
(Source: ASM, 2008)

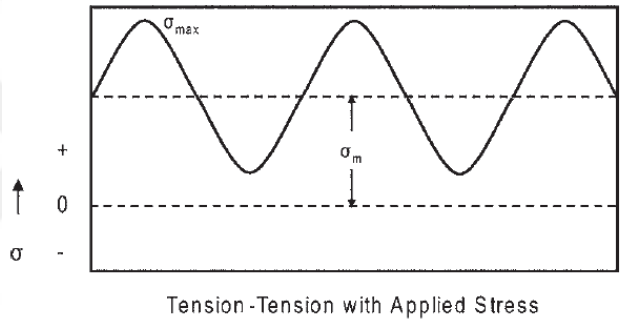

Figure 2.13. Tension – tension with applied stress
(Source: ASM, 2008)

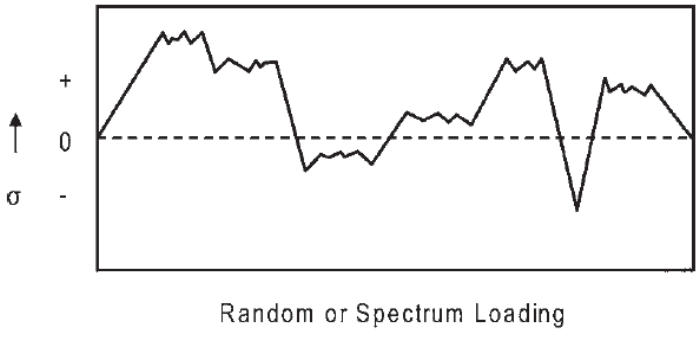

Figure 2.14. Random or spectrum loading
(Source: ASM, 2008)

The full reversed loading type shown in Fig. 2.12 is commonly used test technique and there are many studies which the experiments have been performed according to this

profile. The maximum and minimum stress amplitudes are equal in this type of loading. This type of stress can be produced by using rotating beam fatigue test machine shown in Fig. 2.15.

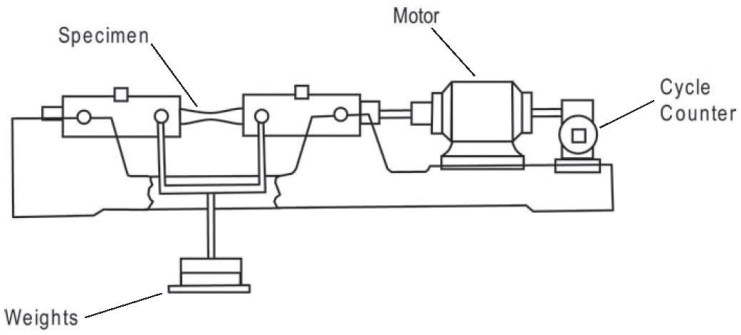

Figure 2.15. Schematic view of R.R.Moore reversed-bending test machine
(Source: ASM, 2008)

It should not be forgotten that there is very few produced fatigue data with no effect of mean stress by using R.R.Moore reversed-bending test machine. The second common type of stress cycle is repeated stress cycle with effect of mean stress on top of the maximum and minimum applied stresses. The Fig. 2.13 represents this type of loading and it can be whether in tension or compression mode. It is not necessary to have equally applied maximum and minimum stresses for this type of application. If the part is subjected to a random loads during service conditions shown in Fig. 2.14 so that, it is not possible to explain load profile with periodic (sinusoidal) curve. Even the big portion of fatigue data in the literature has been produced for fully reversed loading, there are also axial fatigue test machines which are able to do test in tension or compression mode shown in Fig. 2.16 (ASM, 2008).

Figure 2.16. Hydraulic – axial fatigue test machine
(Source: IYTE – ME, 2017)

2.4.2. Terminology of Fatigue

There are many terms to explain the apllied stress cycle such as, constant or variable amplitude loading, proportional or non-proportional loading, stress ratio, mean stress etc. Each of these terms will be explained with physical meanings and represented by own equation.

- ✓ Constant amplitude: The amplitude of applied stress cycle is not changed by time.
- ✓ Variable amplitude: The amplitude of applied stress can be changed randomly.
- ✓ Proportional loading: The ratio of principal stresses is constant
- ✓ Non-proportional loading: It means that, there is no implied relationship between the stress components

- The stress amplitude, σ_a is defined as,

$$\sigma_a = (\sigma_{max} - \sigma_{min}) / 2 \tag{2.11}$$

- The mean stress, σ_m is defined as,

$$\sigma_m = (\sigma_{max} + \sigma_{min}) / 2 \tag{2.12}$$

- The range of stresses $\Delta\sigma$ is defined as,

$$\Delta\sigma = (\sigma_{max} - \sigma_{min}) = 2\ \sigma_a \tag{2.13}$$

- The stress ratio R is defined as,

$$R = \sigma_{min} / \sigma_{max} \tag{2.14}$$

Finally the each component of stress cycle for constant amplitude and proportional loadind is demonstared in Fig.2.17,

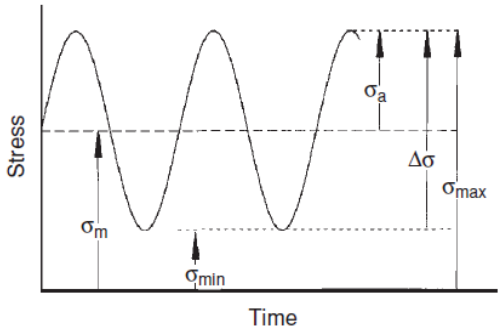

Figure 2.17. Demonstration of cyclic stress with several terms
(Source: Hosford, 2010)

2.4.3. High-Cycle Fatigue

If the number of cycles to failure bigger than N> 10^5 cycles and the stress is applied elastically the fatigue can be classified as high cycle. Even the stress is applied within the elastic limits, the crack initiation can take a place due to the plastic deformation. The fatigue data are usually represented by S-N curve in logarithmic scale. The relationship between stress amplitude and number of cycles to failure can be obtained with specified mean stress value, stress ratio or amplitude ratio. The amplitude ratio is given both in terms of ratio of stress amplitude - mean stress and stress ratio shown as in Eq. 2.15.

$$A = \sigma_a / \sigma_m = (1-R) / (1+R) \tag{2.15}$$

2.4.4. S – N Curves

The fatigue data are mostly presented in S-N curve form which are plots of the cyclic stress amplitude versus the number of cycles to failure. The S-N curve is conventionally plotted on the logarithmic scales. The fatigue tests are usually made for zero mean stress conditions to obtaion this type of curves. As a nature of experimentation, as the stress amplitude increases the number of cycles to failure will be decrease. The typical S-N curves for annealed 4340 steel and an aluminum alloy 7075-T6 shown in Fig. 2.18 respectively. (Hosford, 2010)

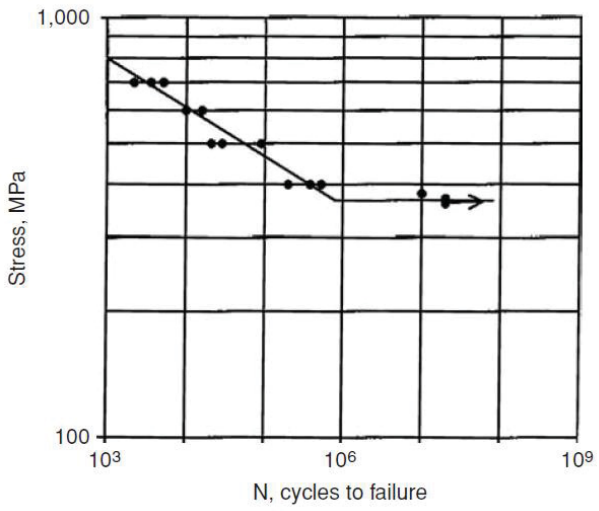

Figure 2.18. The S-N curve of annealed 4340 steel
(Source: Hosford, 2010)

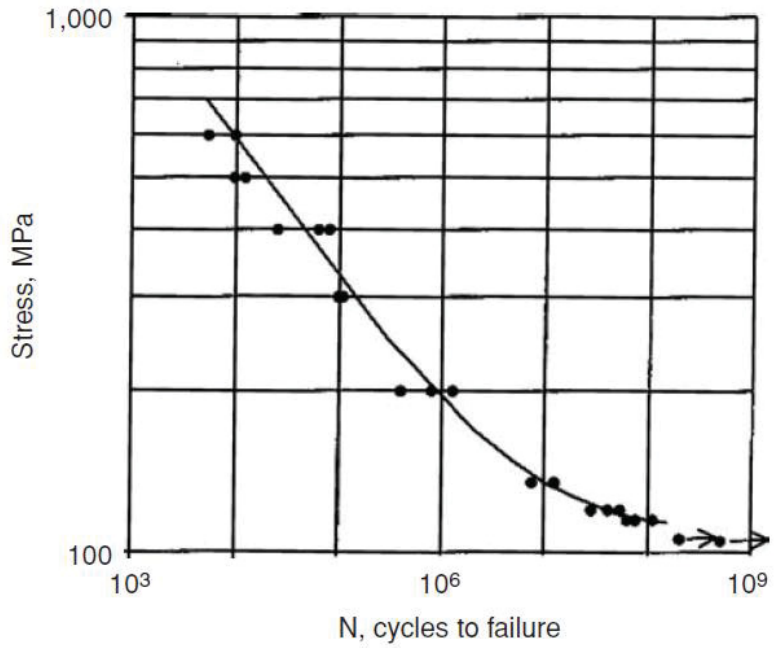

Figure 2.19. The S-N curve of an aluminum alloy 7076-T6
(Source: Hosford, 2010)

The main difference between S-N curves of 4340 steel and 7073-T6 aluminum alloy is observed cycles to failure which means the endrurance limit. The endurance limit of 4340 is determined as 10^6 cycle but, there is no true endurance - breakage (fatigue) limit for aluminum alloy. (Hosford, 2010)

The most commonly used model for the representation of stress life based fatigue curve is Basquin's relation and it provides an analytical expression of the S-N curve, for finite life approach especially in high cycle fatigue. (Q.Bader et al, 2014)

The simple Basquin's curve is represented as;

$$\sigma_a = a.N_f{}^b \tag{2.16}$$

where the parameters of equation,

σ_a: Stress amplitude of fatigue (MPa)

N_f: Number of cycles to failure

The parameters a and b are both costant and they are depend on the geometry and material.
a, is approximately equal to tensile strength of material

b, is the fatigue strength exponent.

The linearization process is neded to find out these coefficients and parameters and Power-law can be used as a linearization procedure in logarithmic form.

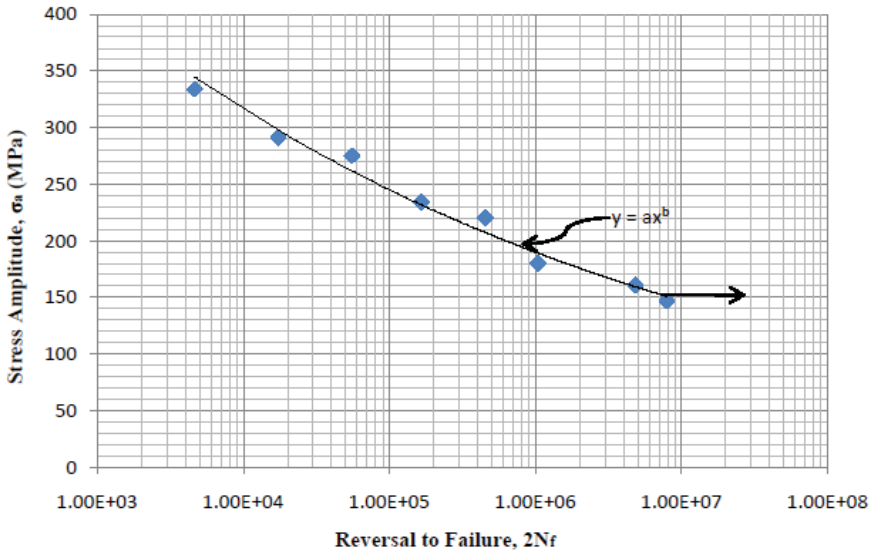

Figure 2.20. Typical S-N curve of 316L SS steel with fitted Basquin's equiation (Source: K.A.Mohammad et al, 2012)

The S-N curve of austenitic type 316L stainless steel is represented in Fig. 2.20. Finally, the most important point that the experimental points of S-N curve must be a statistically confident to have undiverged and more robust results. The robustness of a curve is usually measure by R^2 value of obtained equation. The number of experimental repititations can be changed according to type of application.

2.4.5. Low Cycle Fatigue

The relationship of stress and strain can directly be explained over the modulus of elasticity during cyclic loading. But, if there is a plastic strain formation under applied cyclic stress the structural response will be a more complex than elastic regime. In this case, it is must to use hysteresis loop of stress vs strain. The loop can be obtained by loading and unloading of material as represented in Fig. 2.21. The hysteresis loop path is given in below order respectively,

- ✓ O-A: The compoment is under tension
- ✓ A-D: The strain response during unloading, no stress at a point D
- ✓ D-B: The componenst is subjected to a compressive stress
- ✓ B-A: Releasing compressive stress and reapplying tension, no stress at a point C

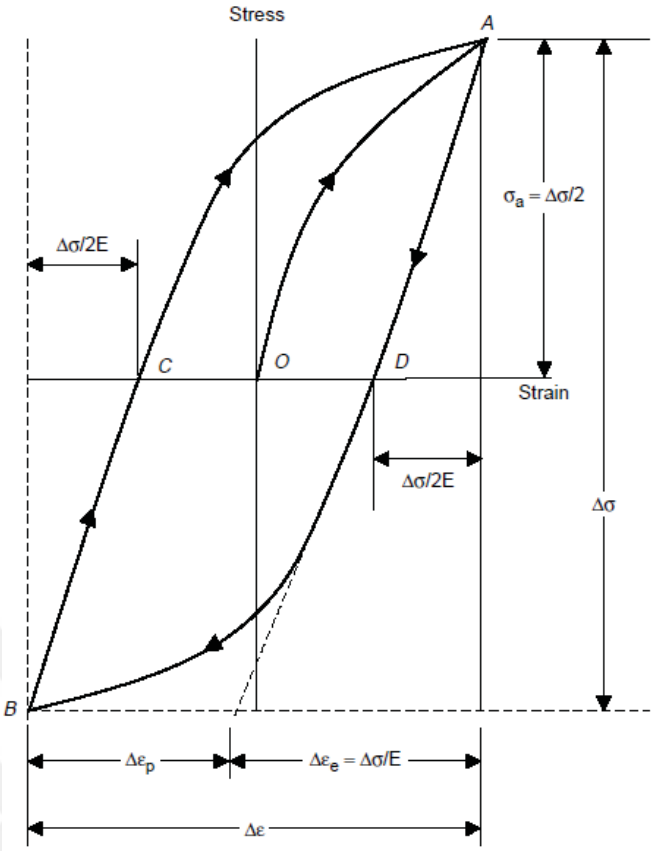

Figure 2.21. Stress-strain hysteresis loop for cyclic loading
(Source: ASM,2008)

The accumulated total strain on the material can be found by Eq. (2.17),

$$\Delta\varepsilon = \Delta\varepsilon_p + \Delta\varepsilon_e \tag{2.17}$$

The Eq.2.17 come out of elastic and plastic strain, so the expansion of each strain component,

$$\Delta\varepsilon = \Delta\sigma / E \tag{2.18}$$

$\Delta\varepsilon_p$: Distance between *C* and *D* in Fig. 2.21 (plastic strain range)

The strain amplitude must be held constant during cyclic strain-controlled fatigue tests. It is important that the plastic deformation is not fully reversible process, so that the material response can be changed during cyclic loading. The change of the material behaviour is strongly depends on the initial conditions of the metallic material. The metal can either expose to the cyclic strain hardening or cyclic strain softening. Besides that, it can remain stable during cyclic loading. The increase of peak strain by increasing cycles can be defined as *cyclic hardening* while the *cyclic softening* is defined as the decreasing of strain levels by increasing cycles. (ASM, 2008)

Generally, the high strength metals have a tendency of cyclically soften and the low strength metals have a tendency of cyclically harden. As a typical rule, the ratio of ultimate tensile strength to yield strength shown in Eqs. 2.19 and 2.20 are given both for cylically harden and soften materials respectively (ASM, 2008).

$$\sigma_u / \sigma_y \geq 1{,}4 \tag{2.19}$$

$$\sigma_u / \sigma_y \leq 1{,}2 \tag{2.20}$$

σ_y: yield strength of material

σ_u: ultimate tensile strength of material

The reason behind the cyclic hardening or softening can be explained with the effect of dislocations in microstructure of metallic material. If the material is largely strain hardened in initial conditions which means the dislocation density is high, the dislocations will be activated to rearrange by cyclic strain thus the stress had been reduced at which plastic deformation occurs. In contrast, when the initial dislocation density is low, the elastic strain and stress formation will be increased by the cyclic strain increases. (ASM, 2008)

2.4.6. $\Delta\varepsilon_p$ – N Curves

The representation of low-cycle fatige test data are often given as a logarithmic plot of the plastic strain range ($\Delta\varepsilon_p$) versus cycles to failure (N). The curve which is shown in Fig. 2.22 is defined by Coffin-Manson equation shown in Eq. 2.21.

$$\Delta\varepsilon_p / 2 = \varepsilon_f' (2N)^c \tag{2.21}$$

where the parameters of equation,

- $\Delta\varepsilon_p / 2$: plastic strain amplitude
- ε_f': the fatigue ductility coefficient
- 2N: number of strain reversals to failure
- c: fatige ductility exponent

It is important that to give some remarks about the strain-life equation parameters,

- ✓ One strain cycle is equal to two reversals
- ✓ The fatigue ductility coefficient must be calculated by strain intercept at 2N=1
- ✓ The fatigue ductility coefficient is given as approximately equal to the true fracture strain for several metallic materials
- ✓ The fatigue ductility exponent usually is alternates between -0,5 and -0,7.
- ✓ Finally, a smaller values of the exponent tends to longer fatigue life-time.

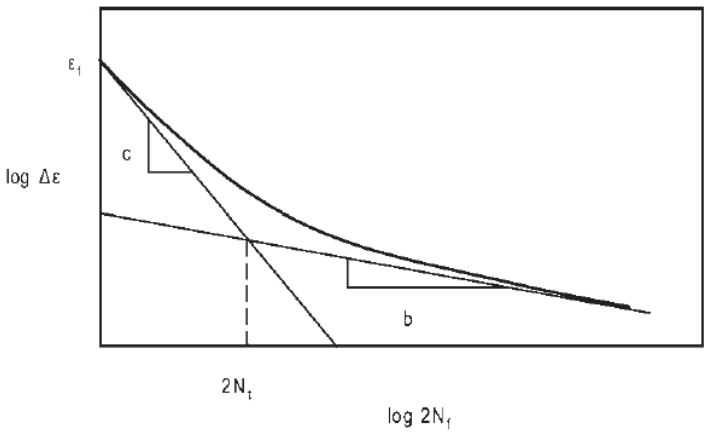

Figure 2.22. Fatigue life in terms of total strain
(Source: ASM, 2008)

2.4.7. The Effect of Mean Stress and Mean Stress Theories

The most of experimental fatigue data have been determined for the fully reversed loading conditions $\sigma_m = 0$, in the past. But, the many service condtions are often include non-zero mean stress loading. There are several ways to predict effect of mean stress on the S-N curve. The most common techniques are presented as maximum stress versus cycles to failure and alternating stress versus cycles to failure shown in Fig. 2.23 and Fig. 2.24 respectively.

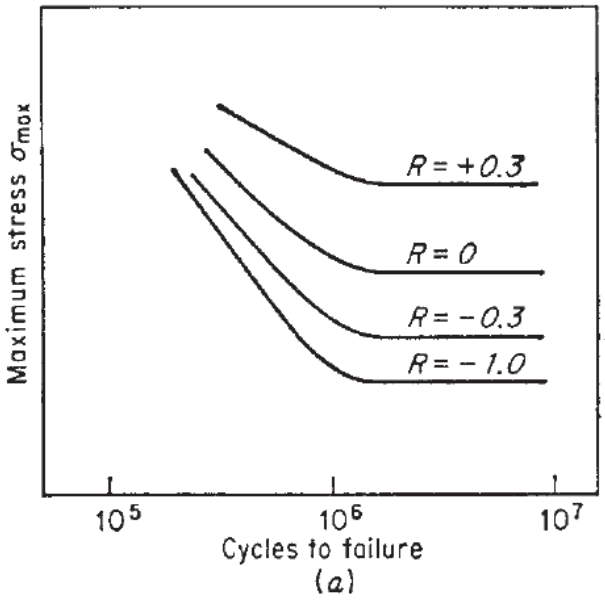

Figure 2.23. Stress ratio method of plotting fatigue data when the mean stress is not zero
(Source: George E. Dieter, 1988)

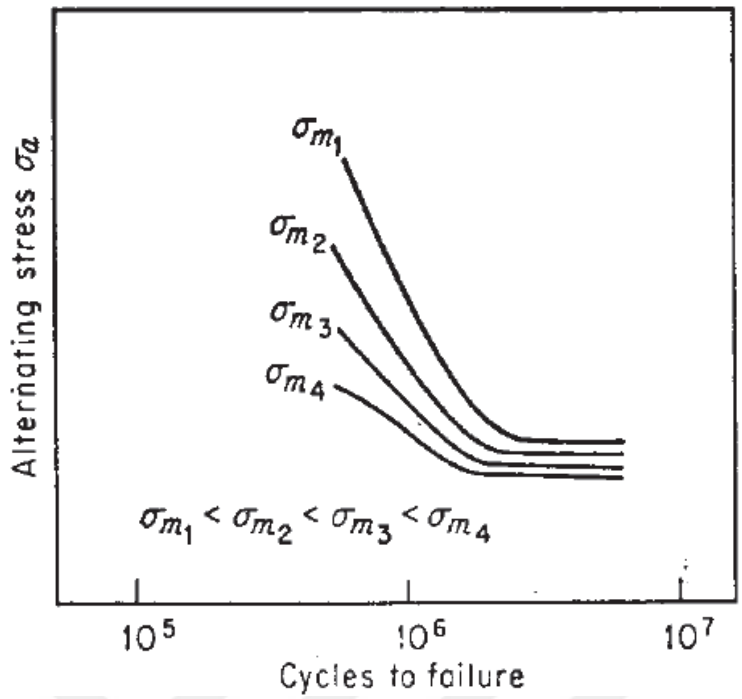

Figure 2.24. Mean stress method of plotting fatigue data
(Source: George E. Dieter)

The Fig. 2.23 is composed by S-N curves with different stress ratios. The experiments performed that applying the series of stress cycles by decreasing maximum stress while the minimum stress kept as constant. However, the same data is represented in terms of the alternating stress versus cycles to failure at constant value of mean stress in each S-N curve. Finally, it is possible to plot these data by taking constant mean stress for Fig. 2.23 and by taking constant minmum stress for Fig. 2.24. (George E. Dieter, 1988)

The influence of mean stress has been investigated by several theories. Within the context of this thesis, the brief explanations and fundamental equations will be given only for Goodman, Soderberg and Gerber. The theories can be defined with mathematical expressions shown in Eq. 2.22, 2.23 and 2.24 respectively.

$$(\sigma_a / \sigma_e) + (\sigma_m / \sigma_u) = 1 \quad (2.22)$$

$$(\sigma_a / \sigma_e) + (\sigma_m / \sigma_y) = 1 \quad (2.23)$$

$$(\sigma_a / \sigma_e) + (\sigma_m / \sigma_u)^2 = 1 \quad (2.24)$$

where the parameters of mean stress equations are, σ_a: alternating stress, σ_m: mean stress, σ_y: tensile yield strength, σ_e: endurance fatigue limit, σ_u: ultimate tensile strength.
The graphical illustration of each theory is given in Fig. 2.25 for the better understanding of mean stress effect on the S-N curve.

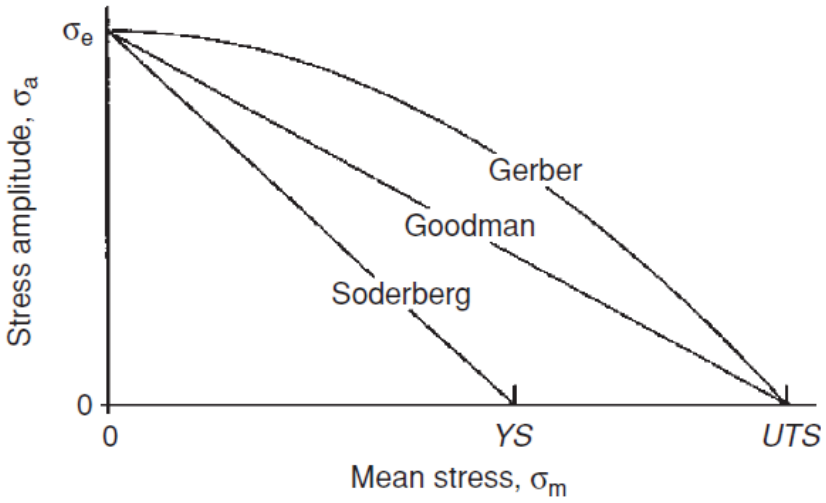

Figure 2.25. The graphical illustration of mean stress theories
(Source: Hosford, 2008)

Soderberg is proposed more conservative expression than Gooodman by taking the yield strength of material is a reference. Goodman and Soderberg is proposed a linear relationship while the Gerber is offered to use second order parabola. The selection of mean stress theory strongly depends on the design criterion. Even the more conservative than others, the Soderberg is often used that if the design based on yield strength. The Goodman is suitable for brittle materials but there is no correction for the compressive mean stresses. The usage of Gerber parabolic curve is more proper than the others for ductile materials especiallt in tensile mean stresses. (ANSYS Inc. , 2015)

The modified Goodman diagram shows the effect of mean stress on failure which is caused by fatigue and yielding shown in Fig. 2.26.

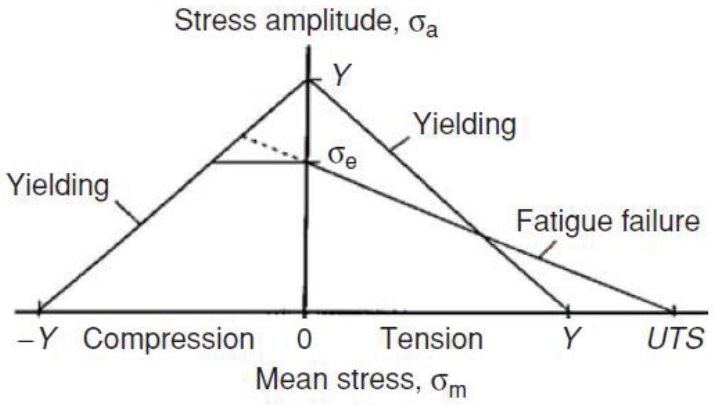

Figure 2.26. The modified Goodman diagram
(Source: Hosford, 2008)

Besides the effects of mean stress, there are other important factors which can effect the S-N curve of material such as notch, temperature, grain size and direction, surface treatments, environments, specimen – component size diffrence etc. All these factors can be represented by *fatigue strength factor* K_f. This approach is sutiable especially for numerical analysis but, it is frequently used in hand calculations by multiplying all effective factors to have a single value. The value of K_f must be smaller than 1. (Source: ANSYS Inc. , 2015)

2.5. Yielding Criterion in Multiaxial State of Stress

Although, the mechanical properties of materials are determined by the tensile test, in real life, the parts are working under multi-axial loading. Thus, the material which will work under the multi-axial state of stress that is necessary to decide limit criteria for the starting of permanent (plastic) deformatin. It so called as *failure criteria*. As in this study, there is a necessity for a failure criteria in order to be able to guide proposed design solutions. (Irizalp, 2015)

The most general form of yield (failure) criteria can be given as a functions of multi-axial state of stress shown as,

$$f(\sigma_x,\sigma_y,\sigma_z,\tau_{xy},\tau_{yz},\tau_{zx}) = C \tag{2.25}$$

where C is a constant value specific to material, and this relation can be given in terms of principal stresses for isotropic materials shown as,

$$f(\sigma_1,\sigma_2,\sigma_3) = C \tag{2.26}$$

It is important that the yielding (failure) criteria for most of solid material independent from sign of stress which means. So that, the yielding strength of most metallic materials equal in tension or compression. (Hosford, 2008)

With in this context, there will be only discussed Rankine, Tresca and Von-Mises failure criterion. The Rankine's and Von-Mises theories has been used during the evaluation of numerical results of the investigated problem in this study. The fatigue safety factor calculations have been done according the these failure criterion.

2.5.1. Rankine's Failure Theory (Maximum Principal Stress Theory)

This theory, which is also called as *maximum principal (normal) stress* theory has been developed by W.J.M. Rankine in 1800's. The approach of theory is said that the failure will occur when the biggest tensile stress exceeds the uniaxial tensile strength.

Firstly, the principal stresses σ_1, σ_2, and σ_3 must be calculated for given state of stress, hereby, the yield function will be obtained as,

$$f = \max(|\sigma_1|, |\sigma_2|, |\sigma_3|) - Y \tag{2.27}$$

The yielding (failure) conditions have been given according the sign of defined function in Eq. 2.27,

If, $f < 0$, there will be no yielding

If, $f = 0$, there will initiate the yielding

If, $f > 0$, the condition is not defined with in the scope of theory.

The Mohr's circle and graphical representation of maximum principal theory is given in Fig. 2.27.

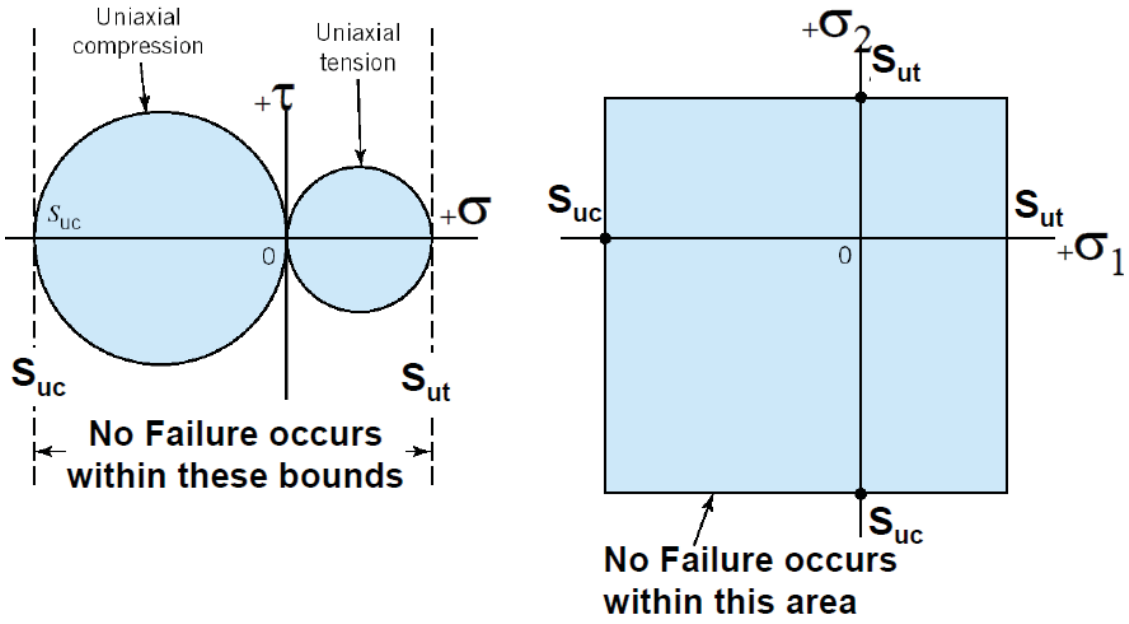

Figure 2.27. Mohr's circle and graphical representation of Rankine's yield function (Source: Thompson & Müller, 2005)

2.5.2. Tresca Criteria (Maximum Shear Stress Theory)

The theory has ben developed by French Mechanical Engineer Tresca in 1860's. The main claim of theory is that if the plastic deformation is caused by shear stresses, a critical shear stress value is also required for plastic deformation in case of multi-axial state of stress. The tensile stress is considered for this critical shear stress value. The maximum shear stress has been expressed as a yield function of maximum principal stresses shown in Eq. (2.28).

$$f = \max \{ |(\sigma_1 - \sigma_2)/2|, |(\sigma_2 - \sigma_3)/2|, |(\sigma_3 - \sigma_1)/2| \} - K_T \; (= Y/2) \qquad (2.28)$$

The failure will occur when maximum shear stress exceeds shear strength in uniaxial tension. K_T represents the maximum shear strength of material.

If the $f < 0$, there will be no yielding.

If the $f = 0$, there will initiate the yielding.

S_y has been defined as yield strength of material in uni-axial tensile testing and the Mohr's circle and graphical representation of Tresca failure criteria has been illustrated as shown in Fig. 2.28.

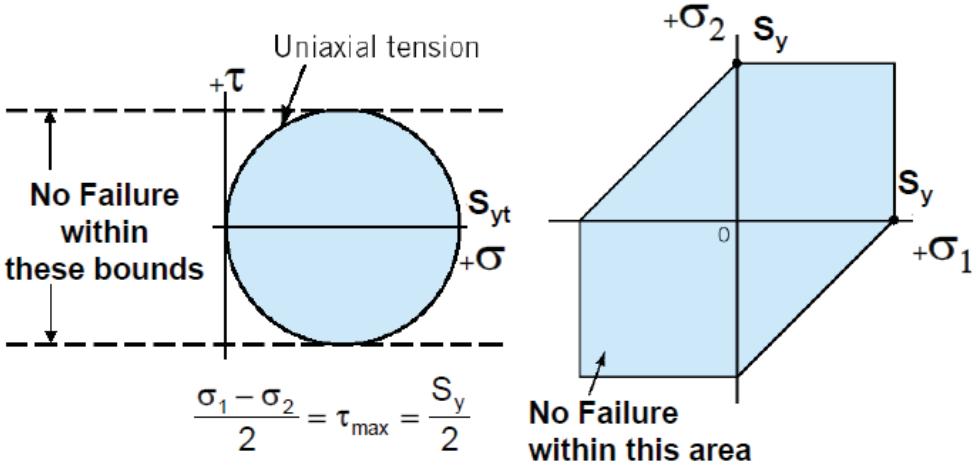

Figure 2.28. Mohr's circle and praphical representation of Tresca yield function (Source: Thompson & Müller, 2005)

It can be easily seen from graphical representations shown in Fig. 2.27 and 2.28 that the Tresca ceriteria is more conservative than Rankine's maximum principal stress theory.

Because, the Tresca is taking into account the yield strength of material while the Rankine's theory is considering tensile strength as a base value.

2.5.3. Von Mises Distortion Energy Yielding Criteria

The theory has been proposed by Austrian scientist Richard Von Mises, 50 years after the Tresca. It is more complicated and sophisticated than Tresca. The theory is based on the stress tensors unlike the other theories Tresca and Rankine. The stress tensor is composed of hydrostatic aand deviatoric components. The hydrostatic component of tensor represents only normal stresses and so that, it would not cause any plastic deformation on the material. Whereas, the deviatoric component of tensor in that comprises a shear stress components, it will lead to a plastic deformation. The Von Mises theory said that the yielding will occur after the second invariant of the stress deviator J_2 exceeds a limit critical value. The second stress J_2 has been expressed as,

$$J_2 = 1/6\ [(\sigma_1 - \sigma_2)^2 + (\sigma_2 - \sigma_3)^2 + (\sigma_3 - \sigma_1)^2] \tag{2.29}$$

The critical limit value for second invariant of the stress deviator has been described to be constant values shown as,

$$J_2 = k^2 \tag{2.30}$$

The evaluation of constant k value and link it with yielding in tension test, it is necessary to take the principal stress components as $\sigma_1 = \sigma_0$, $\sigma_2 = \sigma_3 = \sigma_0$ for the realization of yielding in uniaxial tensile test.

Then, the σ_0 can be written in terms of k shown in Eq. (2.31),

$$\sigma_0 = \sqrt{3}\ k \tag{2.31}$$

Thus, by substitution of Eq. 2.31 into Eq. 2.29, the expression will take a form as in Eq. (2.32), and also it can be expressed in terms of normal and shear stresses as in Eq. (2.33) respectively.

$$\sigma_0 = (1/\sqrt{2})\ .\ [(\sigma_1 - \sigma_2)^2 + (\sigma_2 - \sigma_3)^2 + (\sigma_3 - \sigma_1)^2]^{1/2} \tag{2.32}$$

$$\sigma_0 = (1/\sqrt{2})\ .\ [(\sigma_x - \sigma_y)^2 + (\sigma_y - \sigma_z)^2 + (\sigma_z - \sigma_x)^2 + 6.(\tau_{xy} + \tau_{yz} + \tau_{xz})]^{1/2} \tag{2.33}$$

To sum up the Von Mises theory, the yeilding will occur when the the differences of principal or axial stresses which are right side components of Eq. 2.32 and 2.33, exceeds the yield stress in uni-axial tension σ_0.

(George E.Dieter, 1988)

The graphical representation of Von Mises theory is given in Fig. 2.29. It is clear that the results of Von Mises criteria are more refine than Tresca. The reason of refinement that the Tresca is taking into account only 1st and 2nd principal stresses while the Von Mises obtain the all principal stresses.

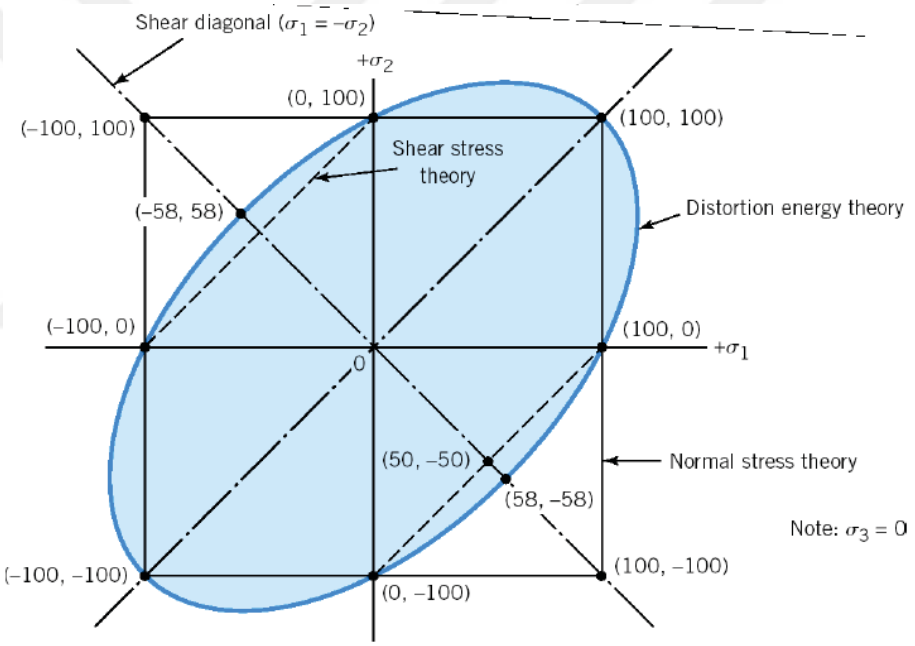

Figure 2.29. Graphical representation of Von Mises theory and differences with others (Source: Thompson & Müller, 2005)

2.6. Vacuum Brazing

Brazing is one of the oldest method to connect materials. It is applied for more than 5000 years. In 1900's changing from experimental to industrial brazing has been realized. Brazing is defined as a joining process that is carried out at a temperature above 450 ˚C, but below the melting point of the materials being joined. The filler metal, heat

input and protective cover (environment) can be said as a core elements of brazing process. The fundamental required works to have good brazing are classified and explained as,

- ✓ *Reduction* of the oxides from the parent metals
- ✓ *Wetting* of the braze metals on the parent metals (contact angle)
- ✓ *Spreading*, flowing of the liquid braze filler metal over the surface of the parent metal
- ✓ *Capillary action*, driving force, viscosity and density of the molten metal and geometry of the braze gap
- ✓ *Alloying,* interaction between filler metal and parent metal
- ✓ *Vapor pressure* of all elements
- ✓ *Thermal expansion* of different materials
- ✓ *Process coefficient* = Solidus parent metal / braze temperature in ˚K.

To have good interaction and alloying between the base metal and filler metal, it is necessary that the contact angle angle β should be as small as possible. If the contact angle β is smaller than 30 ˚, there will be a good wetting shown in Fig. 2.30.

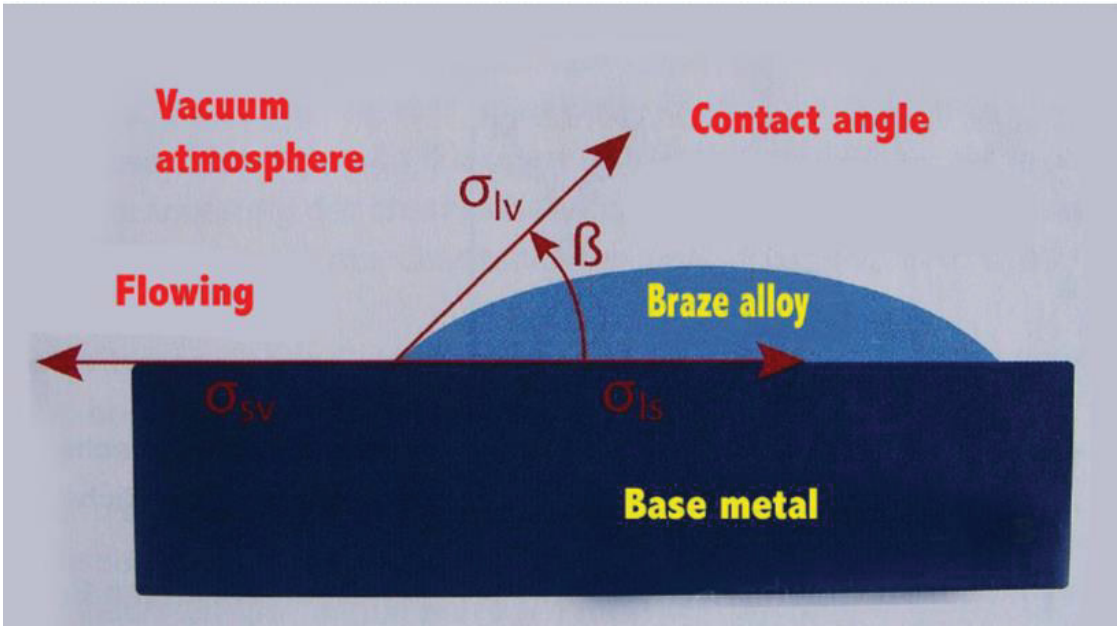

Figure 2.30. Schematic representation of contact angle
(Source: Peter Steege, 2015)

The excellent vacuum brazing examples are shown in Fig. 2.31,

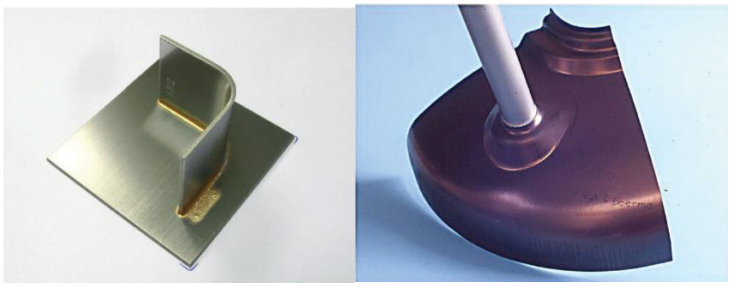

Figure 2.31. The brazing of steel to copper and steel to steel

(Source: Peter Steege, 2015)

The five elements of brazing process are defined by AWS Brazing Handbook as,

I. Design
II. Base materials
III. Filler metals
IV. Source of heat
V. Protective cover

Each of elements of brazing process has a crucial importance on the brazement of materials. The thickness of base and filler materials, geometry and clearance of the brazing gap, position of the filler material, design of fixture are most important parameters of design. The several types of brazement design are illustrated in Fig. 2.32 such as, flunched T, flush lap and crimped etc.

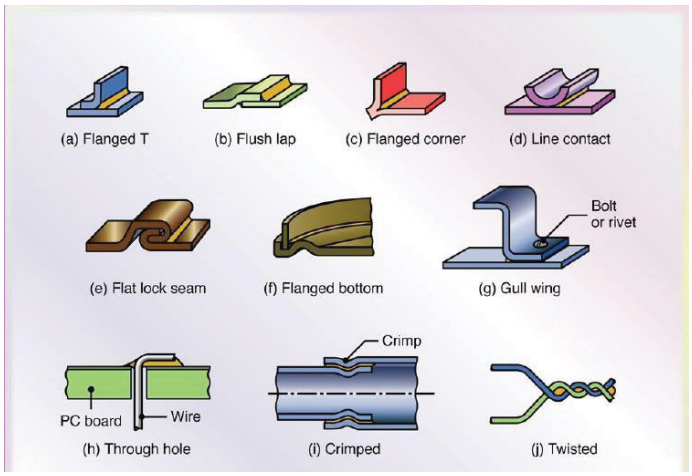

Figure 2.32. Various types of brazement design
(Source: Peter Steege, 2015)

The chemical, metallurgical, physical and mechanical characteristics of base material is directly effect the final propeties of brazed interface. The most of stainless steels are commonly used base materials in industrial applications especially in energy industry. The 316L, 304 and 430 stainless steels are good examples due to the high corrosion resistance and thermal conductivity. The silver, copper, nickel, gold, palladium, iron, cobalt and titanium are popular filler materials among the others. The process coefficient was defined as a ratio of the brazing temperature to solidus temperature of base material in ˚K. However, the value of process coefficient must be smaller than 0,9 to have brazement. The calculation of that coefficient is given for 316 L stainless steel shown as below.

The solidus tempeature of AISI 316L: 1640 ˚K

The vacuum brazing temperature: 1400˚ K

Process coefficients (PC) = 1400 / 1640 = 0,85 < 0.9

The vacuum furnaces are commonly used to as a heat source in industrial brazing processes. Because, the vacuum atmosphere are used during brazing to prevent the formation of oxides on the surface of the base metal to permit the brazing filler metal to wet and flow on clean base metal. The commerical vacuum furnace has been shown in Fig. 2.33.

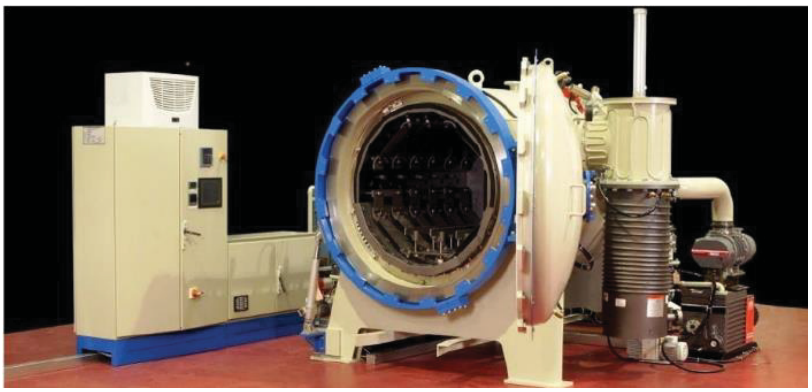

Figure 2.33. The commerical vacuum brazing furnace
(Source: Peter Steege, 2015)

To prevent vaporize of elements in base or filler metal protective gas environments is used. It is so called as partial-pressure gas atmosphere. Nytrogen, Argon and Hydrogen are most common types of protective gases. The term vapour pressure denotes the

pressure exerted at a given temperature at which the material is in equilibrium with its own vapour. If the vacuum or temperature is increased the material will vaporize and the vapours will condense on the colder parts of the hot zone. The vacuum brazing has been preferred as a production method of plate heat exchangers (PHE) in recent years due to it has provided the structural requirements of PHE's shown in Fig. 2.34. The burst pressure and thermal fatigue test behaviour of chevron type brazed PHE are given for three different types of filler metals shown in Fig. 2.35 and 2.36 respectively.

Figure 2.34. Chevron type brazed plate heat exchanger
(Source: Peter Steege, 2015)

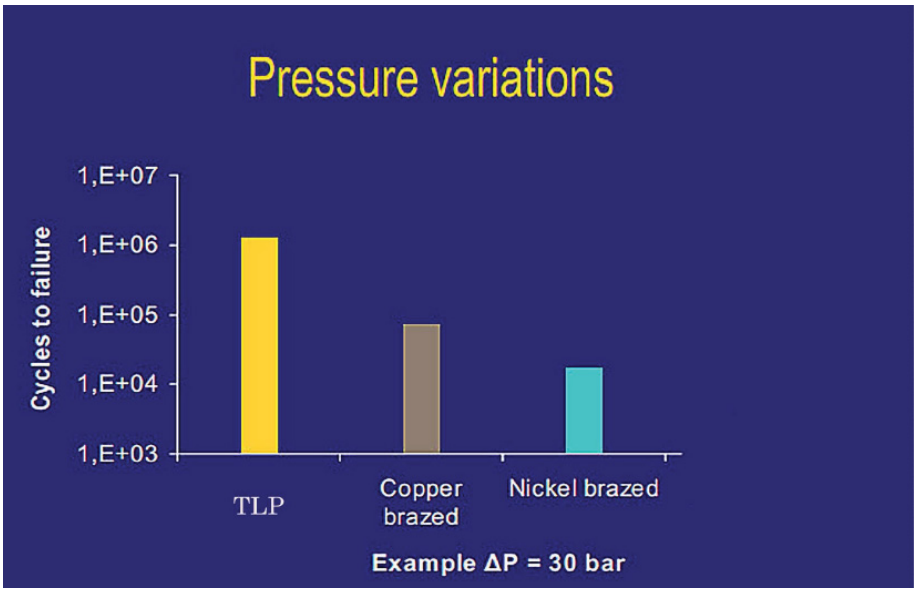

Figure 2.35. Burst pressure fatigue test behaviour of PHE
(Source: Peter Steege, 2015)

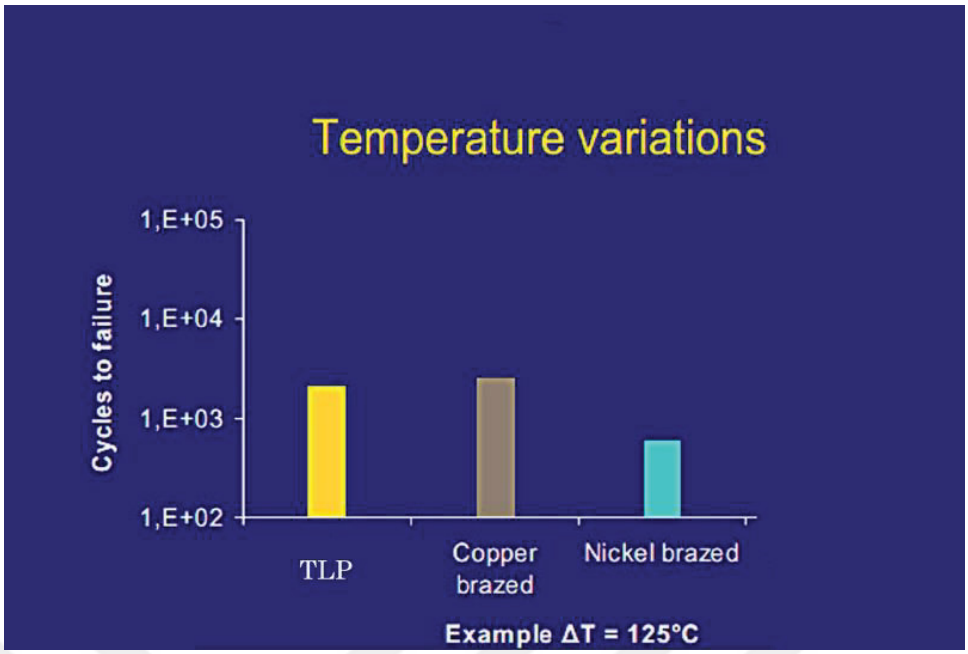

Figure 2.36. Thermal fatigue test bhevaiour of PHE
(Source: Peter Steege, 2015)

As can be seen from Fig. 2.35 and 2.36 the titanium based filler material and copper based filler material are superior properties in terms of burst pressure and thermal fatigue behaviour.

2.7. Finite Element Analysis (FEA)

Finite element analysis is a method which has been developed for solving engineering problems that can not be solved by analytical techniques. For example, the mechanics of materials and theory of elasticity is can be used to obtain stress and strain distributions of curved beam problem, but the analytical method neither will be very useful and powerful for complex geometries such as car suspension sytem, airplane wings etc. The method is firslty used to calculate the stresses and strains of engineering components under loading. The physical behaviour of any component that is mechanically designed can be predicted by finite element method before the starting of fabrication. It is the fact that the product whose structural behaviour is determined by the finite element analysis among the important point is validation of numerical solution by experimental techniques. This is to ensure the workability of the finished product, as well as for cost effectiveness in the manufacturing process. The development of the finite element method (FEM) has gained acceleration along with the technological

improvements in computers. The method is currently applicable for wide range of physical pheonomena and engineering problems including structural mechanics, mechanical vibrations, heat transfer, fluid mechanics and electrostatics. (The University of Manchester, 2010)

The FEM is basically cuts a structure into several elements to compute the requested outputs such as displacement, strain or stress, then the piecewise elements are reconnected at 'nodes'. It is so called as *discretization technique (meshing).* The elements can be a several shapes in one, two or three dimensions as can be shown in Fig. 2.37.

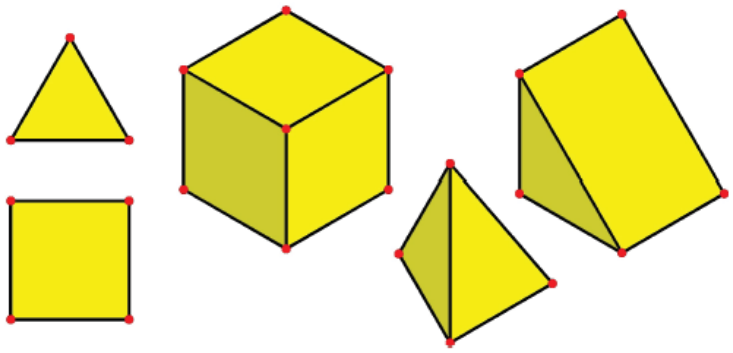

Figure 2.37. Commonly available several types of finite elements
(Source: The University of Manchester, 2010)

The degrees of freedom, which are the independent movements possible, are represented by nodes. The behaviour of each node has been defined with equilibrium equations and the mathematical description of it has been expressed in forms algebraic equations in matrix notation. The solution procedure of finite element method is that the formulation of each equation and then combine them to achieve whole domain. The results of finite element problem are given with calculation of the displacements at each node and the forming of stresses within the each element.

2.7.1. General Steps of Finite Element Method

The behaviour of physical phenomenon depends on the complexity of geometry, defined initial and boundary conditions and the material properties of geometry. In engineering systems, when the geometry, boundary conditions and material properties are very complex, the analytical solution of corresponding differential equation which represents the problem is very difficult. Thus, the mathematical descriptions of many

engineering problems in practice are solved by the finite element method. The solution of a continuum problem by the finite element method always follows an orderly step by step process. The numerical solution procedure of engineering problem are stated as follows;

i. Discretization

The first step of finite element analysis is comprised the definition of suitable element type by dividing solution domain into finite elements. As soon as the type of elements vary with used software in analysis, the convergence and sensitivity of solution is directly effected by the type of elements. The one dimensional (1D), two dimensional (2D) and three dimensional elements (3D) can be used in finite element analysis as can be seen in Fig. 2.38.

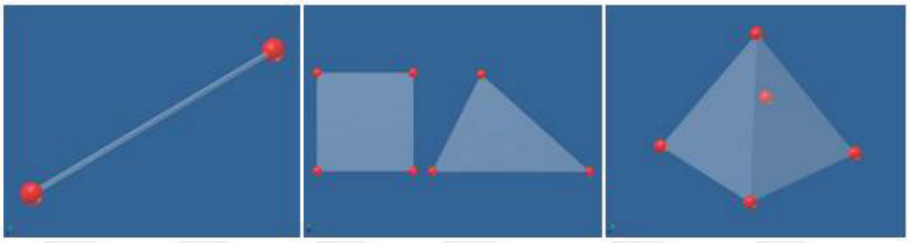

Figure 2.38. Representation of 1D, 2D and 3D element types
(Source: fea-cae-engineering.com, 2018)

ii. Definition of interpolation functions: The polynomial functions are most preferred types as an interpolation functions. The degree of polynomial function is relied on the number of nodes in the single element.

iii. Identifying of element properties: The variational approach and Galerkin's method are most convenient algorithms for the installation of governing matrix equation.

iv. Assembly of the element equations: The fourth step of procedure involves the combining of discretized elements for global solution. It is important that the boundary conditions and material properties should be defined before solution.

v. Post-processing: the last step of procedure is processing of obtained data from numerically solved engineering problem to display the output of analysis in terms of known metrics such as, principal stresses, strains etc.

2.7.2.Finite Element Analysis by Using ANSYS

The ANSYS is the widely used finite element analysis softaware used to determine physical behaviour of engineering system. The first from of ANSYS numerical solution concept has been come up in early 1976. The development process of ANSYS concept has been started with generation of solutions for one and two dimensional problems. Nowadays, ANSYS is used to for many types of engineering problems having very complex geometry and boundary conditions such as fatigue analysis, cooling analysis of nuclear poer plants, biomedical applications etc.

With in the scope of this thesis, the Workbench module of ANSYS software has been used to predict the structural behaviour of chevron type brazed plate heat exchanger under its operating conditions and results have been evaluated in terms of static structural analysis. Additionaly, the fatigue assesment of numerically studied geometry has been done based on static structural results of software. The modelling procedure and details of ANSYS has been listed as below;

1. For a linear structural analysis, the global displacement vector is solved in the form of matrix equation shown as in Eq. (2.34).

$$[K] \cdot \{x\} = \{F\} \tag{2.34}$$

2. Significant classes of structures do not have a linear relationship between force and displacement as shown in Fig. 2.39. Because a plot of F versus u (x) for such structures is not a straight line, such structures said to be nonlinear.

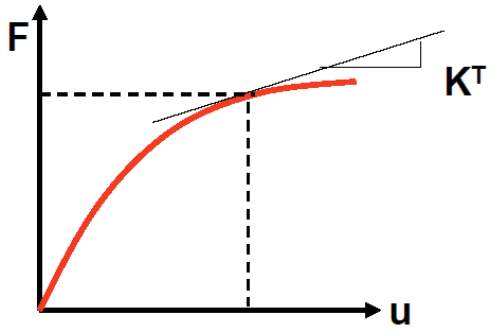

Figure 2.39. Force vs displacement
(Source: ANSYS Inc., 2016)

A structure is nonlinear if the loading causes significant changes in stiffness. Typical reasons for stiffness change are; strains beyond the elastic limit

(plasticity), large deflections on the geometry and changing status between two bodies (contact). There are three main sources of nonlinearities: geometrical, material and contact. In a nonlinear analysis, the structural response can not be predicted directly with a set of linear eqautions. However, a nonlinear structure can be analyzed using an iterative series of linear approximations, with corrections. The Mechanical module of ANSYS Workbench is used an iterative process called the *Newton Raphson* method.

3. In our modelling approach in this thesis, there are two main sources of nonlinearity, geometry based large deflection and modelling of plasticity. Large deflection has been activated due to the high pressure loading and the material has been modelled with *multilinear kinematic hardening model* which represented the plastic deformation behaviour of system.

4. Thereafter, the fatigue analysis has been performed by results of static structural simulation. It should not forgotten that although, the fatigue is related to repetitive loading, the results are based on static analysis and linear material model. The stress based fatigue approach in ANSYS is not considered the effect of plastic behaviour of material.

CHAPTER 3

EXPERIMENTAL STUDY

In this chapter, it is aimed to give information about sample preperation techniques, material testing, processing of experimental data and results of performed tests. Modelling of mechanical behaviour of material for understanding of its response under defined loading conditions is crucially important. According to this manner, in this study within the scope of thesis the mechanical behaviour and structural response of materials and brazing interfaces are investigated by experimental methods. Tensile and stress based fatigue tests are performed respectively to find out mechanical properties of brazing interfaces. Additionaly, the tensile test results of 316L stainless steel sheets which previously prepared by Atılım University are given.

3.1. Sample Preperation

There are many studies in the literature which the proper sample dimensions are presented (W.Jiang et al, 2009, W.Jiang et al, 2011, R.Hormozi et al, 2015, M.Laurent et al, 2016). Moreover, there are several standarts for producing of sample, the dimensioning of test samples may be changed according to proposed work. The dimensions of brazed tensile and fatigue specimens are taken from Jiang's study (W.Jiang et al, 2011 - ASTM E8 / E8M – 16a) are presented in Figure 3.1 and the bulk stainless steel parts and copper foil has been joined for that purpose shown in Fig. 3.3. The reason behind the selection of Jiang's sample is that the smallest area of sample and the brazing cross-sectional area of numerically studied plates are nearly the same.

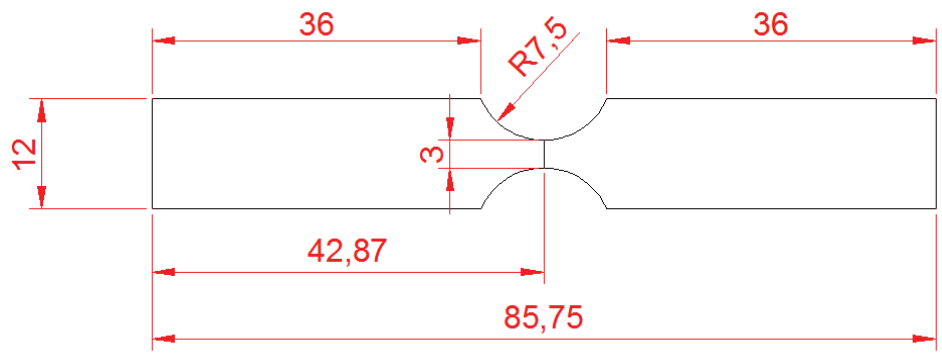

Figure 3.1. Tensile and fatigue test sample dimensions (mm)

3.1.1. Brazed Slab Production by Vacuum Brazing Technique

The manufacturing of tensile and fatigue test specimens without any effect of temperature and other environmental factors are extremely important in order to obtain more realistic and undiverged data from experiments. According to this manner two stainless steel slabs have been purchased from raw material supplier APERAM. The material chemical composition of stainless steel is given in Table 3.1 and three dimensional view and dimensions of stainless steel slabs are given respectively in Fig. 3.2 and 3.3. The tensile and fatigue test specimens have been obtained from the slabs produced by vacuum assisted brazing method. The production methods of tensile and fatigue specimens are given below.

i. Grinding of stainless stel slab surfaces to have claer regions in brazing process
ii. Placing of copper foil between slabs and positioning in vacuum furnace
iii. Vacuum brazing operation
iv. Cleaning of residual coppers from slab surfaces
v. Placing of brazed slabs for wire erosion machining
vi. Wire erosion machining
vii. Tensile and fatigue test specimens with good dimensional property

Table 3.1. Chemical composition of 316 L stainless stel

Type of element	C	Mn	Si	Cr	Ni	Mo	Co	N (ppm)
Percent by % or ppm	0,019	1,30	0,450	16,70	10,01	20,019	0,217	318

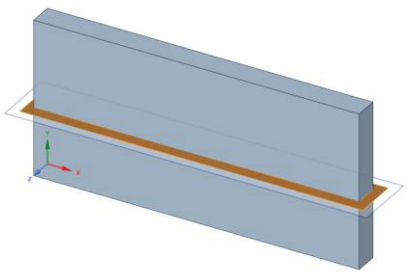

Figure 3.2. Positioning of stainless steel slabs for brazing process with copper foil

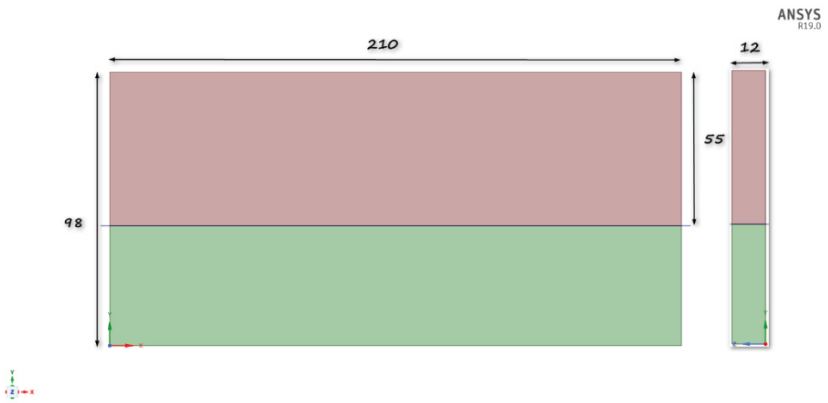

Figure 3.3. Dimensions of stainless steel slabs

The sample production should be performed as in the given order to have undiverged results from experiments. Brazing operation is strongly noncontrollable production method especially when it is in vacuum furnace. The schematic views of operations; positioning of slabs in palletes, covering system of slabs and brazed slabs after vacuum furnace are given in Fig. 3.4, 3.5, 3.6, respectively. The temperature profile of vacuum brazing furnace is shown in Fig.3.7 and the maximum temperature is fixed at 1100°C during brazing phase.

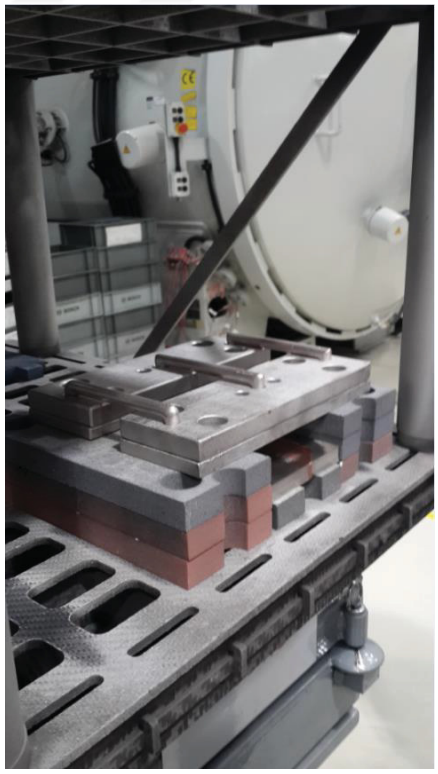

Figure 3.4. The positioning of stainless steel slabs on palletes before brazing (Source: Bosch, 2017)

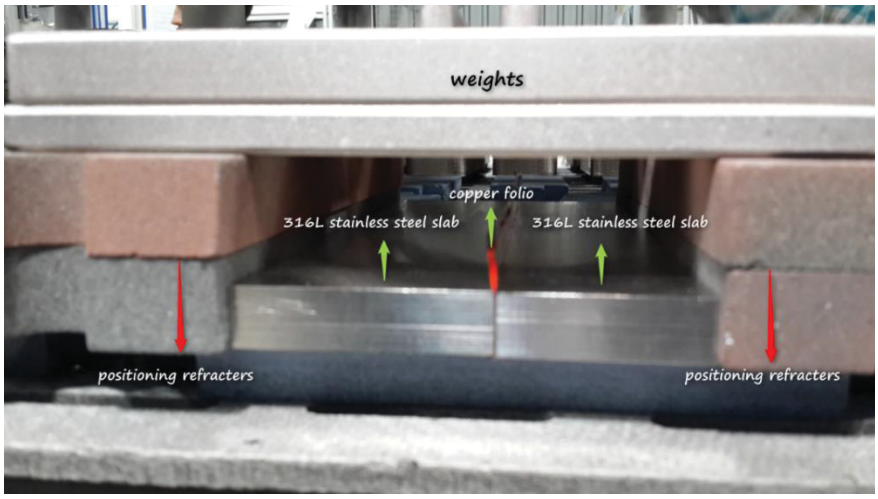

Figure 3.5. Covering system for success brazing operation in the vacuum furnace (Source: Bosch, 2017)

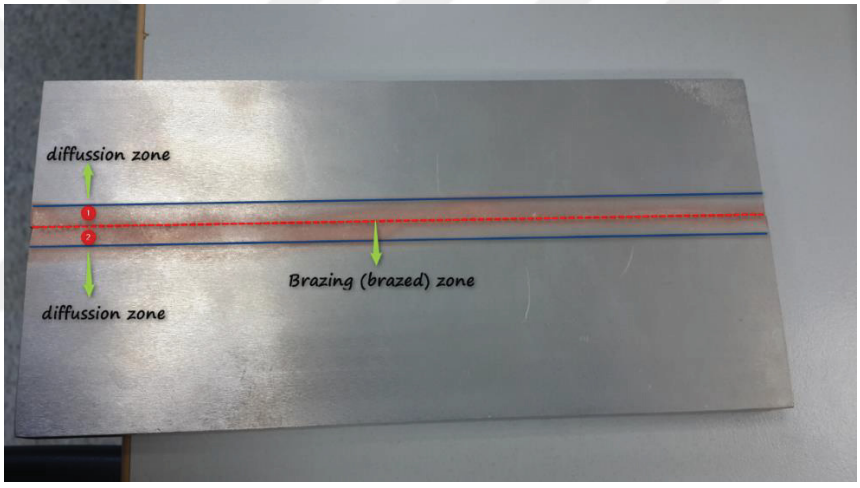

Figure 3.6. Brazed slabs after vacuum furnace with brazing and diffusion zones (Source: Bosch, 2017)

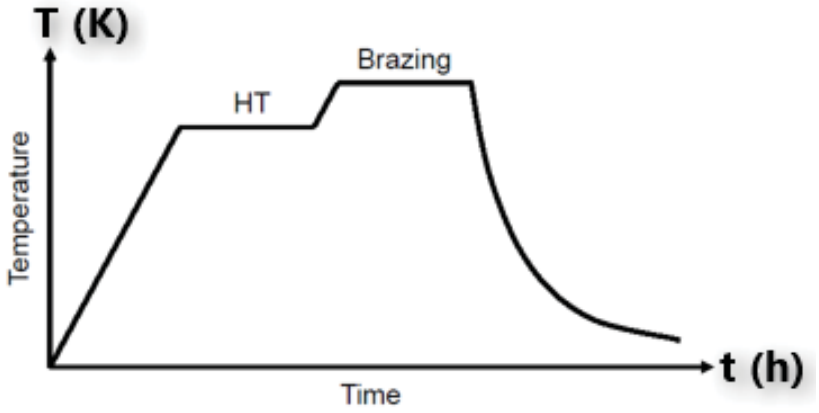

Figure 3.7. Temperature profile of vacuum brazing furnace (Source: Uhlig et al. , 2016

3.1.2. Specimen Production by Wire Erosion Machining

After the brazed stainless steel slabs are produced in vacuum furnace, tensile and fatigue specimens without any effect of temperature during machining process have been prepared. The wire erosion machining method, however the time consuming and being expensive has been preferred. At the end of wire erosion operation, tensile and fatigue samples have been obtained as shown in Fig. 3.8.

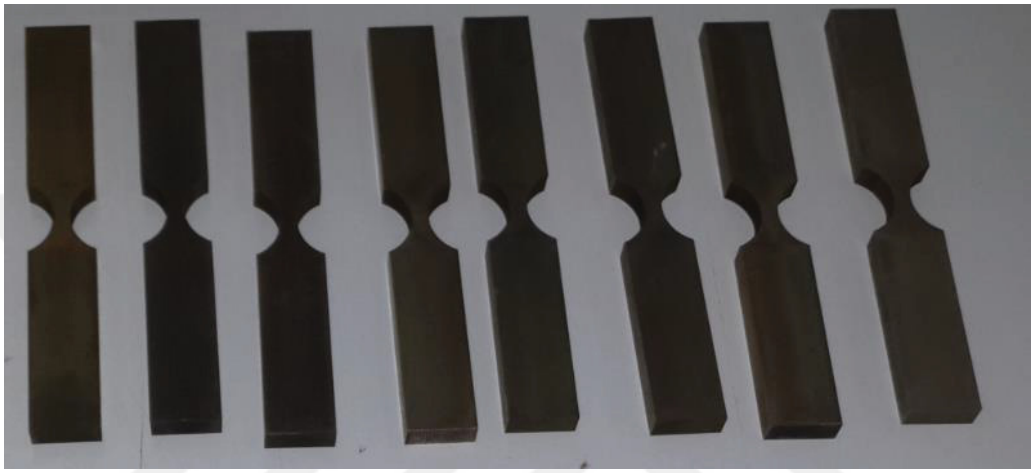

Figure 3.8. Tensile and fatigue test specimens
(Source: BOSCH TT, 2017)

3.2. Tensile Test Results of Brazed Specimens

The mechanical properties of brazed specimens have been determined by uniaxial tensile testing in IYTE Mechanical Enginering laboratories. These properties are used as an input data of material models which have been proposed for numerical analysis. The test conditions are presented in Table 3.2.

Table 3.2. Tensile test conditions

Test condition	Specific value
Temperature	22°C
Relative humidity	35 %
Test Speed	1 mm / sec

The tensile tests have been repeated for the four different samples and σ-ε curves are shown in Fig. 3.9.

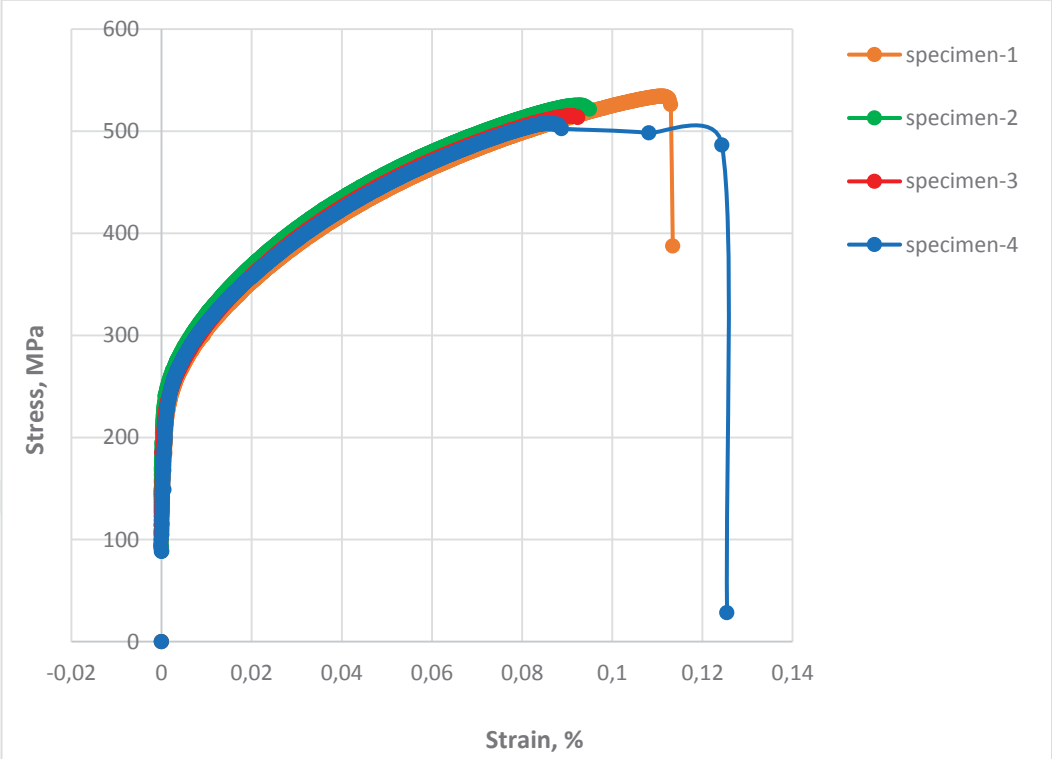

Figure 3.9.Engineering stress-strain curve of brazed specimens

The mechanical properties of brazed test samples are given in Table 3.3 and 3.4 respectively.

Table 3.3. Tensile testing results of brazed specimens

Sample	Ultimate Tensile Strength (MPa)	Young's Modulus (GPa)	Yield Load (kN)	Yield Strength (MPa)
1	534.3	240.05	3.831	249.1
2	525.4	230.27	4.085	264.7
3	515.0	271.14	3.919	254.4
4	507.5	256.68	3.954	257.9
Average	**520.5**	**249.53**	**3.947**	**256.5**
Standart Deviation (+ / -)	**11.7**	**18.0**	**0.105**	**6.5**

The tensile test results of brazed specimens have shown that although, the standard deviation values between the repitations are somewhat high, the experimental observations are found to be meaningful. The deviation can be decreased by increasing the number of repitations.

The homogeneous plastic deformation region of the engineering stress – strain curve which is shown in Fig. 3.9 has been converted to true stress-strain curve (plastic flow curve) and the characteristics of the curve has been discussed in detail. The plastic flow curve or homogenious plastic deformation region of stress – strain curve have been obtained to understand deformation mechanism of brazed specimens shown in Fig. 3.10. The Hollomon's parameters are found by linearization in logarithmic scale of this region of curve. It is important that the plastic flow curve of material must be drawn for true stress and strain values. In this regard, the engineering values have been converted to true values by using Eq. 2.3 and Eq. 2.4. Finally, the linearization procedure has been applied to obtain Holloman's parameters, K and n.

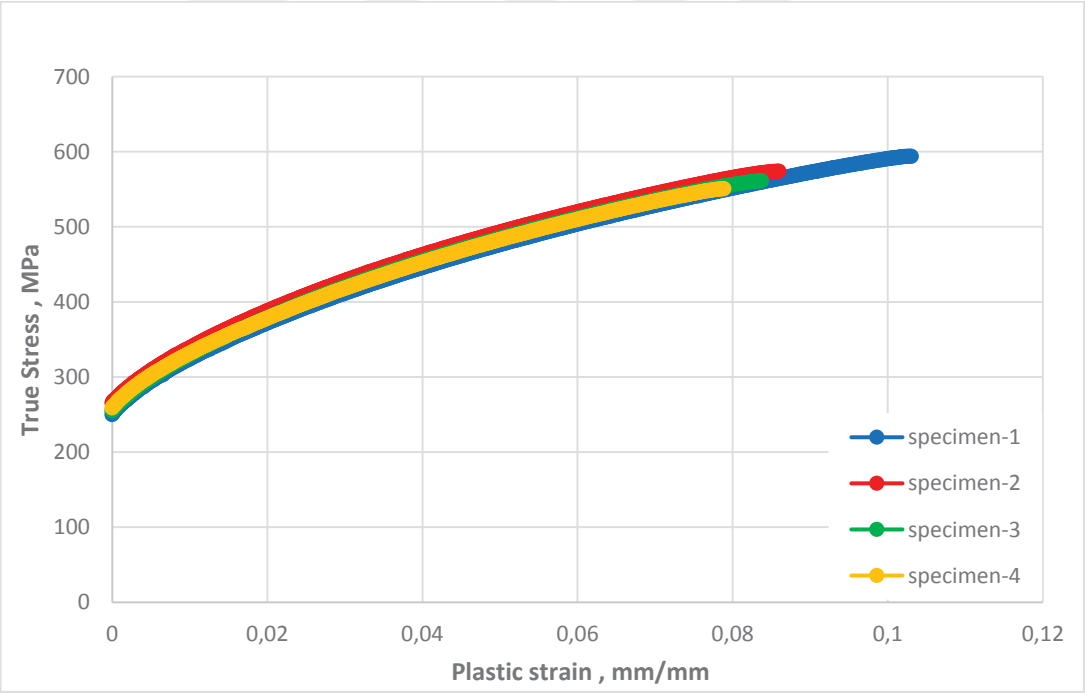

Figure 3.10. Plastic flow curve of brazed specimens

The true stress- strain curves of the specimens 1, 2, 3 and 4 have been given in logarithmic scale with own fitted equations are shown in Fig. 3.11, 3.12. The logarithmic scale true stress-strain curves have been curve fitted to find out Hollomon's parameters K and n.

These parameteres for each specimen are presented in Table 3.4. The R^2 values in Fig. 3.11 and Fig. 3.12 represents the statistically robustness of fitted curve and parameters.

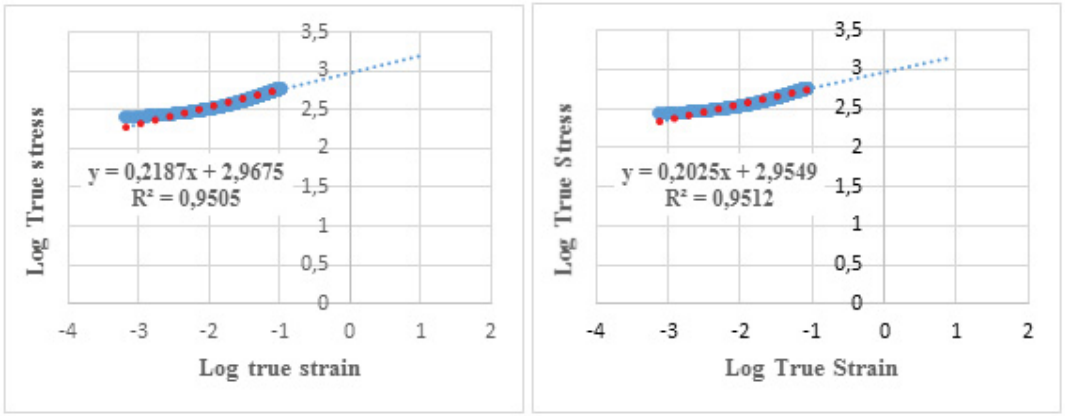

Figure 3.11. Logarithmic true stress-strain graph of specimen 1 and 2

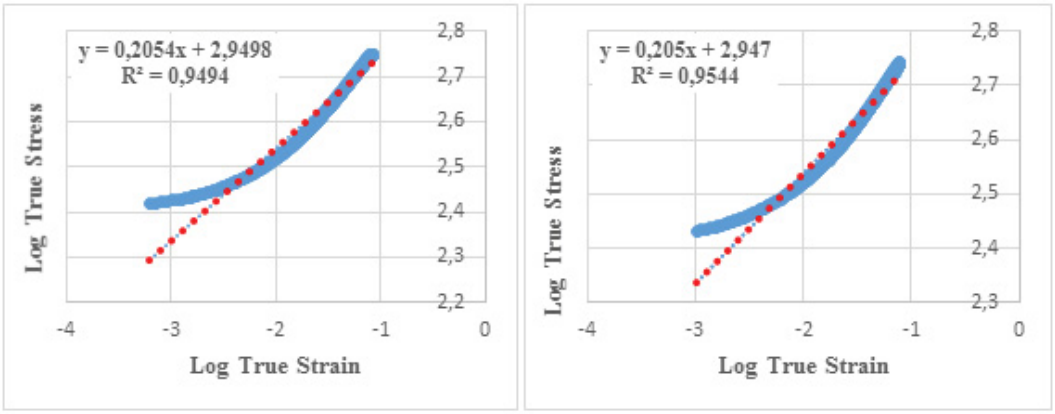

Figure 3.12. Logarithmic true stress-strain graph of specimen 3 and 4

Table 3.4. The Hollomon's parameter of brazed specimens 1, 2, 3 and 4

Specimen	Strength Coefficient (K) MPa	Strain hardening exponent (n)
1	927.89	0.218
2	899.49	0.202
3	890.84	0.205
4	885.11	0.205
Average	**900.8325**	**0.2075**
Standard deviation (+ / -)	**18.9820**	**0.007141**

It has been observed from the Table 3.4 that the value of strain hardening exponent (n) of the brazing interface is different from the n value of stainless steel which is base metal and the n value of copper which is filler metal given in Table 3.5. The same difference has been observed for the strength coefficient as well. Moreover, the comparison between these values for different materials are given in Table 3.5. The deviations for n and K between the repitations can be seen in Fig. 3.13

Table 3.5. Comparison table of different materials for n and K

Material	Strength Coefficient (K) MPa	Strain hardening exponent (n)
Low carbon steel	525-575	0.20-0.23
Stainless steel (austenitic)	400-500	0.40-0.55
HSLA steels	650-900	0.15-0.18
Copper	420-480	0.35-0.50
Brazed interface	**900.8325**	**0.2075**

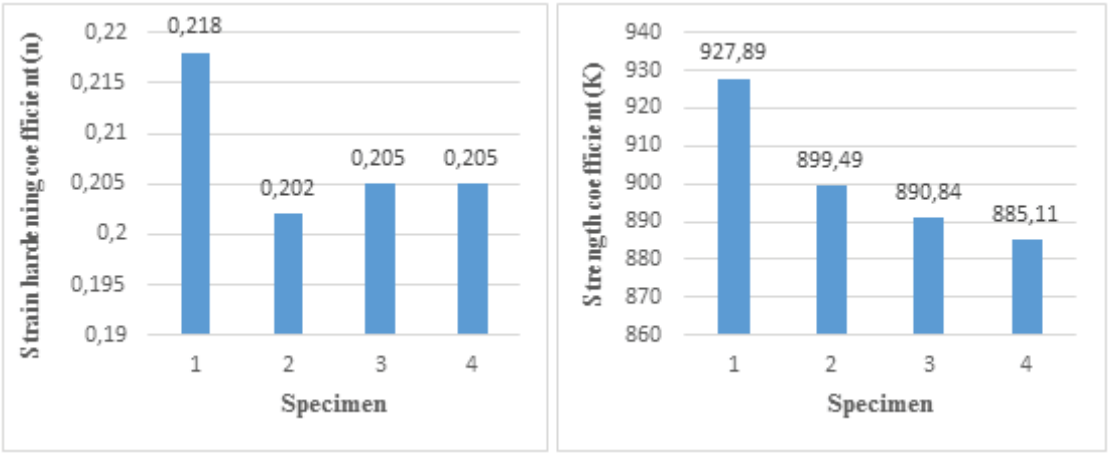

Figure 3.13. Comparison of experimental repitations for n and K

It is also understood from the obtained experimental data that the brazed interface material can not be considered as stainless steel or copper. Because, the strain hardening exponent and K values of brazed interface material is significantly different from the base and filler material shown in Table 3.6. This can be explained basically with diffusion mechanism during vacuum brazing process. The microstructural evaluations of stainless steel and copper interface have been done previously by Thomas Uhlig and colleagues especially

for brazed joints in plate heat exchangers. The scanning electron microscopy images of brazing sections in PHE are given in Fig. 3.14 and 3.15, respectively.

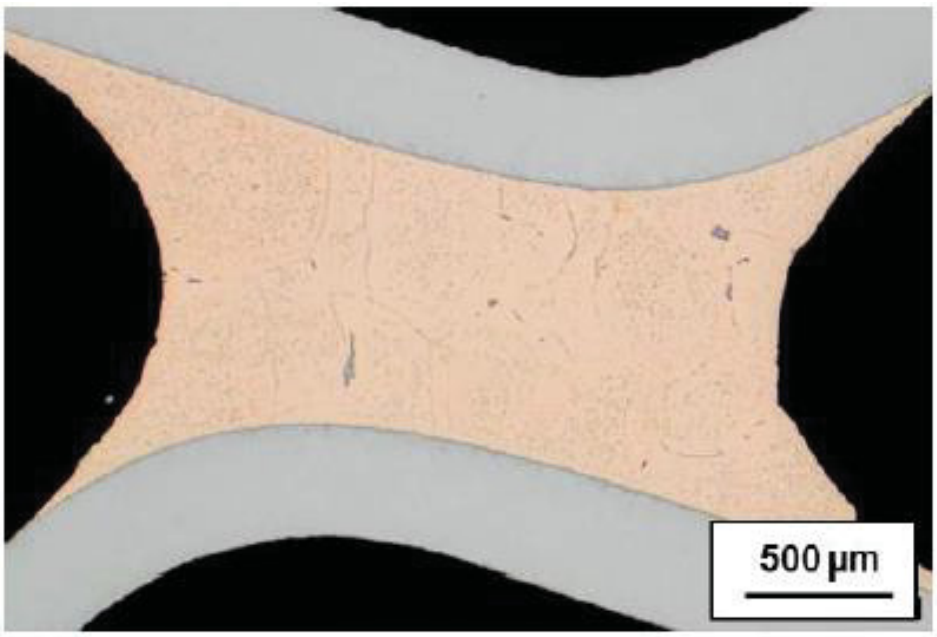

Figure 3.14. Section view of brazing point in PHE taken by SEM
(Source: Uhlig et al. , 2016)

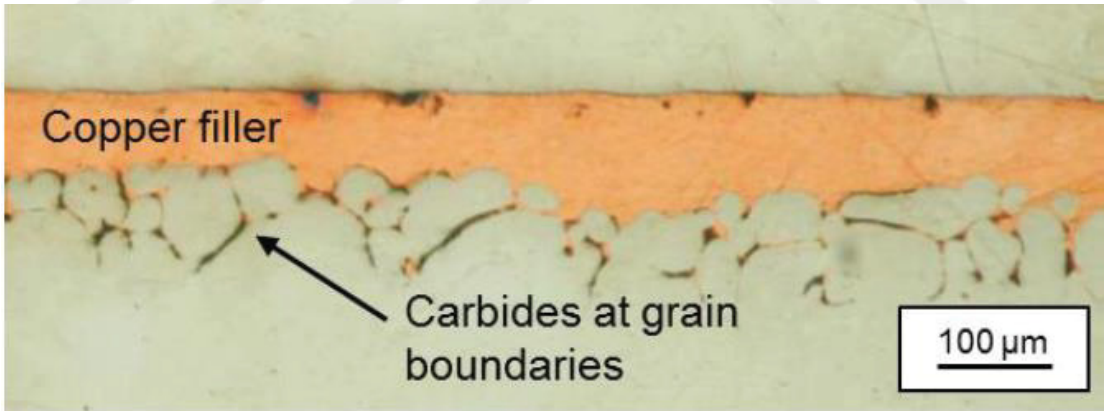

Figure 3.15. Illustration of carbide formation in stainless steel-copper brazing interface
(Source: Uhlig et al. , 2016)

Referring the Fig. 3.15, the grain boundaries can be infiltrated by copper filler during brazing process. This can be caused by residual stresses or carbide precipitations at grain boundaries. So that, the ductility of material can be reduced. The precipitation phases can be seen at a higher magnitude and resolution of SEM shown in Fig. 3.16.

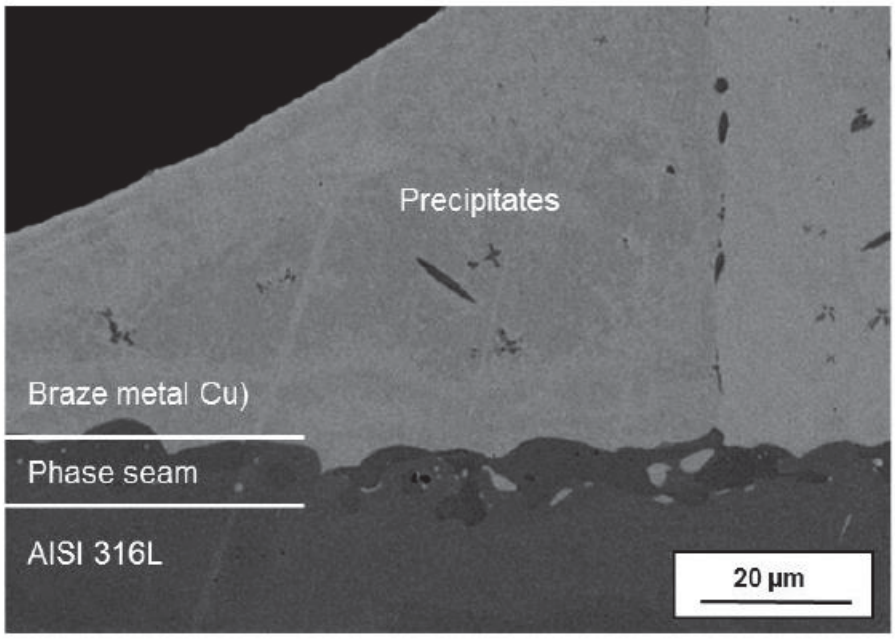

Figure 3.16. The precipitations and phase seam of brazing section by SEM (Source: Uhlig et al. , 2016)

Additionaly, the element contaminations of each region and phase of brazing intersection shown in Fig. 3.16 are calculated by EDXS analysis of SEM and represented in Table 3.6.

Table 3.6. Element contaminations of each region (Source: Uhlig et al., 2016)

EDXS [wt %]	Cu	Fe	Cr	Ni	Mn	Mo
Steel plate	-	70	17	9	1	2
Braze metal	98	2	-	-	-	-
Phase seam	-	69	24	3	-	4
Precipitates	62	26	8	3	1	-

Finally, all of these microstructural evaluations have shown that the behaviour of the brazed interface is different from that of the base metal and filler metal.

3.3. Fatigue Test Results of Brazed Specimen

The stress based fatigue tests have been performed to find out the S-N curves of brazed interface in IYTE Mechanical Engineering laboratories. The test condtions are presented in Table 3.7.

Table 3.7. Fatigue test conditions

Test condition	Specific value
Temperature	22°C
Relative humidity	35 %
Test Frequency	5 Hz

At the first stage of the tests, load-controlled fatigue tests have been applied based on the ultimate tensile strength of material. Then, the fatigue tests have been carried out at four different load levels by assuming maximum force values corresponding to 90, 80, 70 and 60 % of the ultimate tensile strength. The maximum load calculations are given in Table 3.8.

The cross sectional area of fatigue specimens are measured as $A_{specimen}$ = 15,44 mm^2. The minimum force F_{min} was kept constant at 94 N during the fatigue experiments for each values of ultimate tensile strength. Finally, the stress ratio R has been calculated by dividing mimimum stress amplitude to maximum stress amplitude. As can be seen in Table 3.8 the values of stress ratio is close to zero regarding tension – tension loading.

Table 3.8. Maximum load calculations of fatigue test according to UTS

Parameters	**Obtained values**			
UTS %	**90 % UTS**	**80 % UTS**	**70 % UTS**	**60 % UTS**
Fmax	7200	6408	5607	4806
σ_{min}	6.088	6.088	6.088	6.088
σ_{max}	466.321	415.026	363.148	311.269
R	0.0131	0.0147	0.0168	0.0196

Two fatigue experiment specimens have been tested for each load level. It is accepted that the fracture (rupture) formation as a failure (damage) criterion and the cycles to failure has been determined as the fatigue life of the relevant material (brazed interface) for applied load levels. The Table 3.9 shows the fatigue lives for each load level.

Table 3.9. Fatigue life for each load level

Load level (S)	Cycles to failure of 1st specimen	Cyles to failure of 2nd specimen
90 %	1940	6577
80 %	12035	18081
70 %	34225	53571
60 %	143918	124152

The experiments showed that all the fractured surfaces have been observed in the gauge section of the samples. The S-N curve is obtained from experimental data is shown in Fig. 3.17. Then, the S-N curve in logarithmic scale is also presented in Fig. 3.18.

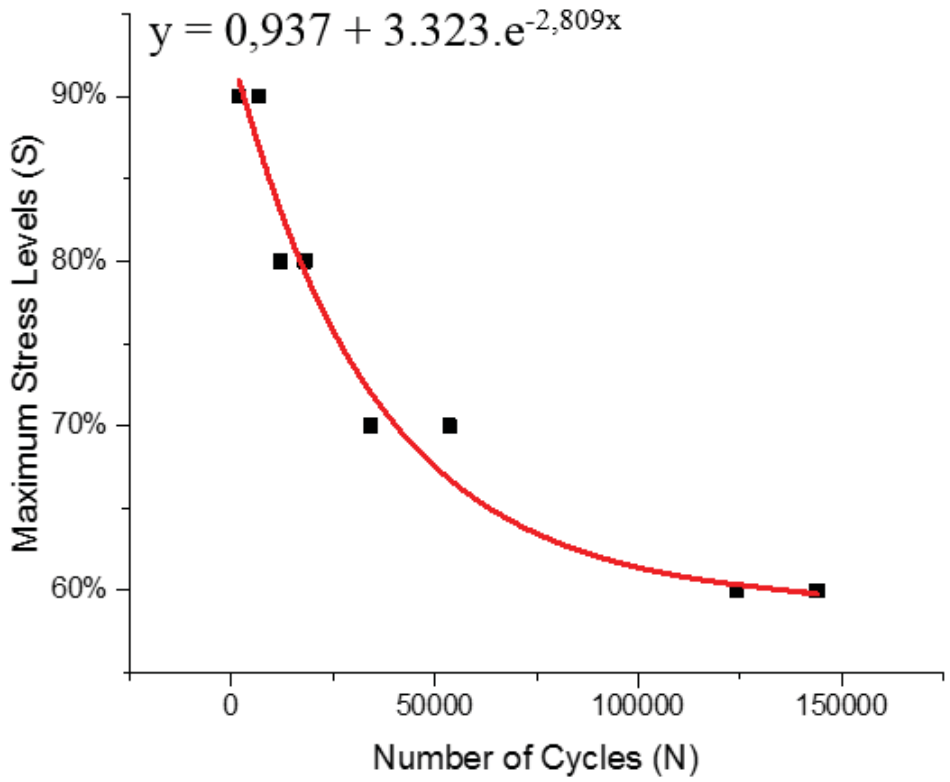

Figure 3.17. The S-N curve of brazed specimen

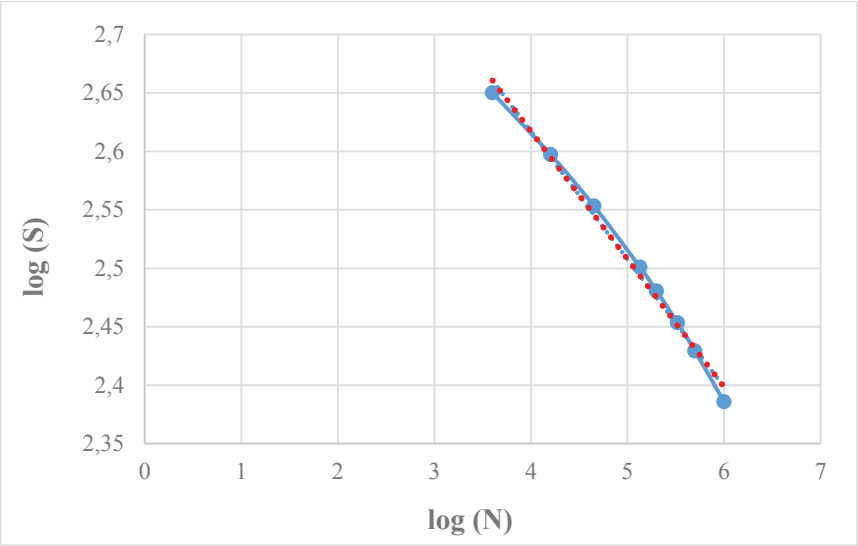

Figure 3.18. The S-N curve in logarithmic scale

The Basquin's equation constant parameters have been calculated by using data in Fig. 3.18 as a = 1133.44 and b = -0.1093 respectively.

The load contorolled fatigue tests have been carried out in second stage by reference to the yield strength value obtained from mechanical tensile tests. In a second stage fatigue tests, the force value corresponding to 90 % and 80 % of the yield strength have been considered as the maximum applied force on a specimen. The minimum load is assumed to be 94 N and the maximum load calculations of fatigue tests are given in Table 3.10.

Table 3.10. Maximum load calculations of fatigue tests according to yield strength

% Yield strength	% 90 Yield	% 80 Yield
F_{max} (kN)	3.564	3.168
σ_{min} (MPa)	6.088	6.088
σ_{max} (MPa)	230.85	205.2
R	0.026	0.029

In the experiments, the rupture have been detected on the specimen when 90 % percent of yield load applied, but, the specimen which is subjected to a 80 % yield load, there have not been experienced any rupture even though it has been completed one million cycle. Thus, the fatigue test has been finalized at that yield load level. Because, the rupture

failure (fracture) has been selected as a damage criterion for fatigue experiments. The cycles to failure for applied yield load level have been given in Table 3.11.

Table 3.11. Fatigue life for yield strength based applied load level

Load level (S)	Cycles to failure
90 % yield strength	261200
80 % yield strength	+1.000.000

3.3.1. Fractographs of Fatigue Specimens

The fractographies of fatigue specimens which have been tested at different load levels according to ultimate tensile strength are presented in Fig. 3.19, 3.20, 3.21 and 3.22, respectively. It is noted that the all fractographies have been taken by conventional camera. The brittle fracture has been observed in all fatigue tests at different load levels. It is also clearly visible that the fracture has been occured from the copper dense phase. For further investigations, it is necessary to perform SEM and other characterization tests.

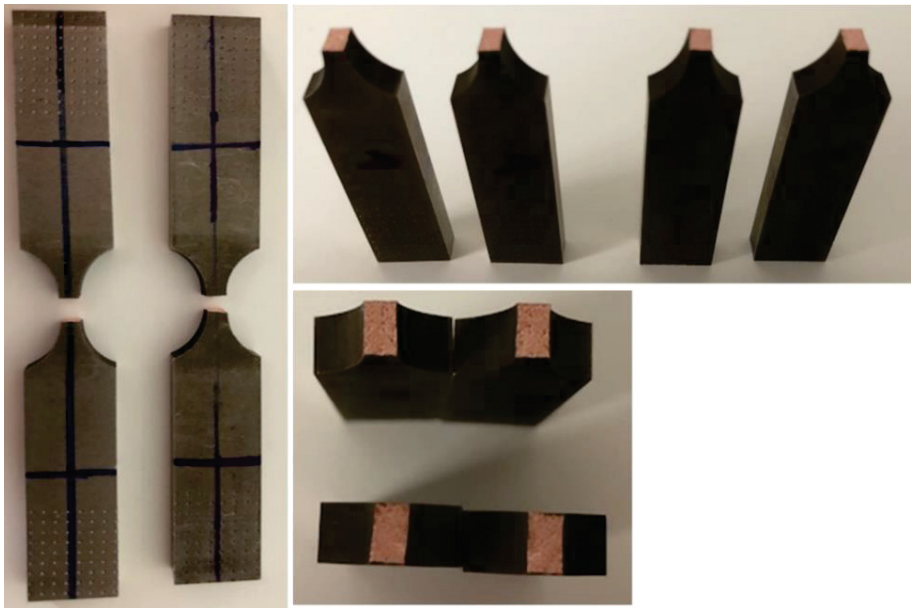

Figure 3.19. The fractographs of UTS based fatige specimens at 90 % UTS
(Source: BOSCH TT, 2017)

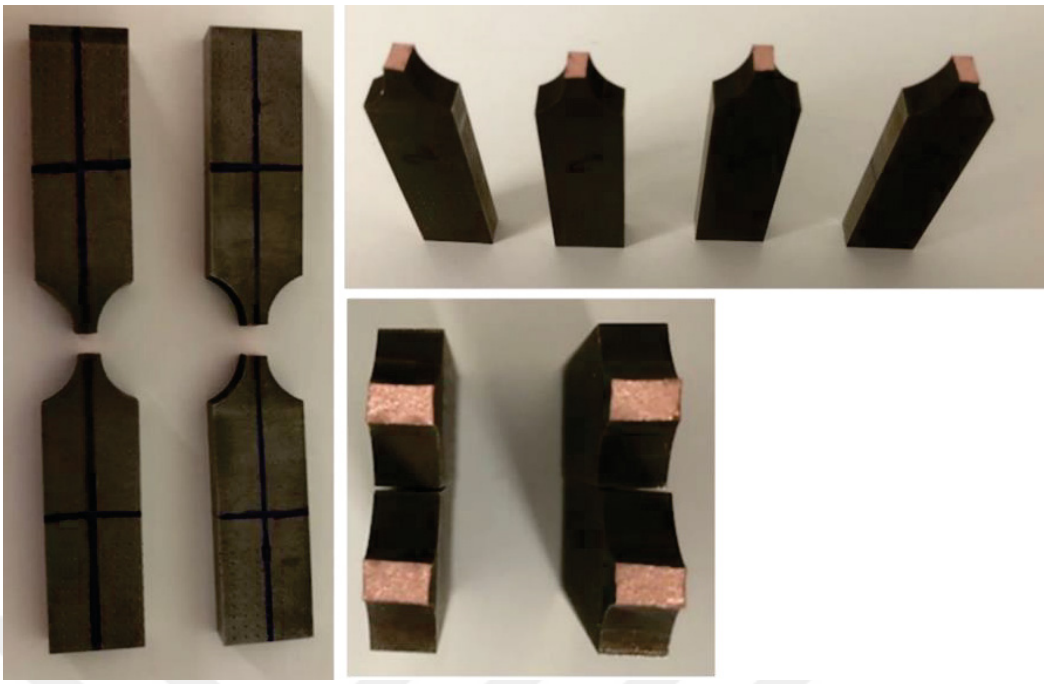

Figure 3.20. The fractographs of UTS based fatige specimens at 80 % UTS
(Source: BOSCH TT, 2017)

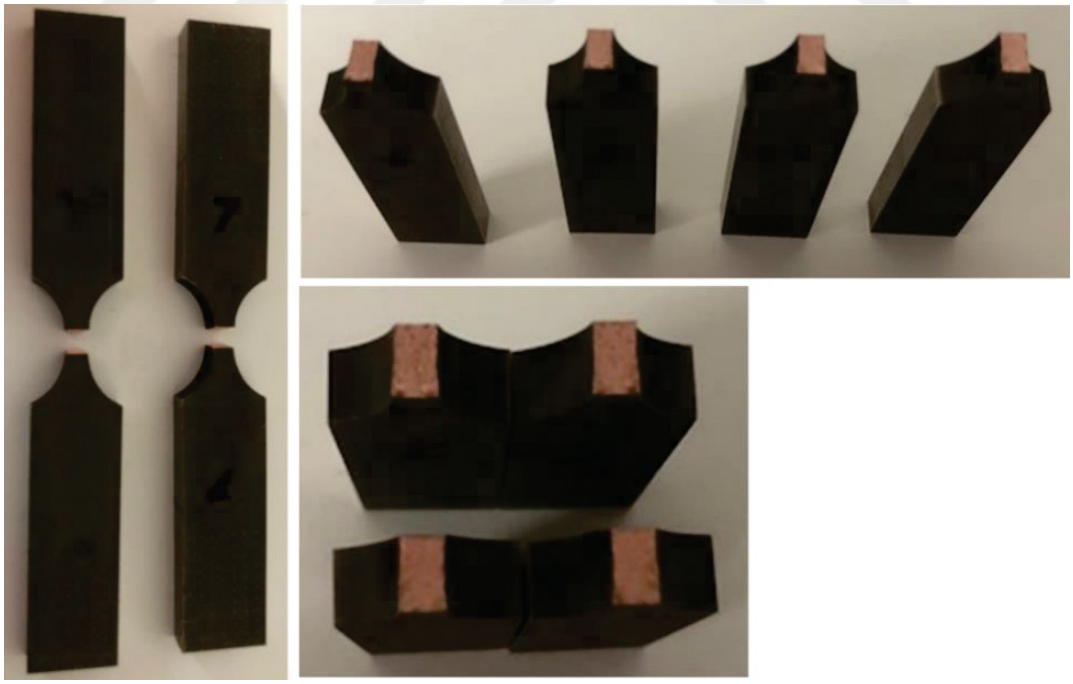

Figure 3.21. The fractographs of UTS based fatige specimens at 70 % UTS
(Source: BOSCH TT, 2017)

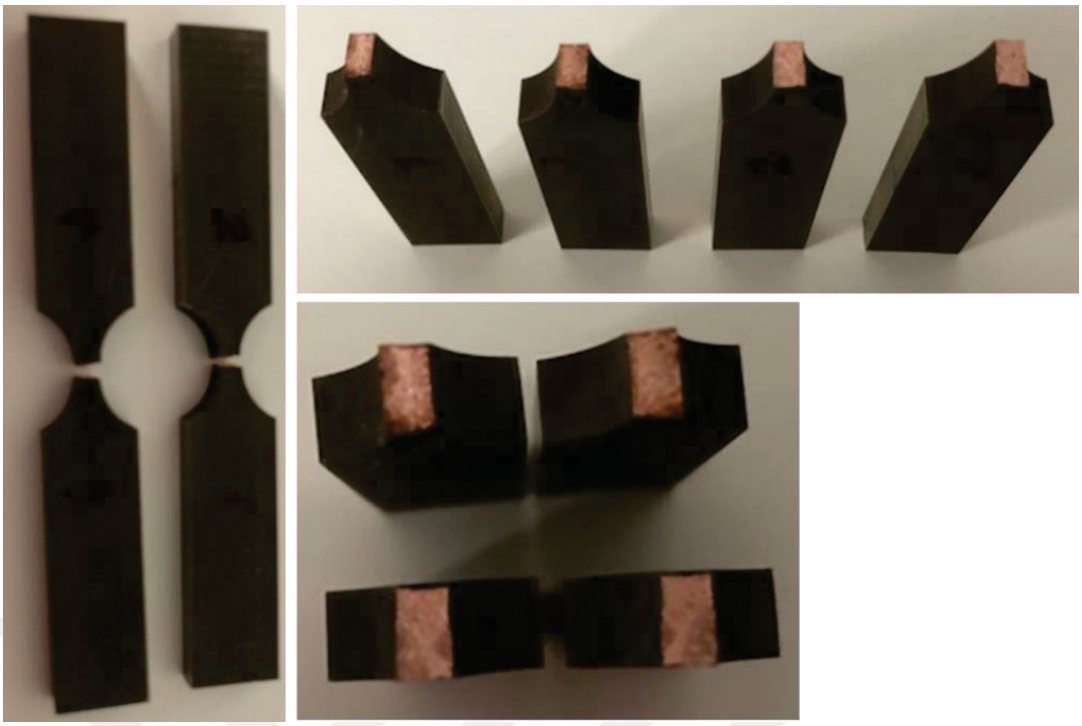

Figure 3.22. The fractographs of UTS based fatige specimens at 60 % UTS
(Source: BOSCH TT, 2017)

To summarize the experimental studies carried out within the scope of thesis;

i. The specimen production methodology has been discussed in detail.
ii. The tensile tests have been carried out to obtain a linear-elastic material properties and plastic flow region properties of brazed interface.
iii. Young's modulus, yield strength, ultimate tensile strength and Hollomon's parameters of plastic flow curve have been calculated.
iv. Stress based fatigue tests have been carried out for ultimate tensile strength and yield strength based diffent load levels.
v. S-N curves and Basquin's parameters have been obtained as a result of fatigue tests.
vi. The fractographies of fatigue test specimens have been presented.

3.4. Tensile and Fatigue Properties of 316 L Stainless Steel

The tensile properties of 316L austenitic stainless steel (SS) has been obtained by tensile testing at Metal Forming Center of Exellence in Atılım University. Meanwhile, the S-N curve of 316L SS has been taken from Zhao's study.

3.4.1. Tensile Test Results of 316L Stainless Steel

The tensile tests have been carried out by staying within the elastic deformation limits with the specimen (Fig. 3.23) prepared from the sheet material having 0.3 mm thickness to determine the modulus of elasticity. The elongation during elastic loadings has been masured precisely using a macro extensometer shown in Fig. 3.24.

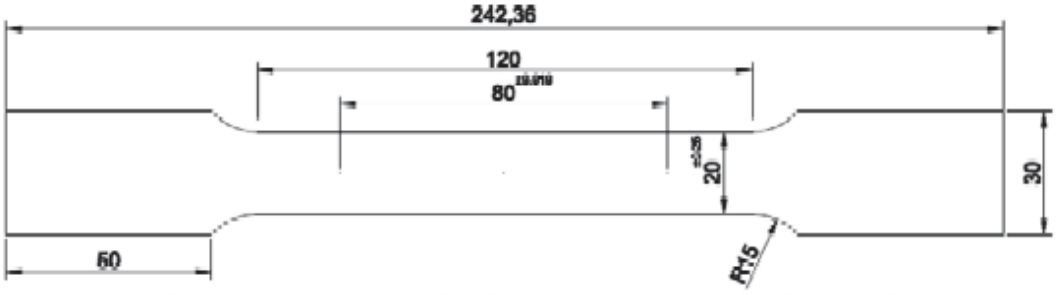

Figure 3.23. Standard flat tensile specimen
(Source: Atılım University, 2016)

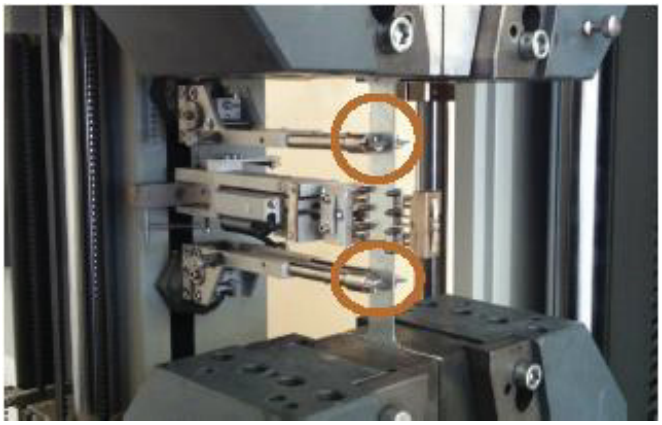

Figure 3.24. Macro extensometer
(Source: Atılım University, 2016)

When determining the modulus of elasticity, the rolling directions of 316L stainless steel shets are also taken into consideration. The tests were repeated five times for each sample.

The average values of the modulus of elasticity for each rolling direction are given in Table 3.12.

Table 3.12. The average values of modulus of elasticity for each rolling direction

Material	Thickness (mm)	Rolling direction (°)	Youg's Modulus (GPa)	Standard deviation
316L	0.3	0	190	+ / - 1.10 GPa
		45	189	+ / - 0.78 GPa
		90	197	+ / - 0.37 GPa

The plastic flow curve of 316L stainless steel has been obtained shown in Fig. 3.25.

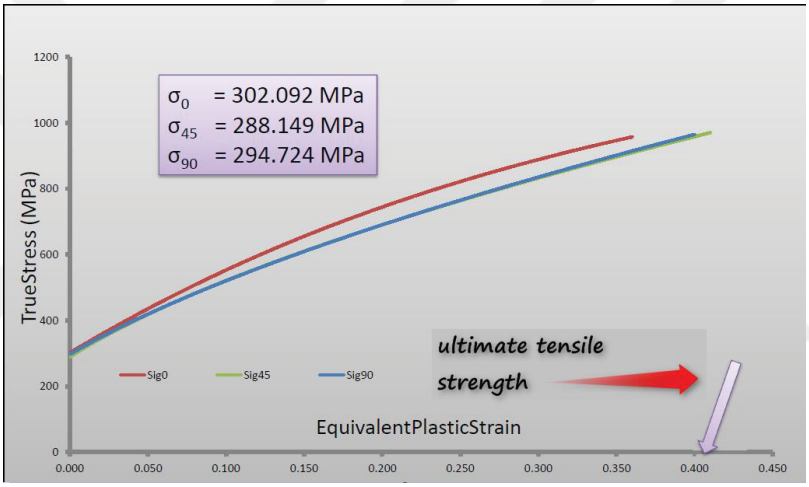

Figure 3.25. Plastic flow curve of 316L stainless steel material
(Source: Atılım University, 2016)

The yield strengths of 316L stainless steel for each rolling direction are given in Table 3.13.

Table 3.13. Yield strengths of 316 L SS for each rolling direction

Material	Thickness (mm)	Rolling direction (°)	Yield strength (ave) (MPa)
316L	0.3	0	302.092
		45	288.149
		90	294.724

3.4.2. S-N Curve of Stainless Steel

The S-N curve of 316L austenitic type stainless steel has been taken from Zhao, 2012

The experiments have been carried out for tension – tension mode by using a servo-valve controlled electro-hydraulic machine at room tempeature. Before performing the stress based fatigue experiments, uniaxial tensile test has been done to obtain ultimate tensile strength of material. The fatigue tests are conducted according to maximum tensile load at different levels such as, 90, 80 % percentage etc. The S-N curve is depicted both for true and logarithmic scales in Fig. 3.26 and 3.27 respectively. The parameters of the Basquin's equation are taken as a = 2804.14 and b = -0.1629.

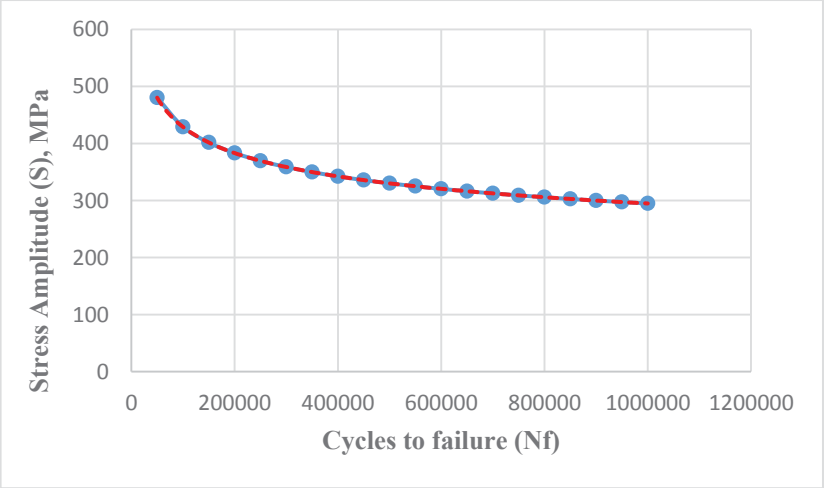

Figure 3.26. S-N curve of 316L stainless steel according to Basquin's equation

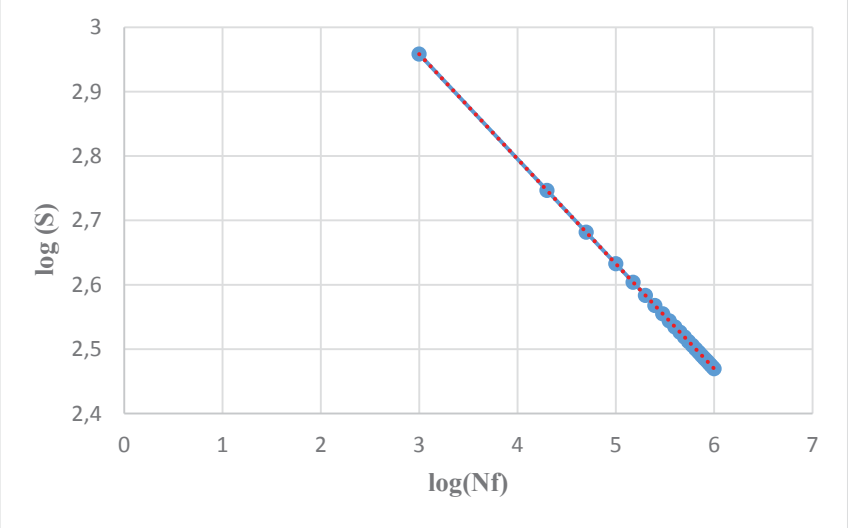

Figure 3.27. Logarithmic S-N curve of 316L stainless steel (Power-Law equation)

The material properties obtained from experiments and taken from reference studies will be input data for material models used in numerical analysis. In addition to this, it should be noted that the all material data are processed for the use in structural analysis of brazed plate heat exchangers. Thus, it could not been guaranteed for all other usage. Because, all experimental parameters are identified proper to Bosch Thermotechnology use cases and test conditions.

CHAPTER 4

MODELLING AND SIMULATIONS

In this chapter, it is intended to introduce definition of problem and modelling procedures. Furthermore, the validation of numerical approach will be introduced by tensile testing experimental inputs.

4.1. Problem Definition

The plate heat exchangers (PHE) are located in the combi boilers as a secondary heat exchanger to provide hot water for domestic installation line (kitchen, bathroom etc.). They operate at relatively high pressures. The PHE is comprised several number of channel plates to meet heat output requirements. The minimum and maximum number of plates are determined according to heat power of boilers. The PHEs consist of two different water channels such as central heating (CH) and domestic water (DW). The central heating channel carries the water which is coming from primary heat exchanger called as heat cell or combustion chamber. The domestic water (DW) channel carries to tap (potable) water coming from mains water system of city. The location of hydraulics and PHE in combi boiler and the schematic three dimensional view of PHE are illustrated in Fig. 4.1 and 4.2, respectively.

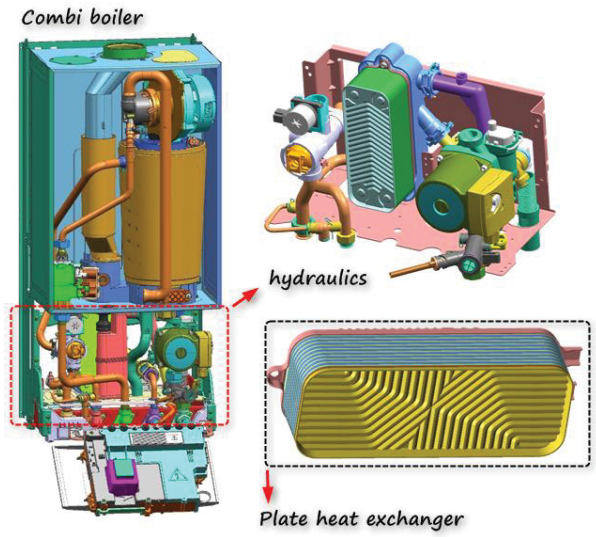

Figure 4.1. The location of hydraulics module and PHE in combi boiler
(Source: BOSCH TT, 2015)

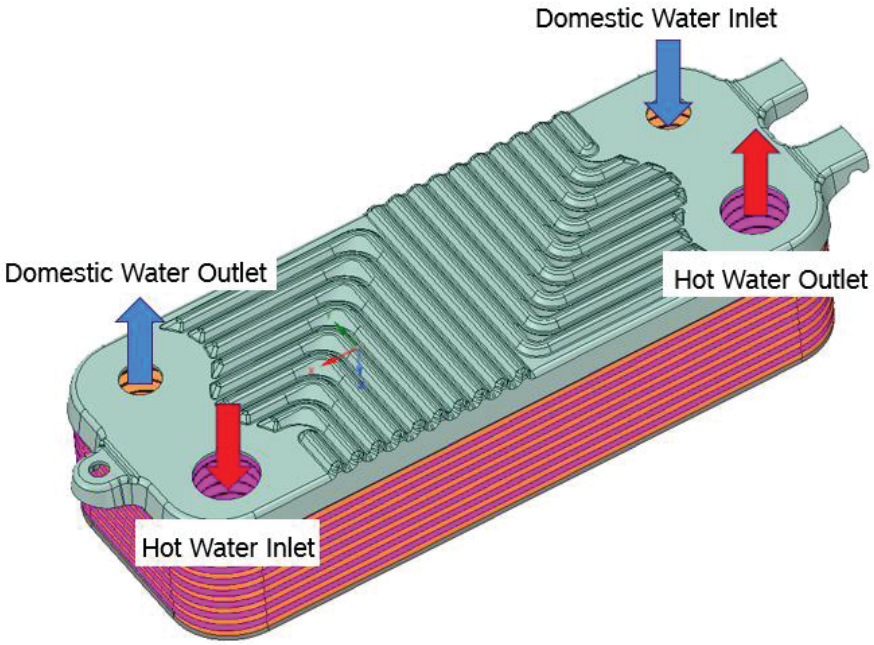

Figure 4.2. The three dimensional schematic view of PHE
(Source: BOSCH TT, 2015)

The plates of PHE are made of austenitic type 316 L stainless steel and the plates have 0.3 mm thickness. The thickness of plates is critical because of the efficient heat transfer and structural robustness of PHEs. The structural stability of PHE (plates, brazing regions) strongly depends on the operating conditions of heat exchanger. The channel pressure and water temperature (central heating and domestic) are main activators. The CH and DW channel pressures are different from each other and the potable water can fluctuate according to installation line behaviour. Additionaly, the central heating channel pressure values are determined by combi boiler's heat power.

In the plate heat exchangers at domestic hot water circuit, the sudden fluctuations are occured in channel pressure because of the user habbits. On the other hand, this phenomenon can easily be observed with the sudden closure of the tap in the kitchen, bathroom or similar domestic water line. This behaviour so called as '*water hammer*' effect. The magnitude of water hammer pressure strongly depends on the mains water system of city or country. The statistical study has been made to evaluate water hammer pressure peak values over the countries by Bosch Thermotechnology and it's mean peak values assumed to be as minimum *16 bar*. Also, the determination of peak value calculation complies with EN standards. Additionaly, it is inevatible to evaluate fatigue, since the water hammer peak will occur during the life-time of plate heat exchangers.

Within the scope of this thesis the static structural behaviour and fatigue evaluation of chevron type plate heat exchangers will be carried out by numerical methods. For that purpose, the three different PHE designs have been studied numerically by using experimentally derived material models. The chevron angle has been selected as a main design variables for the plates of PHE between the others. The main design variables have been illusrated in Fig.4.3 for the single plate of chevron type plate heat exchanger.

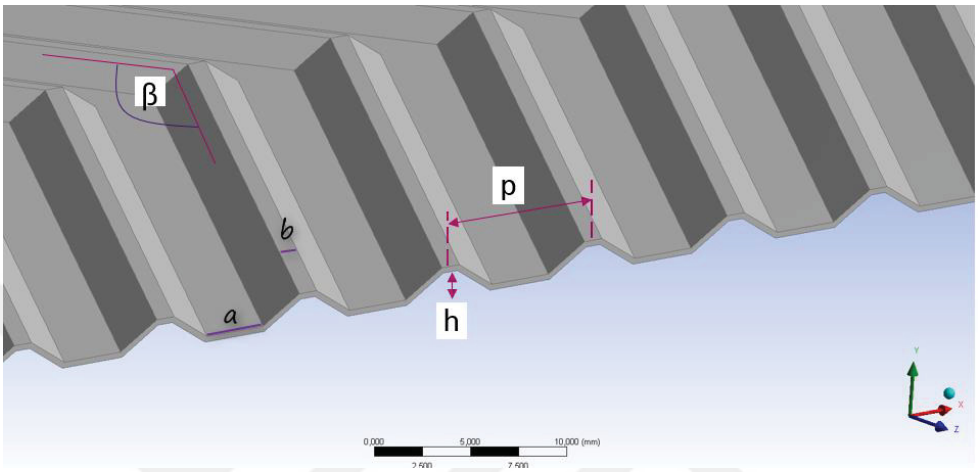

Figure 4.3. The main deisgn variables of chevron type PHE
(Source: BOSCH TT, 2015)

β: chevron angle**,** p: the distance between two chevron, h: form height, a: bottom base width, b: top base width

It is important that the most of design variables are depend on each other, that means the single variable is a function of others. Thus, despite the fact that the *chevron angle* has been choosen as a design variable, the other geometrical parameters (β, p, h etc.) will automatically changed. The chevron angle values has been considered as 90°, 110° and 130° shown in Table 4.1.

Table 4.1. The numerical values of chevron angle

Design parameter	**Numerical values of chevron angle β (°)**		
Chevron angle	$\beta_1 = 90°$	$\beta_2 = 110°$	$\beta_3 = 130°$

It is previously mentioned that the PHE consists of several number of plates such as from 10 to 32. However, the numerical studies has been done by using only two channel

plates to save computational time. The reason behind that is, the PHE has a repetitive geometrical configuration shown in Fig. 4.4. The channel types versus nominal pressure and pressure ranges are also given in Table 4.2.

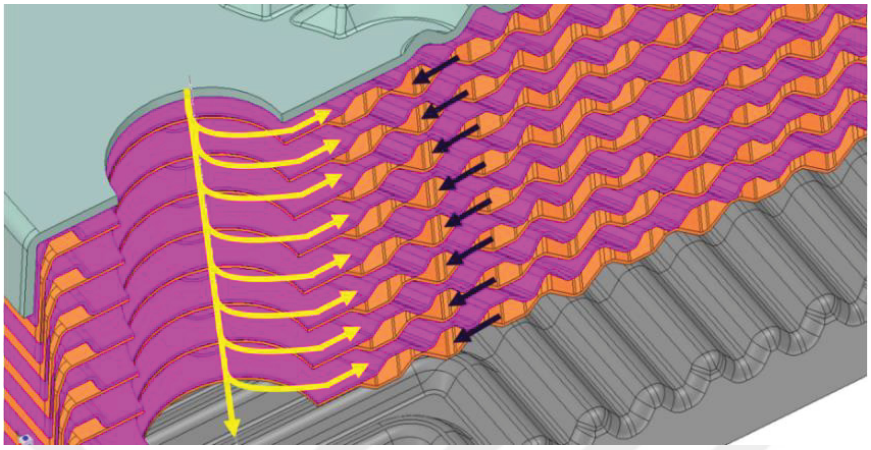

Figure 4.4. The central and domestic heating channels of PHE
(Source: Bosch TT, 2015)

Table 4.2. Water channel type versus channel pressures

Water Channel	Arrow	Channel Pressure
Central heating (CH)	→	1.5 bar (nominal)
Domestic heating (DHW)	→	16 – 50 bar

The water hammer induced mechanical loading on the plates has been shown in Fig. 4.5.

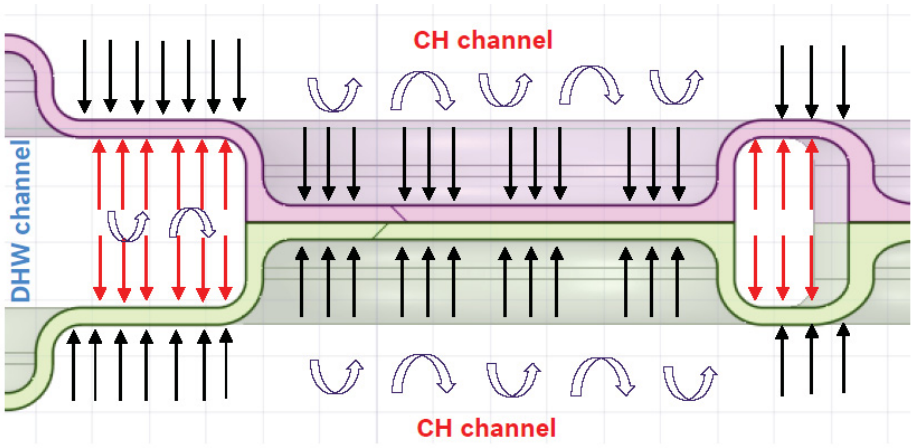

Figure 4.5. Representation of water hammer induced mechanical loading on the plates

Finally, the main intension of this study will be to investigate static structural response of brazed plate heat exchangers for three diffrent chevron angles under several pressure loadings from 16 bar nominal value up to 50 bar. In addition to that, the fatigue assesment of PHE will be done by using static structural analysis results. Since, the water hammer pressure fluctuations takes place in domestic heat water channel, the nominal value of central heating channel pressure has been kept constant at 1.5 bar in numerical analysis.

4.2. Modelling Approach, Simplifications and Assumptions

The assumptions and simplifications considered for the numerical studies have been listed as,

i. The plates of PHE has been converted from solid to shell due to t/L ratio is quite small than 10, where *t* is the thickness of plate and *L* is a length of plate.
ii. As already mentioned, even tough the PHE consists of several number of channels, only two plates have been considered in numerical analysis due to geometrical repitation.
iii. The nominal pressure of central heating channel and water hammer induced domestic heating channel pressures have been defined seperately. But, the net pressure has been used as a initial conditions for analysis and listed in Table 4.3

Table 4.3. The net applied pressure values inside the channel

Domestic heating pressure (P_{DHW}), bar	**Central heating pressure (P_{CH}), bar**	**Pnet = P_{DHW} - P_{CH} , bar**
16	1,5	14.5
25	1,5	23.5
30	1,5	28.5
50	1,5	48.5

iv. The connection of brazing points to plates have been modelled as *'Bonded'* contact. The physical meanings of bonded contact is defined as, it is not allowed that any seperation between connected parts during mechanical loading. The reason for the definition of *bonded contact* that, there is no breakage expected

between the plates and brazing points. The plates and brazing points connections have been represented in Fig. 4.6.

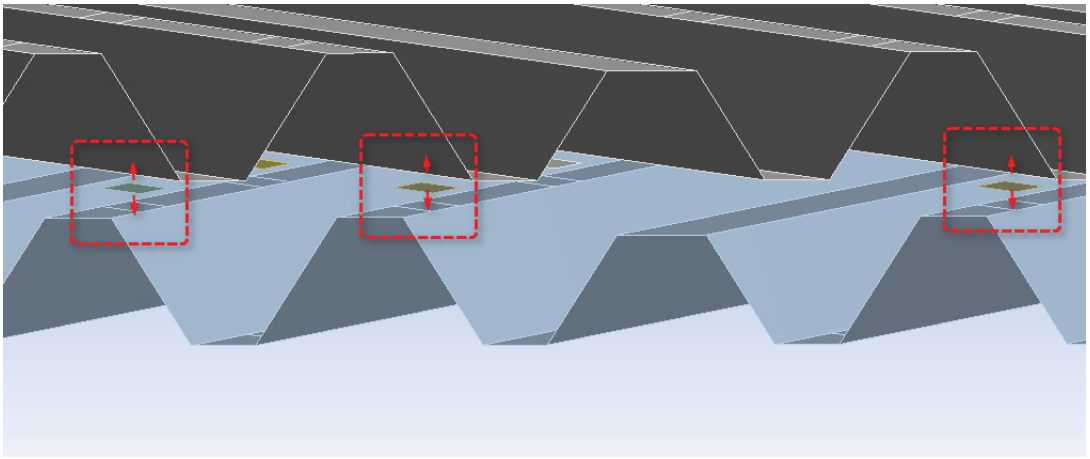

Figure 4.6. Representation of brazing points and connection with plates

v. Since, the design of the inlet and outlet port regions of plate heat exchangers differs from the mid-region, the structural analysis has been carried out only for middle region of PHE shown as in Fig. 4.7. The design of inlet and outlet port zones are significantly depend on the thermal and flow behaviour of PHE.

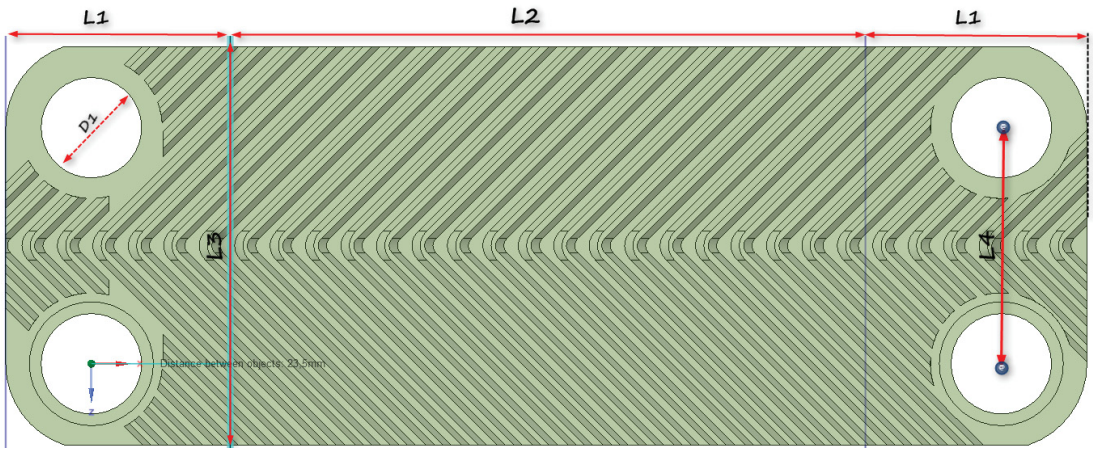

Figure 4.7. A complete chevron type heat exchanger plate

The geometrical dimensions of plates are given in Table 4.4 and the numerically investigated domain has been defined as (L_2 x L_3) rectangular area. It is so called as middle region of plate heat exchanger.

Table 4.4. Geometrical dimension of plate (mm)

L_1	L_2	L_3	L_4	D_1
28	130	28	40	17

4.2.1. Development of Numerical Modelling Approach

Since there is no modelling approach that defines the mechanical behaviour of the plate heat exchangers under water hammer induced pressure loading, the proposed methodology used in numerical analysis has originally been developed within the scope of study. In numerical analysis the all listed assumptions and simplifications have been considered.

The brazing points in chevron type plate heat exchangers consist when two different plates which are cental heating and domestic heating are stacked in opposite directions and the copper foil is placed between these plates. It should not be forgotten that the geometrical configuration of CH and DHW plates can be the same or different. The brazing points will be in the form of *parallelogram* with the overlapping of chevron bases in opposite directions shown in Fig. 4.8.

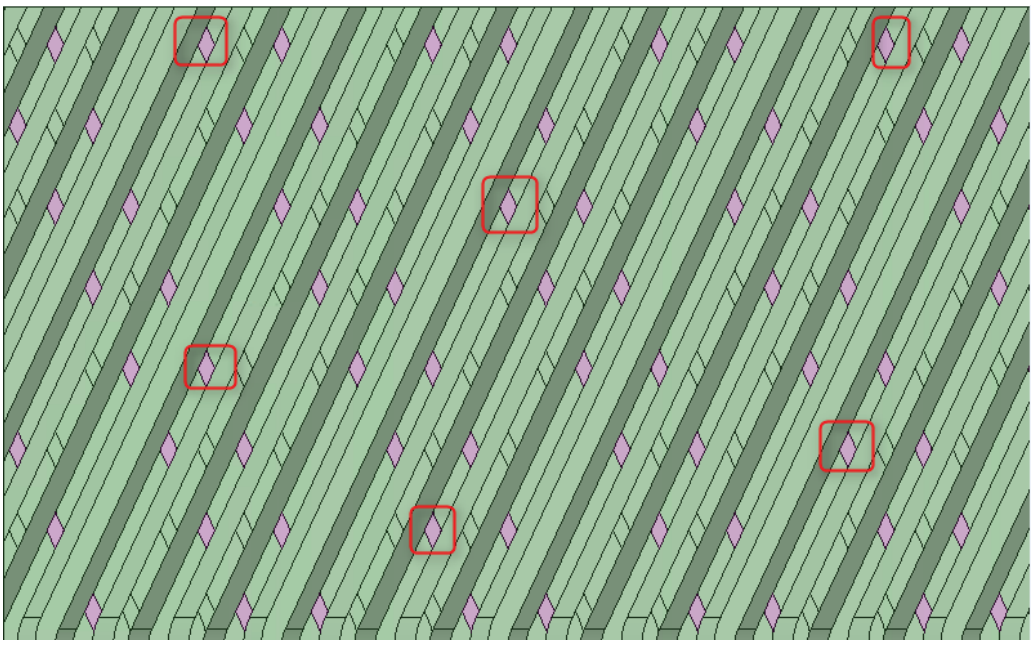

Figure 4.8. Parallelogram shaped brazing points on the chevron type PHE

The brazing points have been modelled seperately as shell elements and the thickness of shell's has been defined as 0.2 mm. The upper and lower surfaces of parallelograms (brazing points) are connected to channels plates. The physical propety of that connections is defined as ' *Bonded* ' contact. The material properties of these brazing points were obtained by data obtained from tensile and fatigue experiments.

4.2.2. Mesh Sensitivity (Independency) Analysis

The mesh sensitivity analysis has been carried out to eliminate and decrease the numerical solution errors. The independency study has been applied for all variations of PHEs (90˚, 110˚ and 130˚ chevron angles) at 50 bar channel pressure and the total deformation was selected as an evaluation metric. The sensitivity analysis results have been represented in Fig. 4.9.

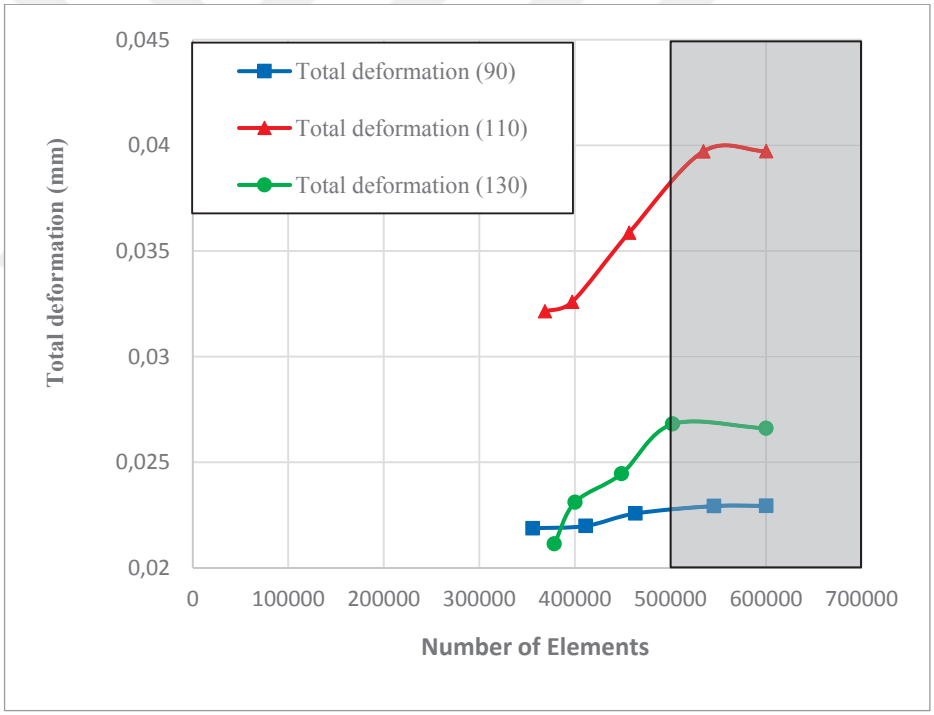

Figure 4.9. Mesh sensitivty analysis graphics of PHE

It is observed from the Fig. 4.9, the total deformation of PHE at 50 bar channel pressure has been converged with approximately 500.000 hexagonal elements for all chevron angle variations. The mesh quality metrics, skewness and orthogonal quality of structural mesh have been given in Table 4.5.

Table 4.5. Mesh quality metrics

PHE chevron angle	Number of elements	Skewness	Orthogonal quality
90˚	600125	0,127	0.982
110˚	611312	0,125	0.981
130˚	607324	0,120	0.979

4.2.3. Boundary Conditions

The loading and clamping conditions representing the real conditions of the plate heat exchanger were taken into consideration during the derivation and definition of boundary conditions in numerical analysis. The inlet and outlet region edges displacements have been restricted along the x,y and z directions as shown in Fig. 4.10.

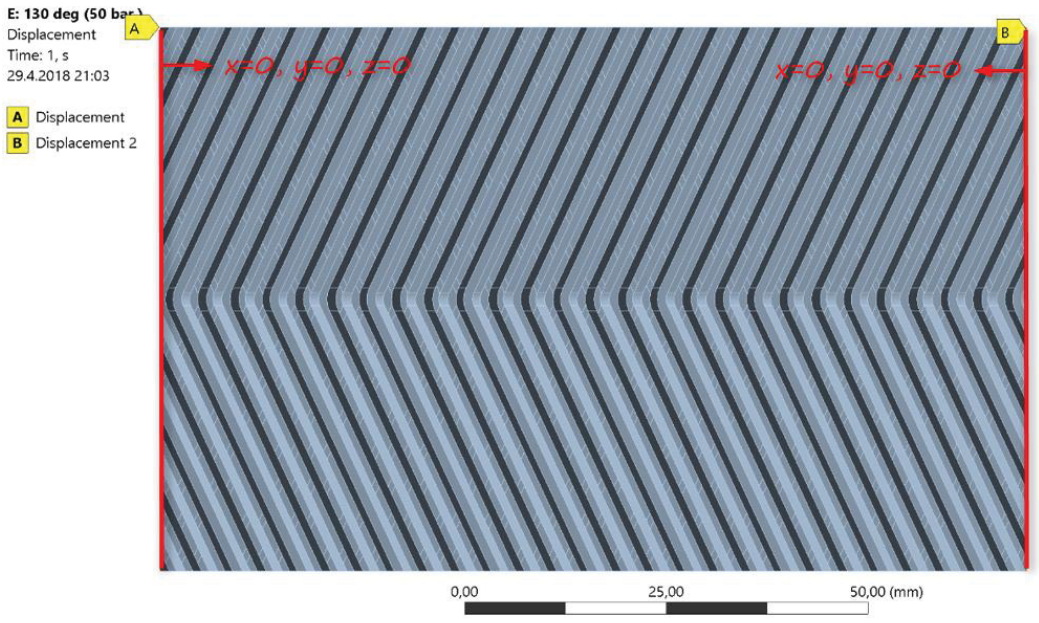

Figure 4.10. Displacement boundary condition for plate edges (x,y,z = 0)

In the structural analysis of plate heat exchanger, the numerical analysis have been carried out by considering only two channel plates due to computational challenges. The brazing points on the upper and lower channel plates have been defined ax fixed support

contact elements shown in Fig. 4.11. The physical meaning of fixed support that there is no allowed displacement and rotation along the all degree of freedoms. Moreover, the side edges of channel plates have been connected with *Bonded* contact due to in real case the plate skirts have been placed and touched onto each other as shown in Fig. 4.12. Lastly, the water hammer induced pressure fluctuation has been applied as a hydrostatic pressure with its maximum acting net value as shown in Table 4.3. Since the pressure distribution over the brazing surface areas are zero, they have been extracted from the total surface area when the definition of hydrostatic pressure boundary condition.

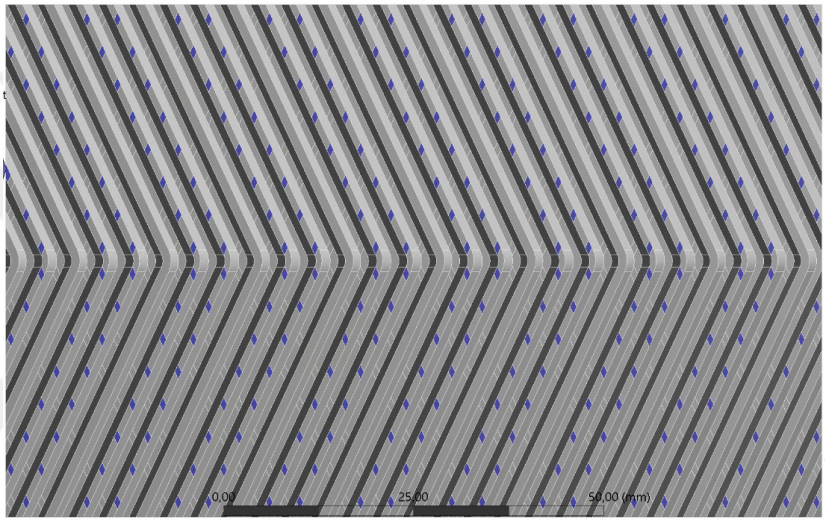

Figure 4.11. Upper and lower channel plates brazing points boundary condition

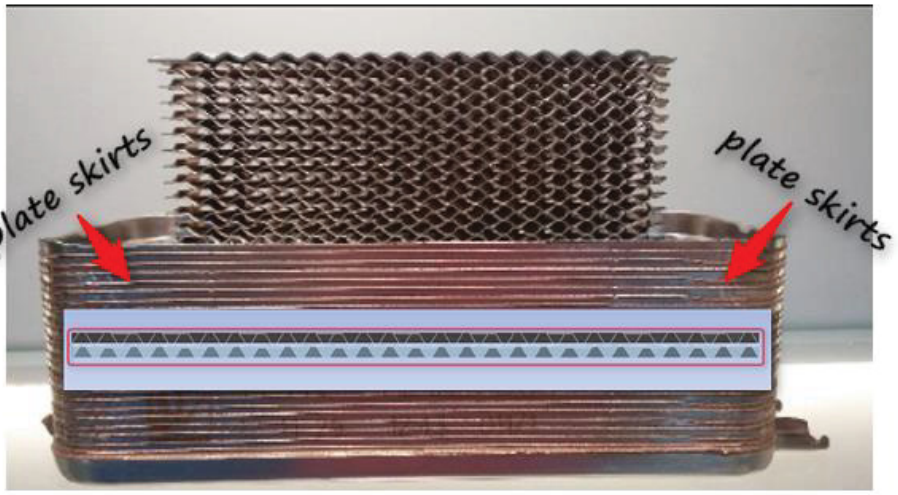

Figure 4.12. Bonded contact between plate skirt boundaries
(Source: BOSCH TT, 2015)

Additionaly, the analysis settings have been arranged according to numerical non-linearities. The large deflection has been activated and time steps have been defined to be maximum 0,01 second for convergence of numerical solution. The multi-linear kinematic hardening material model has been used to determine plastic behavior of both for plates and brazing points.

4.2.4.Validation of Numerical Approach

The tensile test has been performed numerically in order to verify the feasibility and robustness of the proposed methodology. The structural mesh has been built as dense and precise as possible to clearly capture the stress distributions in the interface region and interface-base metal connection regions shown as in Fig. 4.13. The tensile test sample has been modelled using quarterly symmetrical approach and the boundary conditions have been defined in this context shown in Fig. 4.14. The interface material properties have been defined for interface region of tensile specimen to evaluate structural response during tensile loading.

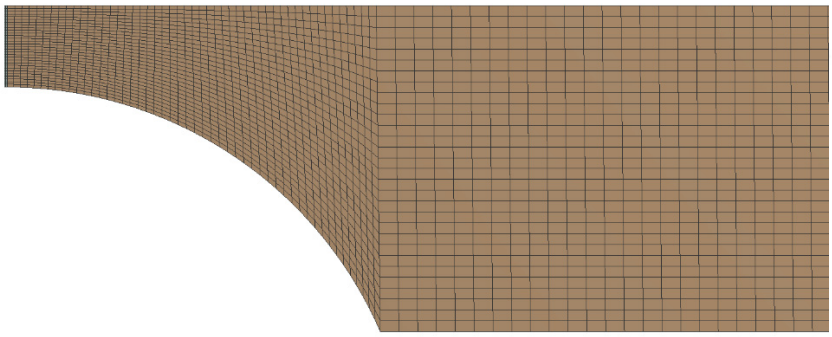

Figure 4.13. Structural mesh of quarter tensile specimen

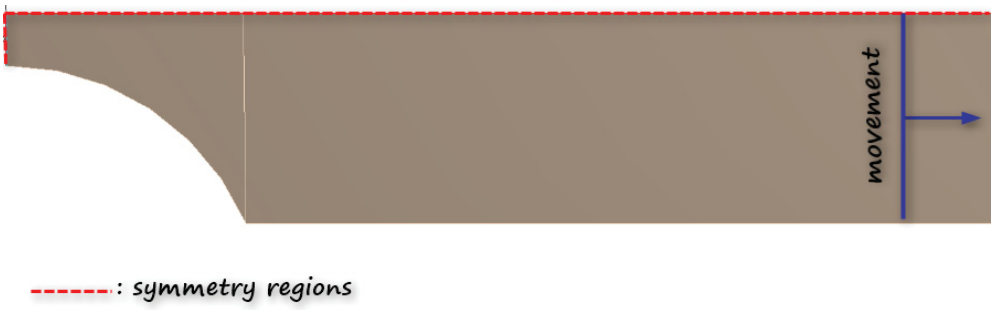

Figure 4.14. Boundary conditions on the tensile test specimen

Since the tensile test is done as quasi-static and there is a certain amount of movement on the specimen, the numerical analysis has been performed explicitly (dynamic numerical analysis). The time steps of explicit analysis are quite small when compared to implicit (static numerical analysis) analysis. Thus, the capture of deformation behaviour of specimen is only possible through explicit analysis.

The ultimate tensile strength (UTS) has been selected as a comparison criteria for experimental and numerical results. The numerical UTS values has been taken from defined paths for stainless steel – copper and brazing interface shown in Fig. 4.15 and 4.16 respectively.

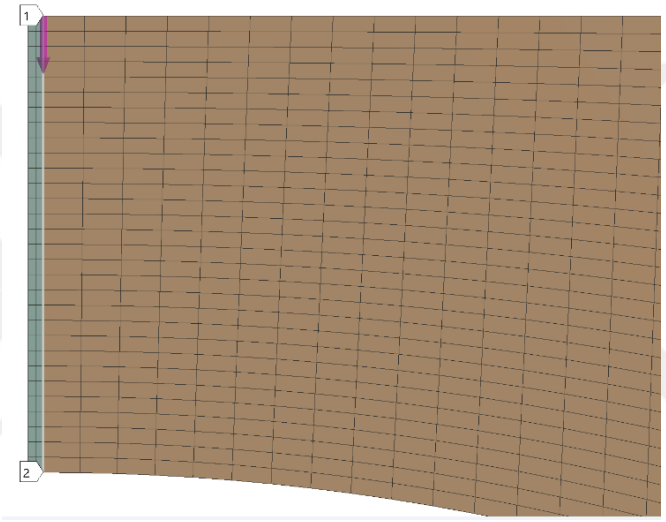

Figure 4.15. Stainless steel-copper interface path (Path-a)

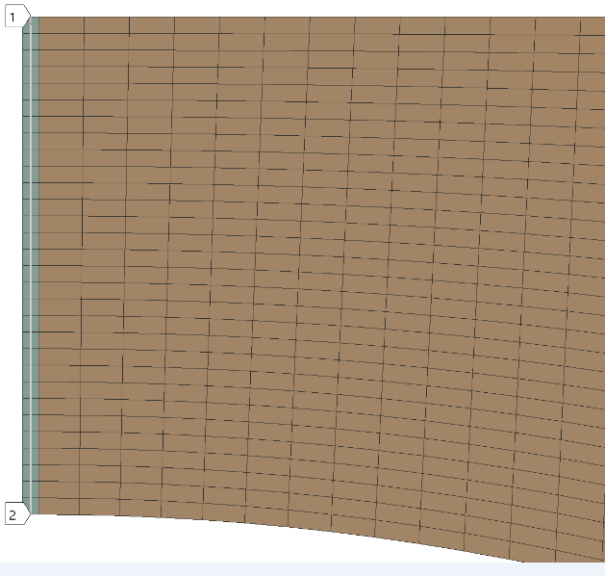

Figure 4.16. The path on the brazing interface material (Path-b)

The maximum principal stresses which are obtained along the defined paths has been presented in Fig. 4.17 and 4.18 respectively.

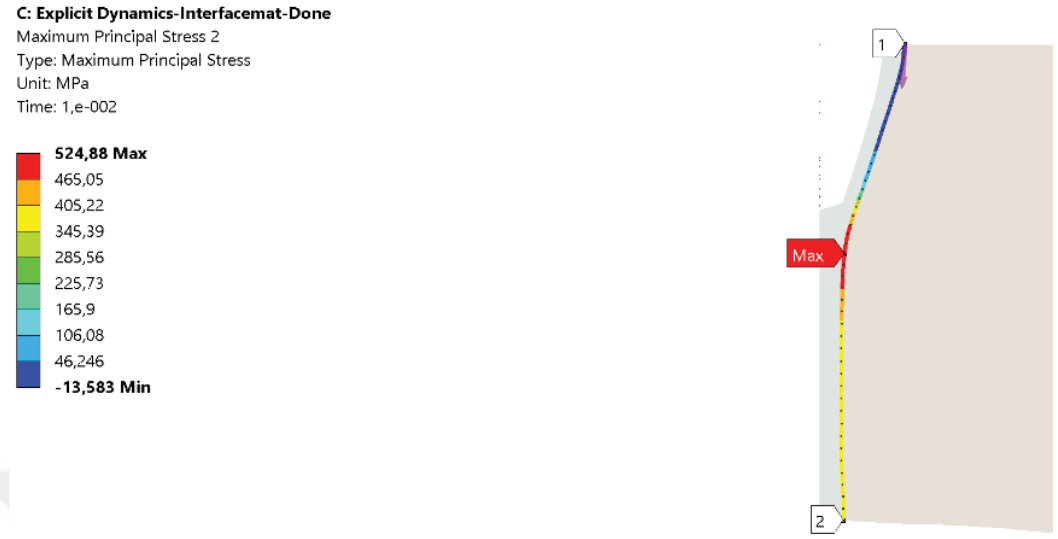

Figure 4.17. The maximum principal stress along the path-a

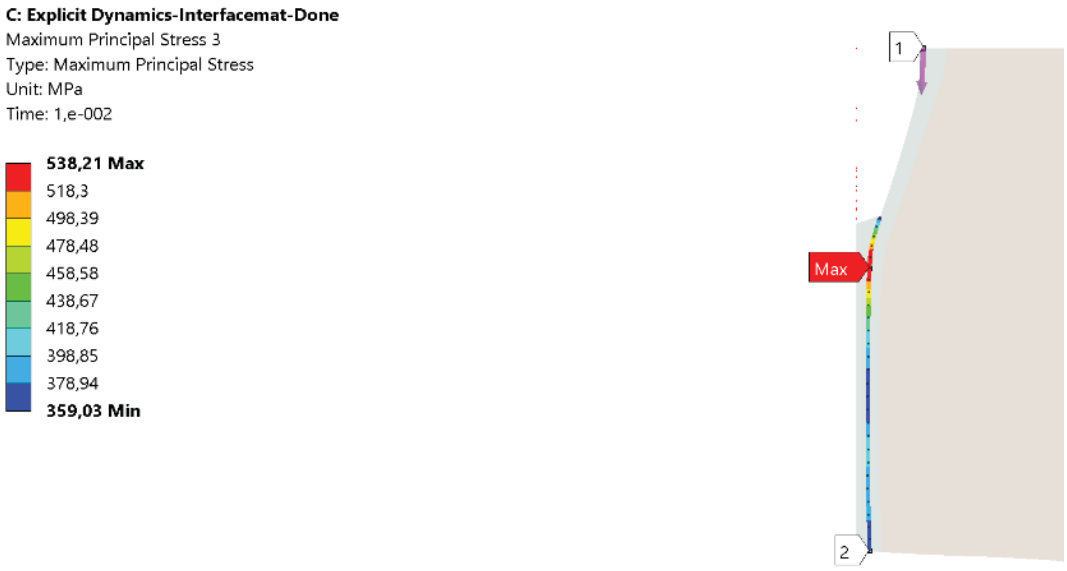

Figure 4.18. The maximum principal stress along the path-b

The numerical analysis of tensile test results have been shown that the maximum principal stress values at the interface are close to experimental UTS value. Thus the material behaviour of brazing interface has been validated and the results are shown in Table 4.6.

Table 4.6. Comparison of experimental and numerical UTS of brazing interface

Experimental UTS (average)	Numerical maximum principal stress through **path-a**	Numerical maximum principal stress through **path-b**	Differences (%)	
			Path-a	Path-b
520.5 MPa	524.88 MPa	538.21 MPa	0.8 %	3.29 %

In this chapter, the numerically studied problem has been introduced in detail. The assumptions and simplifications are shown. The boundary conditions has been explained and the new developed numerical methodology has been presented. Additionaly, the numerical validation of tensile testing with brazing interface material model has been done.

CHAPTER 5

RESULTS AND DISCUSSION

In this chapter, it is intended to give numerical simulation results of brazed plate heat exchanger. The numerical analysis have been performed for three different PHE geometries by arranging the chevron angle of plates. As well, the structural behaviour of plate heat exchanger have been investigated for four different pressure values at each chevron angle. In order to evaluate structural behavior of PHE, the static structural analysis results are given and stress based fatigue assesment have been done by considering strength factor and mean stress effect.

The static loading results of PHE with 90°, 110° and 130° chevron angles have been shown in Table 5.1, 5.2 and 5.3, respectively with maximum value.

Table 5.1. The numerical analysis results of PHE at 90 ° chevron angle

Static Loading Results				
Chevron angle (°)	**90°**			
Total brazing surface area ($mm^{2)}$	**305**			
Channel pressure (P_{net})	**14.5**	**23.5**	**28.5**	**48.5**
Equivalent stress (MPa)	105	192	205	300
Maximum principal stress (MPa)	115	200	220	315
Equivalent elastic strain (mm/mm)	0.00069	0.00111	0.00117	0.00146
Equivalent plastic strain (mm/mm)	0	0	0.00117	0.00171
Equivalent total Strain (mm/mm)	0.00069	0.0012	0.00145	0.00292
Total Deformation (mm)	0.00664	0.0114	0.0137	0.0229

The Table 5.1 shows the static structural analysis results of 90° brazed plate heat exchanger. There is no plastic deformation on the plates up to 30 bar domestic heating channel pressure. The maximum total deformation on the plate has been found as 0,0229 mm. The maximum principal stress contour for 50 bar channel pressure has been given in Fig. 5.1.

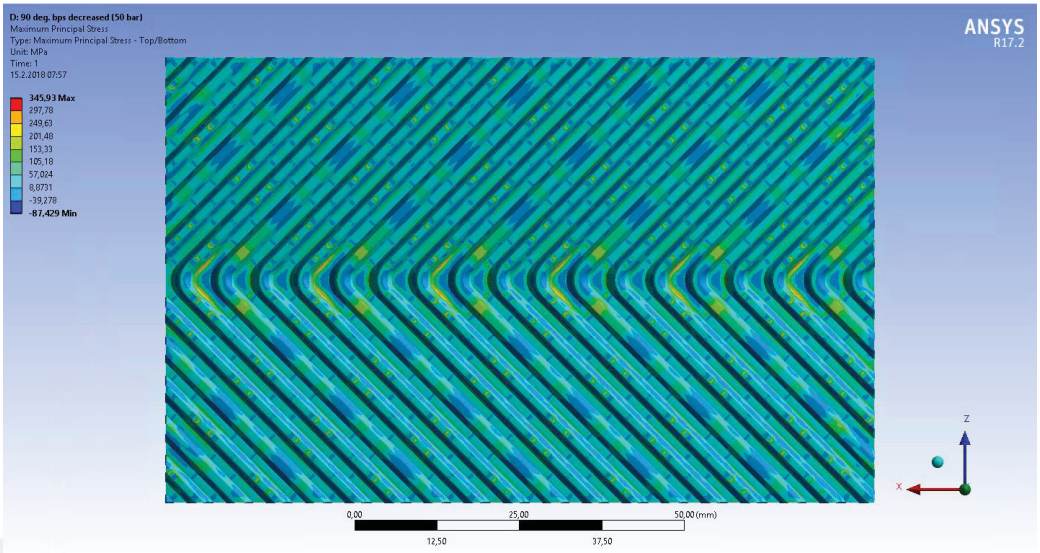

Figure 5.1. Maximum principal stress distribution of 90° PHE at 50 bar pressure

Table 5.2. The numerical analysis results of PHE at 110 ° chevron angle

Static Loading Results				
Chevron angle (°)	**110°**			
Total brazing surface area ($mm^{2)}$	**313**			
Channel pressure (P_{net})	**14.5**	**23.5**	**28.5**	**48.5**
Equivalent stress (MPa)	150	250	290	305
Maximum principal stress (MPa)	160	275	310	318
Equivalent elastic strain (mm/mm)	0.0008	0.00133	0.00141	0.00156
Equivalent plastic strain (mm/mm)	0	0.000072	0.00064	0.00441
Equivalent total Strain (mm/mm)	0.0008	0.001402	0.00187	0.00566
Total Deformation (mm)	0.0009	0.00185	0.0022	0.039

Static loading results of PHE at 110° chevron angles has shown that the plastic deformation is observed that 25 bar domestic hot water channel pressure. Compared with 90°, 41 % difference in total deformation is observed at 50 bar.

The maximum principal stress contour for 50 bar channel pressure has been given in Fig. 5.2.

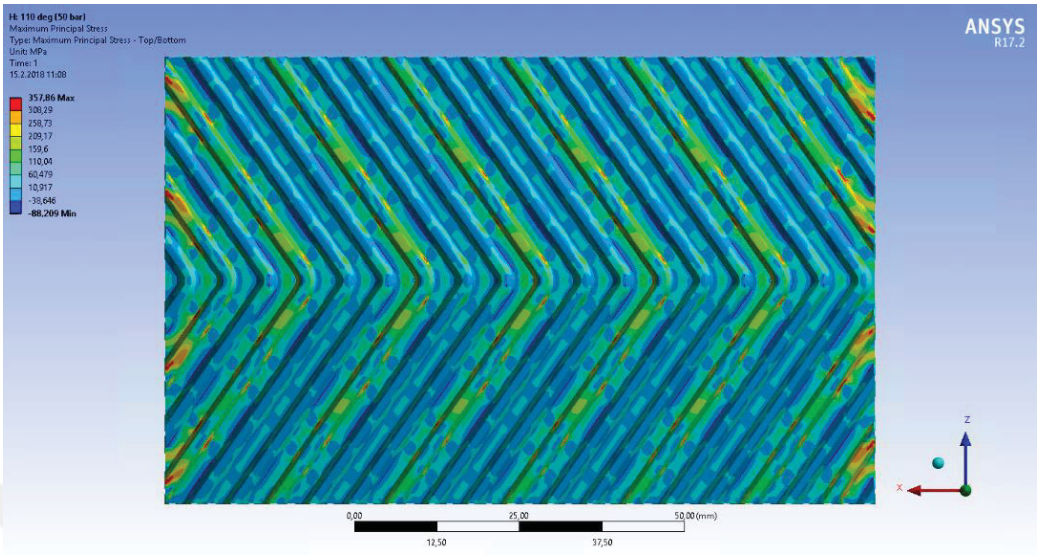

Figure 5.2. Maximum principal stress distribution of 110° PHE at 50 bar pressure

Table 5.3. The numerical analysis results of PHE at 130 ° chevron angle

Static Loading Results				
Chevron angle (°)	**130°**			
Total brazing surface area (mm^2)	**243**			
Channel pressure (P_{net})	**14.5**	**23.5**	**28.5**	**48.5**
Equivalent stress (MPa)	120	230	260	310
Maximum principal stress (MPa)	122	210	252	350
Equivalent elastic strain (mm/mm)	0.000761	0.00123	0.00146	0.00166
Equivalent plastic strain (mm/mm)	0	0.000066	0.000227	0.00194
Equivalent total Strain (mm/mm)	0.000761	0.001296	0.00147	0.0036
Total Deformation (mm)	0.0075	0.0129	0.0155	0.026

It is shown from Table 5.3, although the total brazing surface are of 130° PHE is less than the 110° PHE, the maximum total deformation value of the 110° PHE at 50 bar channel pressure is bigger than the 130° PHE. There is 33 % difference between them.

The maximum principal stress contour of 130° PHE for 50 bar channel pressure has been given in Fig. 5.3.

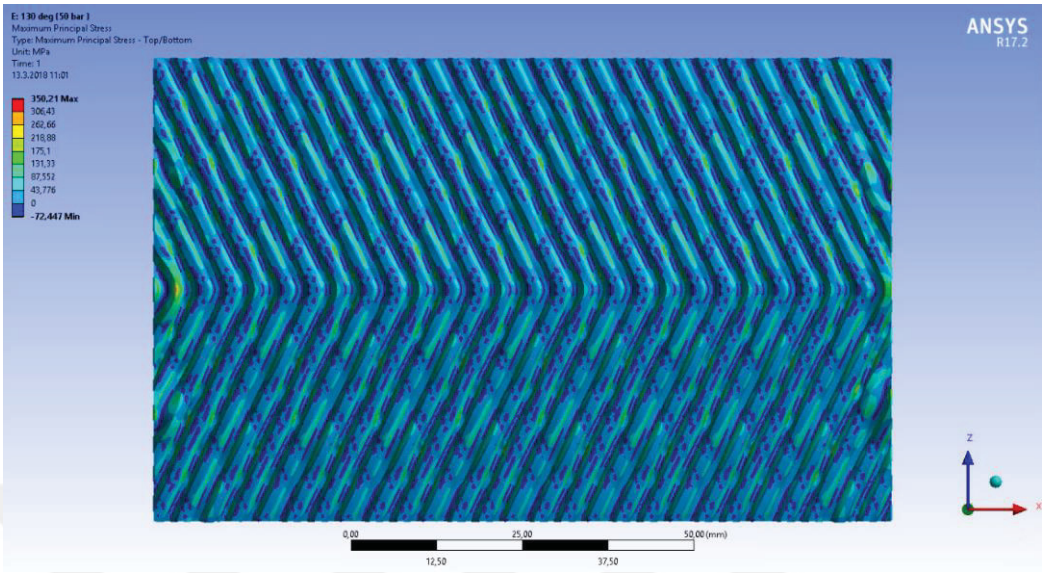

Figure 5.3. Maximum principal stress distribution of 130° PHE at 50 bar pressure

The relations of stress (σ), total deformation (δ) and plastic strain (ε_p) with channel pressure have been shown in Fig. 5.4 and 5.5 respectively.

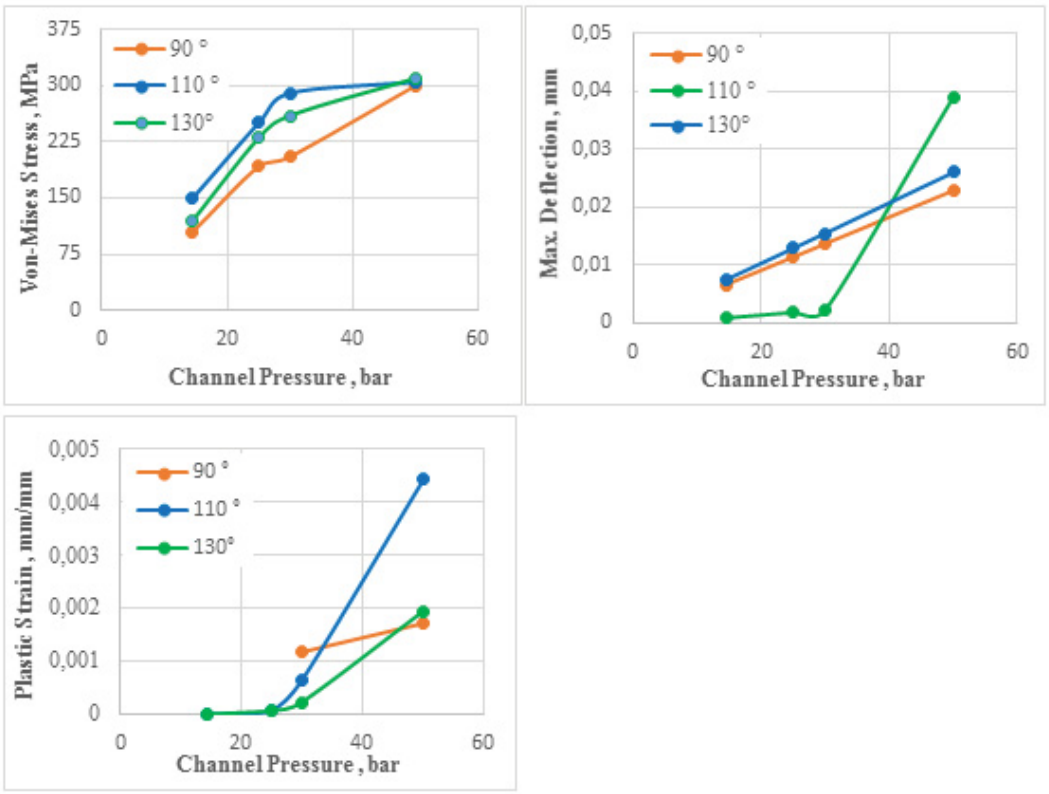

Figure 5.4. σ – P, δ – P and εp - P relations at different chevron angles

The fatigue evaluation of PHE at chevron angles 90°, 110° and 130° have been done by using static structural finite element analysis results based on S-N curve of plate and brazing point materials. The safety factor (SF) has been determined as a fatigue assesment criteria by considering effect of stress theory, fatigue strength factor (K_f) and mean stress theory. The safety factor calculations have been done according to 350.000 cycle endurance limit. The mean stress (MS) effect has been studied only with Goodman crtierion. Because, the fatigue experiments have been performed according to ultimate tensile strength. The tabular safety factor results of 90 ° PHE at minimum value according to Von-Mises and maximum principal stress theories have been shown in Table 5.4 and 5.5, respectively.

Table 5.4. Fatigue results of 90 ° PHE according to Von-Mises stress theory

Von-Mises stress (VM)						
Pressure	$K_f = 1$		Difference (%)	$K_f = 0.8$		Difference (%)
	SF (MS none)	SF (Goodman)		SF (MS none)	SF (Goodman)	
14,5	12.017	5.5297	53.984	9.613	4.959	48.414
25	6.985	3.214	53.987	5.588	2.883	48.407
30	5.799	2.668	53.992	4.639	2.393	48.416
50	4.965	2.284	53.998	3.972	2.049	48.414

Table 5.5. Fatigue results of 90 ° PHE according to maximum principal stress theory

Maximum principal stress (MP)						
Pressure	$K_f = 1$		Difference (%)	$K_f = 0.8$		Difference (%)
	SF (MS none)	SF (Goodman)		SF (MS none)	SF (Goodman)	
14,5	11.791	6.261	46.900	9.432	5.615	40.469
25	6.857	3.617	47.251	5.486	3.244	40.868
30	5.844	3.007	48.546	4.675	2.697	42.310
50	4.53	2.085	53.974	3.624	1.87	48.400

It has been observed that the fatigue safety factor has been differentiated at about 50 % according the effect of mean stress. Similarly, the strength factor K_f has been included in safety factor calculations in order to predict the effect of geometric factors and others

between the experimental sample and the state of numerically investigated plate heat exchanger. The graphical illustration of all fatigue results of PHE with 90° chevron angle are given in Fig. 5.5.

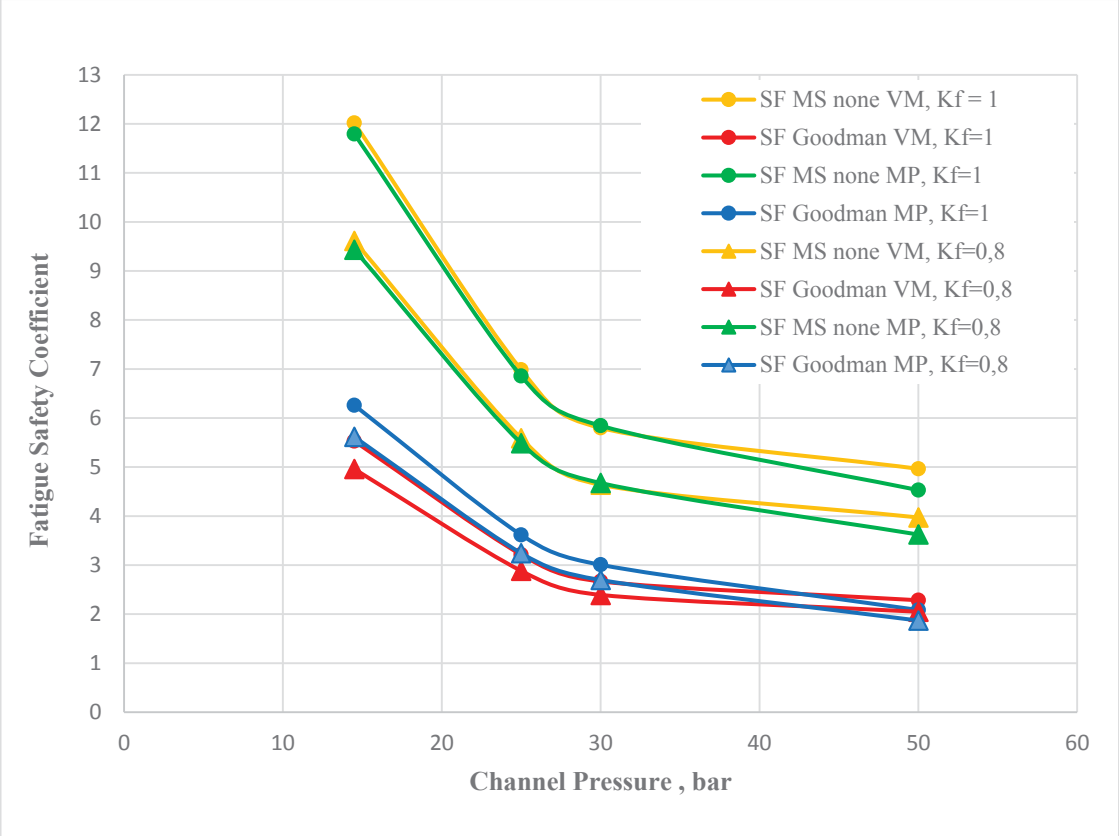

Figure 5.5. Fatigue safety factor – channel pressure relations at 90° chevron angle PHE

The safety factor results of 110 ° PHE at minimum value have been shown in Table 5.6 and 5.7, respectively.

Table 5.6. Fatigue results of 110 ° PHE according to Von-Mises stress theory

Von-Mises stress (VM)						
Pressure	$K_f = 1$		Difference (%)	$K_f = 0.8$		Difference (%)
	SF (MS none)	SF (Goodman)		SF (MS none)	SF (Goodman)	
14,5	5.34	2.45	54.120	4.273	2.204	48.420
25	4.901	2.255	53.989	3.92	2.022	48.418
30	4.762	2.291	51.890	3.809	2.055	46.049
50	2.565	1.66	35.283	2.052	1.428	30.409

Table 5.7. Fatigue results of 110 ° PHE according to maximum principal stress theory

Maximum principal stress (MP)						
Pressure	$K_f = 1$		Difference (%)	$K_f = 0.8$		Difference (%)
	SF (MS none)	SF (Goodman)		SF (MS none)	SF (Goodman)	
14,5	4.712	3.772	19.949	3.769	3.383	10.241
25	4.651	2.308	50.376	3.721	2.07	44.370
30	4.516	2.123	52.989	3.613	1.904	47.301
50	2.539	1.643	35.289	2.031	1.414	30.379

The graphical illustration of all fatigue results of PHE with 110° chevron angle are given in Fig. 5.6.

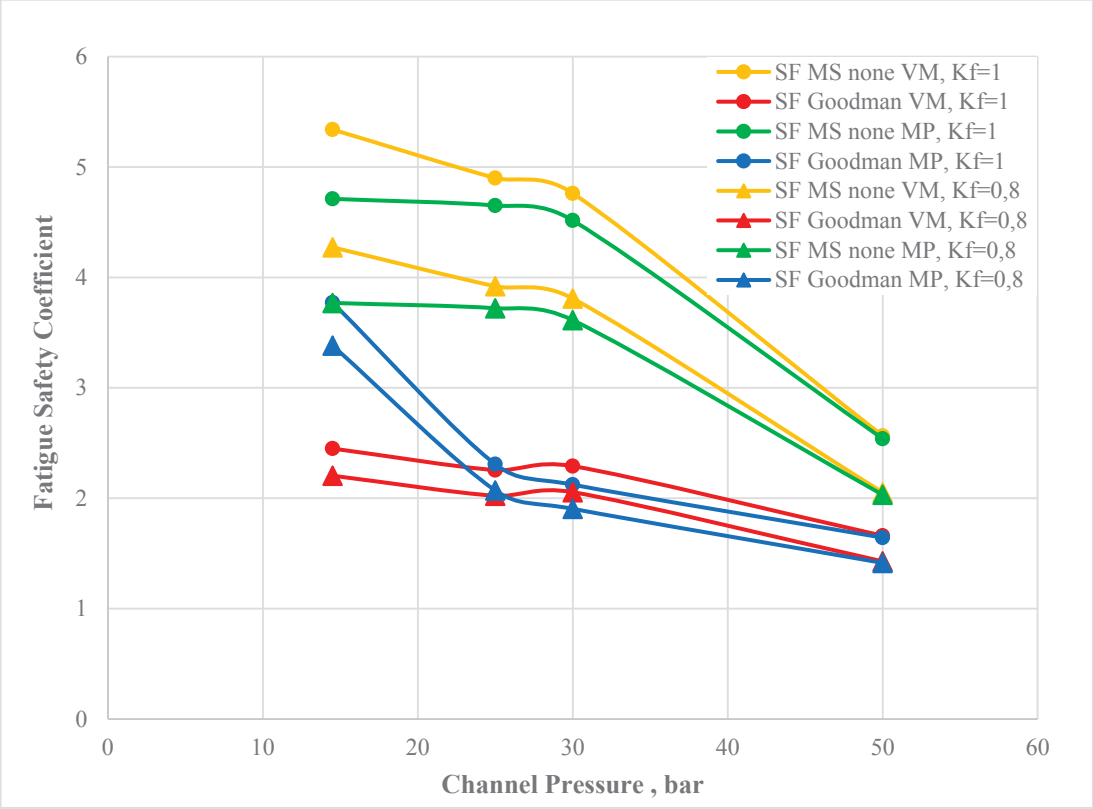

Figure 5.6. Fatigue safety factor – channel pressure relations at 110° chevron angle PHE

When the plate heat exchangers with 90° and 110° chevron angles are compared in terms of fatigue behaviour by considering the safety factors based on Von-Mises and maximum principal theories, the 90° PHE has been observed to be more reliable than the 110° PHE.

The another fact that the difference between the fatigue safety coefficients according to Von-Mises and maximum principal stress theories at the minimum and maximum channel pressures are less than the others. The tabular safety factor results of 130 ° PHE at minimum value have been shown in Table 5.8 and 5.9 respectively.

Table 5.8. Fatigue results of 130 ° PHE according to Von-Mises stress theory

Von-Mises stress (VM)						
Pressure	$K_f = 1$		Difference (%)	$K_f = 0.8$		Difference (%)
	SF (MS none)	SF (Goodman)		SF (MS none)	SF (Goodman)	
14,5	11.516	5.299	53.986	9.212	4.752	48.415
25	6.688	3.077	53.992	5.35	2.76	48.411
30	5.987	2.755	53.984	4.79	2.471	48.413
50	5.003	2.302	53.988	4.003	2.065	48.414

Table 5.9. Fatigue results of 130° PHE according to maximum principal stress theory

Maximum principal stress (MP)						
Pressure	$K_f = 1$		Difference (%)	$K_f = 0.8$		Difference (%)
	SF (MS none)	SF (Goodman)		SF (MS none)	SF (Goodman)	
14.5	11.164	5.926	46.919	8.93	5.315	40.482
25	6.483	3.438	46.969	5.186	3.083	40.551
30	5.552	2.866	48.379	4.441	2.57	42.130
50	4.475	2.059	53.989	3.58	1.847	48.408

Table 5.10. Comparison of fatigue safety factors at maximum channel pressure under specified conditions

Fatigue Safety Factor (FSF) at 50 bar channel pressure (Kf = 0.8 - Goodman)				
Chevron angle (β)	Total brazing surface area (mm^2)	Brazing point surface area (mm^2)	Von-Mises	Maximum Principal
90°	305	1.172	2.049	1.87
110°	313	1.836	1.428	1.414
130°	243	0.861	2.065	1.847

The graphical illustration of all fatigue results of PHE with 130° chevron angle are given in Fig. 5.7.

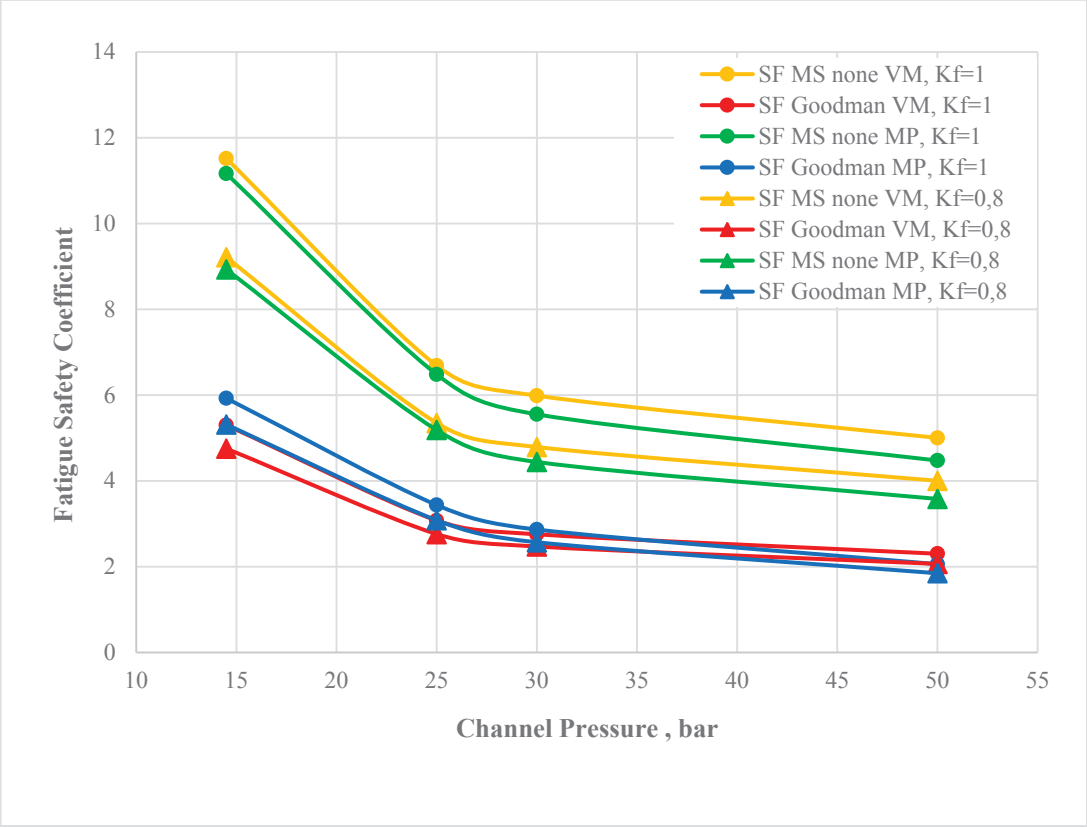

Figure 5.7. Fatigue safety factor – channel pressure relations at 130° chevron angle PHE

The comparison of different PHE designs by considering the chevron angle in terms of fatigue safety factor has been represented in Table 5.10 at worst case conditions; 50 bar channel pressure, $K_f = 0,8$ and Goodman stress theory.

CHAPTER 6

CONCLUSION

Within the scope of this thesis, the mechanical design and numerical analysis of plate heat exchangers having three different chevron angle have been investigated. In this context the material models to be used in numerical analysis have been developed and verified. Based on the studies carried out, the following results have been obtained:

1. The mechanical behaviour of brazing points (interface) of plate heat exchangers have been characterized by tensile and fatigue testing.
2. The mechanical properties of brazing points, modulus of elasticity, yield and ultimate strengths, strain to break etc. have been obtained with tensile testing. It was observed that the obtained mechanical properties have shown distinction from the properties of 316 L stainless steel and copper.
3. The plastic flow curve, representing the area between the yield point and ultimate tensile point of brazing interface material has been obtained.
4. The n and K values characterizing the Hollomon's curve are given tabularly and it is observed that these values are significantly different from the n and K values of typical stainless steel and copper.
5. The S-N curve of brazing interface have been obtained by stress based fatigue experiments for four stress levels, 90, 80, 70 and 60 % UTS and at 5 Hz frequency.
6. The parameters of N_f, a and b of the Basquin's equation which defines the Wöhler's curve (S-N) have been obtained by Power-law linearization method.
7. It is observed that the fatigue life of brazing interface material approximately bigger than the 120.000 cycle when the fatigue specimen is subjected to a 60 % UTS loading.
8. The material model for brazing interface which is used in numerical analysis has been validated according to tensile test conditions by explicit method. It has been shown that the difference between numerical and experimental ultimate tensile strength value is lower than 5 %.

9. The effect of the chevron angle on the mechanical behaviour of the plate heat exchanger has been investigated numerically for different channel pressure values.
10. The static structural analysis results showed that there is no plastic deformation on the plate heat exchangers for all chevron angles 90°, 110° and 130° at 14.5 bar channel pressure. On the other hand, the highest plastic deformation was observed at maximum pressure value of 50 bar with a 0.44 % plastic strain in plate heat exchanger with 110 ° chevron angle
11. The plate heat exchangers with 90° and 130° chevron angle have shown similar structural behaviour as in terms of plastic deformation and total deflection. However, the plate heat exchanger with 110° chevron angle has twice more plastic deformation (52.5 %) than the others. The results have shown that although the plate heat exchanger with 110° chevron angle has the highest total brazing surface area, the worst results both for static and fatigue analysis have been taken from it. From this point of view, the single brazing point surface area and homogeneous distribution of brazing points on the plate are much more critical than the total surface area. The comparison of worst case (50 bar, K_f=0.8 adn Goodman MS) results in terms of fatigue by considering effect of single and total brazing surface area have been illustrated in Table 5.10.
12. The assesment of fatigue analysis have been done by considering the static structural analysis results. It is important that although the plasticity has been defined as material model, the effect of nonlinear material behaviour has not been taken into account during the computation of fatigue results.
13. The fatigue experiments have been conducted to ultimate tensile strength limit of brazing interface material, the fatigue safety factor has been calculated with the effect of Goodman's mean stress theory. The results have been compared by considering no effect of mean stress and Goodman's theory. The fatigue safety coefficients obtained with Goodman's theory are found to have lower values than the others.
14. Since the state of stress and toughness behaviour of plate heat exchangers may be different in the interface zone and on the plate, the fatigue safety factor has been calculated according to Von-Mises and maximum principal stress theories.
15. The all plate heat exchanger designs having 90°, 110° and 130° chevron angles have been achieved a life cycle criteria of 300.000 cycle.

16. The lowest value of fatigue safety factor has been obtained at 50 bar channel pressure and the plate heat exchanger with 110 ° chevron angle as expected due to results of static structural analysis. Furthermore, since the maximum principal stress is bigger than the equivalent stress at 50 bar channel pressure, the fatigue safety factor values which determined by considering maximum principal stress are lower than the equivalent stress. There is a 8 % difference between the fatigue safety factor values for 90° and 130° chevron angles. But there is almost no difference for 110° chevron angle.
17. The strength factor K_f shows that the same effect in all geometric configurations and under all pressure conditions. The fatigue safety factor has been reduced by 20% percent with $K_f = 0.8$.

In conclusion, the structural behaviour of brazed plate heat exchangers can be evaluated numerically with the proposed methodology explained in this thesis. Thereby, the possible problems that can be encountered before the production of molds are foreseen and the geometric design can be updated accordingly. Meanwhile, the methodlogy is enabled to reduce the mold and testing costs as well as decrease the spend time in experimental trial and error. As a continuation of this study, the designed plate heat exchangers can be produced with rapid prototyping and experimental setup can be set for validation of numerical results. Additionaly, the effect of stamping process on the structural behaviour of plate heat exchanger can be investigated.

REFERENCES

Jiang, W., Gong, J. (2011). A study of the effect of filler metal thickness on tensile strength for a stainless steel plate-fin structure by experiment and finite element method, *Materials and Design 31:* 2387-2396.

Mohammad, K. A., Ali, A., Sahari B. B., & Abdullah, S. (2011). Fatigue behavior of austenitic stype 316L stainless steel. *IOP Conf. Series: Material Science and Engineering 36.*

Jiang, W., Gong, J. M., & Tu, S. T. (2011) Fatigue life prediction of a stainless steel plate-fin structure using equivalent-homogeneous-solid method. *Materials and Design 32:* 4936-4942.

Mizokami, Y., Igari, T., Kawashima, F., Sakakibara, N., Tanihira, M., Yuhara, T., & Hiroe, T. (2012). Development of structural design procedure of plate-fin heat exchanger for HTGR. *Nuclear Engineering and Design 255:* 248-262.

Kang, S. H., Park, S. H., Min, J. K., Cho, J. R., & Ha, M. Y. (2012). Evaluation of mechanical integrity on the brazing hoint of a tube-type heat exchanger with considering local material properties. *Mechanical Engineering Science 227 (3):* 420-433.

Shit, J., Dhar, S., & Acharyya, S. (2013). Characterization of cyclic plastic behavior of SS 316 stainless steel. *IJESIT, Volume 2, Issue 5.*

Mohammad, K. A., Zainudin, E. S., Salit, S., Zahari, N. I., & Ali, A. (2013). Fatigue life for type 316L stainless steel under cyclic loading. *Advanced Material Research 701:* 77-81.

Koster, M., Kenel, C., Stutz, A., Lee, W. J., Lis, A., Affolter, C., & Leinenbach, C. (2013). Fatigue and cyclic deformation behavior of brazed steel joints. *Materials Science & Engineering A 581:* 90-97.

Agrawal, R., Uddanwadiker, R., & Padole, P. (2014). Low cycle fatigue life prediction. *Emerging Engineering Research and Technology, Volume 2, Issue 4:* 5-15.

Koster, M., Lis, A., Lee, W. J., Kennel, C., & Leinenbach, C. (2015). Influence of elastic-plastic base material properties on the fatigue and cyclic deformation behavior of brazed steel joints. *Fatigue 82:* 49-59.

Onal, O., Bal, B., Canadinc, D., & Akdari, E. (2015). Experimental and numerical evaluation of thickness reduction in steel plate heat exchangers. *Materials and Technology 137.*

Hormozi, R., Biglari, F., & Nikbin, K. (2015). Experimental study of type 316 stainless steel failure under LCF7TMF loading condtions. *Fatgiue 75:* 153-169.

Brnic, J., Turkalj, G., Canadija, M., Lanc, D., Krscanski S., Brcic, M., Li, Q., & Niu, J,. (2016). Mechanical properties, short time creep and fatigue of an austenitic steel. *Materials, 9(4):* 298.

Laurent, M., Estevez, R., Fabrègue, D. and Ayax, E. (2016). Thermomechanical fatigue life prediction of 316L compact heat exchanger. *Engineering Failure Analysis*, 68, pp.138-149.

Ghovanlou, M., Jahed, H. and Khajepour, A. (2011). Mechanical reliability characterization of low carbon steel brazed joints with copper filler metal. *Materials Science and Engineering: A*, 528(19-20), pp.6146-6156.

Hasanoglu, E. A. (2017). Stacking sequence optimization and modelling of laminated composite plates for free vibration. (Master's thesis, Izmir Institute of Technology, İzmir, Turkey).

Dieter, G. E., (1988), *Mechanical Metallurgy,* McGraw-Hill, Book Company.

ASM International, (2004), *Tensile Testing 2nd edition.*

Hibbeler, R. C. (2016), *Mechanics of Materials,* Pearson, Book Company.

İrizalp, S. (2015), Plastic Deformation. (Lecture notes, Manisa Celal Bayar University, Manisa, Turkey).

Roylance, D. (2001), Stress-Strain Curves. (Lecture notes, Massachusetts Institute of Technology, Cambridge, MA02139, USA)

Hosford, W. F. (2010), *Mechanical Behavior of Materials*, Cambridge University Press.

Roylance, D. (2001), Fatigue. (Lecture notes, Massachusetts Institute of Technology, Cambridge, MA02139, USA)

ASM International, (2008), *Elements of Metallurgy and Engineering alloys: Fatigue.*

Kaymaz, İ. (2015), Fatigue (Lecture notes, Erzurum Technical University, Erzurum, Turkey)

Thompson, B. S., Müller, N. (2005), Mechanical Design (Lecture notes, Michigan State University, Michigan USA).

Steege, P. (2015), Introduction to Vacuum Brazing (Lecture notes, Bosch Thermotechnology, Manisa, Turkey).

NAFEMS, (2010). Introduction to Finite Element Analysis (Lecture notes, The University of Manchester, Manchester, UK).

Bosch Thermotechnology R&D Centre Manisa, (2016), (Mechanical characterization tests report of 316L stainless steel, Atılım University, Ankara, Turkey)

www.fea-cae-engineering.com